MINISTÉRIO DA CIÊNCIA, TECNOLOGIA, INOVAÇÕES E COMUNICAÇÕES
INSTITUTO NACIONAL DE PESQUISAS ESPACIAIS

sid.inpe.br/mtc-m21b/2017/07.24.14.13-TDI

SWAT MODELLING OF STREAMFLOW AND SEDIMENT CONCENTRATION IN AN AMAZONIAN BASIN IMPACTED BY ARTISANAL GOLD MINING

Camila Andrade Abe

Master's Dissertation of the Graduate Course in Remote Sensing, guided by Drs. Evlyn Márcia Leão de Moraes Novo, and Felipe de Lucia Lobo, approved in August 11, 2017.

URL of the original document:
<http://urlib.net/8JMKD3MGP3W34P/3PB94RH>

INPE
São José dos Campos
2017

PUBLISHED BY:

Instituto Nacional de Pesquisas Espaciais - INPE
Gabinete do Diretor (GB)
Serviço de Informação e Documentação (SID)
Caixa Postal 515 - CEP 12.245-970
São José dos Campos - SP - Brasil
Tel.:(012) 3208-6923/6921
E-mail: pubtc@inpe.br

MINISTÉRIO DA CIÊNCIA, TECNOLOGIA, INOVAÇÕES E COMUNICAÇÕES
INSTITUTO NACIONAL DE PESQUISAS ESPACIAIS

sid.inpe.br/mtc-m21b/2017/07.24.14.13-TDI

SWAT MODELLING OF STREAMFLOW AND SEDIMENT CONCENTRATION IN AN AMAZONIAN BASIN IMPACTED BY ARTISANAL GOLD MINING

Camila Andrade Abe

Master's Dissertation of the Graduate Course in Remote Sensing, guided by Drs. Evlyn Márcia Leão de Moraes Novo, and Felipe de Lucia Lobo, approved in August 11, 2017.

URL of the original document:
<http://urlib.net/8JMKD3MGP3W34P/3PB94RH>

INPE
São José dos Campos
2017

Cataloging in Publication Data

Abe, Camila Andrade.

Ab33s Swat modelling of streamflow and sediment concentration in an Amazonian basin impacted by artisanal gold mining / Camila Andrade Abe. – São José dos Campos : INPE, 2017.

xxviii + 114 p. ; (sid.inpe.br/mtc-m21b/2017/07.24.14.13-TDI)

Dissertation (Master in Remote Sensing) – Instituto Nacional de Pesquisas Espaciais, São José dos Campos, 2017.

Guiding : Drs. Evlyn Márcia Leão de Moraes Novo, and Felipe de Lucia Lobo.

1. Hydrological modelling. 2. Sediment. 3. Remote sensing. 4. Amazon. 5. SWAT. I.Title.

CDU 528.8:556

Aluno (a): *Camila Andrade Abe*

Título: "SWAT MODELLING OF STREAMFLOW AND SEDIMENT CONCENTRATION IN AN AMAZONIAN BASIN IMPACTED BY ARTISANAL GOLD MINING".

Aprovado (a) pela Banca Examinadora em cumprimento ao requisito exigido para obtenção do Título de *Mestre* em

Sensoriamento Remoto

Dr. Camilo Daleles Rennó

Presidente / INPE / SJCampos - SP

Dra. Evlyn Márcia Leão de Moraes Novo

Orientador(a) / INPE / SJCampos - SP

Dr. Felipe de Lucia Lobo

Orientador(a) / INPE / São José dos Campos - SP

Dra. Laura de Simone Borma

Membro da Banca / INPE / São José dos Campos - SP

Dra. Maycira Costa

Convidado(a) / UVic / Victoria - CAN

Dr. Yonas B. Dibike

Convidado(a) / W-CIRC/UVic / Victoria - CAN

Dr. Conrado de Moraes Rudorff

Convidado(a) / CEMADEN / São José dos Campos - SP

Este trabalho foi aprovado por:

( ) maioria simples

( ) unanimidade

São José dos Campos, 11 de agosto de 2017

"O, do not pray for easy lives.

Pray to be stronger men!

Do not pray for tasks equal to your powers.

Pray for powers equal to your tasks!

Then the doing of your work shall be no miracle.

But you shall be a miracle."

Phillips Brooks

To my grandmother Mitsuko and to my mother Marieta (in memoriam)

ACKNOWLEDGEMENTS

I thank God, for this opportunity of academic and personal growth, in which I met such special people and could learn with each of them. Many people helped me in this Masters, in several different ways. To all of them, my sincere gratitude!

I am very grateful to my supervisors, Dr. Evlyn Novo and Dr. Felipe Lobo for all advice, dedication, patience, support, and for placing their confidence in me during each step of this work, and even allowing me to take the challenge of developing part of this study abroad.

All members of the defense committee are acknowledged for the much valuable suggestions and corrections that surely improved the quality of this thesis.

I am grateful to Dr. Maycira Costa and Dr. Yonas Dibike, for accepting to supervise my work at the University of Victoria, for all support and attention given, for all great suggestions and advice. Dr. Camilo Rennó, Dr. Laura Borma, and Dr. Lênio Galvão are also acknowledged for the valuable suggestions made in the first steps of this work.

I am grateful to Dr. Francisco Dupas, for the friendship and for introducing me to the research world. To Dr. Patrícia Drach, for the friendship and the kindness always delivered to me, and for supporting and encouraging me to pursue the academic career. Dr. Vanessa dos Santos, for sharing with me the frustrations and triumphs with SWAT, accompanying me on this journey of learning.

I am thankful to all professors and assistants from the Remote Sensing Graduate Program, for the dedication and all shared knowledge.

I acknowledge the Brazilian National Council for Scientific and Technological Development (CNPq) and the Canadian Bureau for International Education (CBIE) for the financial support, as well as the National Institute for Space Research (INPE) and the University of Victoria, for the physical infrastructure and technical support.

Special thanks to my friend Layane Fernandes, for sharing with me the opportunity of the Emerging Leaders in the Americas Program (ELAP) and, despite the distance, keeping such kind friendship and support. I thank all my friends from INPE, for the friendship and partnership in both, good and hard times. I am also grateful to my friends from Spectral Lab, for so warmly receiving me in Victoria, especially Sarah and Andrea, for the much-needed rock climbing nights.

I am especially grateful to my beloved partner, Rodolfo, for all patience, understanding, interest and restless support. And finally, to my grandmother, Mitsuko and to my sister, Dani, whose strength and braveness inspire me every day.

ABSTRACT

Land cover change such as replacing the forest with pasture or bare soil areas can significantly affect the water cycle, altering streamflow regime, accelerating or intensifying erosive processes and influencing water quality and availability. In Crepori River basin, the expansion of gold mining activity has caused an increase in sediment concentration in the river. Sediment concentration in rivers can be quantified using direct or indirect methods, but it is usually difficult to quantify sediment generated by point and non-point sources, such as mining activities and land cover, respectively. In this study, SWAT model (Soil and Water Assessment Tool) was applied in Crepori basin, from 2001 to 2012 to investigate the impacts of land cover change on streamflow regime and on sediment concentration in the river. By comparing simulated sediment concentration and sediment concentration estimated via remote sensing by Lobo et al. (2015) for the same region, this study aimed to define the proportion of sediment concentration due to sheet erosion (non-point source) from that of gold mining activities (point source) in Lobo et al. (2015) estimates. Results show a good adjustment of the model for streamflow (NSE = 0.84, PBIAS = -2.44%, RSR = 0.40) and simulated sediment concentration corresponds to measured values from published studies for period and regions with low or no mining activity. Simulations indicate that land cover change occurred between 2001 and 2012 in Crepori basin were not sufficient to significantly impact the river streamflow, but simulations performed for different scenarios of land cover (referring to the periods of 1973, 1998-2010, a future scenario of 2040 and a hypothetical scenario of complete soil exposure) showed a trend in increasing streamflow given the increase in deforested and bare soil areas in the Basin. Regarding sediments, in average, 14% of sediment concentration estimated by Lobo et al. (2015) in high-water season corresponds to sediment generated by diffuse soil erosion, whereas this average proportion is of 6% in the low-water season. Results also showed that seasonality of sediment concentration generated only due to diffuse soil erosion is the inverse of that observed by Lobo et al. (2015), which includes mining activity. Finally, the increase in deforested and bare soil areas in the basin are associated to the increase in sediment concentration in both wet and dry periods, and the simulations for the hypothetical bare soil scenario indicate that the effects of mining activity on sediment concentration in Crepori River may surpass expected impacts of the scenario with maximum soil exposure to pluvial erosion.

Keywords: Hydrological Modelling. Sediment. Remote Sensing. Amazon. SWAT.

MODELAGEM SWAT DE VAZÃO E DE CONCENTRAÇÃO DE SEDIMENTOS EM UMA BACIA AMAZÔNICA IMPACTADA POR GARIMPO

RESUMO

Mudanças de uso e cobertura da terra podem alterar significativamente o ciclo hidrológico, modificando o comportamento das vazões de rios, além de poder acelerar e intensificar processos erosivos, afetando a qualidade da água. Na bacia hidrográfica do Rio Crepori, o avanço da atividade garimpeira tem levado ao aumento das concentrações de sedimentos no rio. Concentrações de sedimentos em rios podem ser medidas e estimadas por métodos diretos e indiretos, porém é geralmente difícil distinguir quantitativamente as porções de sedimentos geradas por fontes pontuais, como garimpos, de fontes não pontuais, como erosão laminar do solo. Neste trabalho, o modelo SWAT (Soil and Water Assessment Tool) foi aplicado na bacia do Rio Crepori, de 2001 a 2012, para investigar os impactos de mudanças de uso e cobertura da terra sobre o regime de vazões e sobre as concentrações de sedimentos no rio. A partir da comparação entre as concentrações de sedimentos simuladas e valores estimados por Lobo et al. (2015) para a mesma região, busca-se definir a proporção de sedimentos resultantes de erosão laminar do solo (difusa), e a proporção de sedimentos gerada pela atividade garimpeira. Os resultados mostram um bom ajuste do modelo para simulação de vazões (NSE = 0.84, PBIAS = -2.44%, RSR = 0.40), e as concentrações de sedimentos simuladas concordam com valores medidos e estimados, em outros trabalhos, em períodos e regiões com ausência ou baixa atividade de garimpos. Este estudo indica que as mudanças de cobertura da terra ocorridas entre 2001 e 2012 na bacia do Rio Crepori não foram suficientes para impactar as vazões do rio, mas simulações realizadas para diferentes cenários de cobertura do solo (referentes aos períodos de 1973, 1998-2012, um cenário futuro de 2040 e um cenário hipotético de total exposição do solo) mostraram uma tendência de aumento da vazão em função do aumento das áreas de desmatamento e de solo exposto na bacia. Para os sedimentos, em média, 14% da concentração de sedimentos estimada por Lobo et al. (2015) no período de cheia do Rio Crepori correspondem a sedimentos gerados por erosão laminar do solo e, para o período de água baixa, essa proporção média é de 6%. O estudo também mostrou que a dinâmica sazonal da concentração de sedimentos gerados apenas por erosão do solo é inversa àquela observada por Lobo et al. (2015), que inclui a atividade garimpeira. Por fim, o aumento de áreas desmatadas e de solo exposto na bacia estão associados ao aumento ao aumento das concentrações de sedimentos nos períodos seco e úmido, e as simulações para o cenário hipotético de completa exposição do solo indica que os efeitos da atividade garimpeira sobre as

concentrações de sedimentos nas águas do Rio Crepori podem superar os impactos esperados para um cenário de máxima exposição do solo à erosão pluvial na bacia

Palavras-chave: Modelagem hidrológica. Sedimento. Sensoriamento Remoto. Amazônia. SWAT

LIST OF FIGURES

Page.

LIST OF TABLES

Page.

LIST OF ACRONYMS AND ABBREVIATIONS

ANA	Brazilian National Water Agency
ARS	Agricultural Research Service
CERES	Clouds and the Earth's Radiant Energy System
CFSR	Climate Forecast System Reanalysis
DEM	Digital Elevation Model
DNPEA/MA	Brazilian National Department for Agricultural Research - Ministry of Agriculture
ECMWF	European Centre for Medium-Range Weather Forecasts
EMBRAPA	Brazilian Agricultural Research Corporation
EPIC	Erosion-Productivity Impact Calculator
FAO	Food and Agriculture Organization of the United Nations
GIS	Geographic Information System
GOC	Global Optimization Criterion
GOES	Geostationary Operational Environmental System
GPCC	Global Precipitation Climatological Centre
GPM	Global Precipitation Measurement
HIDRO Resources	Database of the Brazilian National System of Water Information
HRU	Hydrologic Response Unit
IBAMA	Brazilian Institute of Environment and Renewable Natural Resources
IBGE	Brazilian Institute for Geography and Statistics
ICMBio	Chico Mendes Institute for Biodiversity Conservation
INMET	Brazilian National Institute of Meteorology
INPE	Brazilian National Institute for Space Research
JAXA	Japan Aerospace Exploration Agency

LBA Amazonia	Large Scale Biosphere-Atmosphere Experiment in
LIS	Lightning Image Sensor
LOWESS	Locally Weighted Scatterplot Smoothing
LUP	Land Use Update Tool
MERRA	Modern-Era Retrospective Analysis for Research and Applications
MSS	Multispectral Scanner System
MUSLE	Modified Universal Soil Loss Equation
NASA	National Aeronautics and Space Administration
NASDA	National Space Development Agency of Japan.
NCEP	National Centers for Environmental Prediction
NSE	Nash-Sutcliffe Efficiency
NDVI	Normalized Difference Vegetation Index
NRC	American National Research Council
OF	Objective Function
ParaSol	Parameter Solution
PBIAS	Percent Bias
PR	Precipitation Radar
PronaSolos	Brazilian Soils National Program
QGIS	Quantum Geographic Information System
QSWAT	Soil and Water Assessment Tool interface on Quantum GIS
RADAMBRASIL	Brazilian Project Radar of Amazonia
RMSE	Root Mean Square Error
RSR Ratio	Root Mean Square Error-Observations Standard Deviation
RT	Real Time
SCS	Soil Conservation Service

SRTM	Shuttle Radar Topography Mission
SSQ	Sum of the Squares of the Residuals
SWAT	Soil and Water Assessment Tool
SWAT-CUP Uncertainty	Soil and Water Assessment Tool - Calibration and Programs
TauDEM	Terrain Analysis Using Digital Elevation Models
TMI	Tropical Rainfall Measuring Mission Microwave Imager
TMPA 3B42 Precipitation	Tropical Rainfall Measuring Mission Multisatellite Analysis Daily Product
TRMM	Tropical Rainfall Measuring Mission
TSS	Total Suspended Solids
USA	United States of America
USDA	United States Department of Agriculture
USGS	United States Geological Survey
USLE	Universal Soil Loss Equation
VIRS	Visible and Infrared Scanner
WMO	World Meteorological Organization

LIST OF SYMBOLS

a	Shape parameter in the rating curve
ALPHA_BF	Baseflow alpha factor
ALPHA_BNK	Baseflow alpha factor for bank storage
$area_{HRU}$	Area of the HRU
b	Shape parameter in the rating curve
BARR	Barren land cover (in SWATv.2012 database)
C_{ch}	Channel cover factor
CFRG	Coarse fragment factor
CH_COV1	Channel erodibility factor
CH_COV2	Channel cover factor
CH_K2	Effective hydraulic conductivity in main channel alluvium
CLAY	Soil clay content
CN2	Initial runoff curve number for moisture condition II
$CONC_{sed,ch}$	Sediment concentration in the channel
$CONC_{sed,ch,mx}$	Maximum sediment concentration that can be transported through the channel
C_{USLE}	USLE cover and management factor
E_a	Evapotranspiration
FF	Plinthosols
FRSE	Forest evergreen land cover (in SWATv.2012 database)
GW_DELAY	Groundwater delay time
GWQMN	Threshold depth water in the shallow aquifer required for return flow to occur
H	Water level
h	Water level to which discharge is zero
HYDGRP	Soil hydrological group

K_{ch}	Channel erodibility factor
K_{USLE}	USLE soil erodibility factor
LS_{USLE}	USLE topographic factor
LV	Red-yellow Ferralsols
NLAYERS	Number of soil layers
NSE	Nash-Sutcliffe efficiency coefficient
PAST	Pasture land cover (in SWATv.2012 database)
PBIAS	Percent bias
P_{est}	Estimated precipitation
$\bar{P}_{est}$	Average estimated precipitation
P_{obs}	Observed precipitation
$\bar{P}_{obs}$	Average observed precipitation
P_{USLE}	USLE support practice factor
Q	Discharge
Q_{gw}	Groundwater flow
Q_{obs}	Observed streamflow
$\overline{Q}_{obs}$	Average observed streamflow
q_{peak}	Peak runoff
Q_{sim}	Simulated streamflow
$\overline{Q}_{sim}$	Average simulated streamflow
Q_{surf}	Surface runoff
r	Correlation coefficient
r__	Relative change
R^2	Coefficient of determination
R_{day}	Precipitation of the day
REVAPMN	Threshold depth of water in the shallow aquifer for “revap” or percolation to the deep aquifer to occur

ROCK	Soil rock content
RSR	RMSE-observations standard deviation ratio
SAND	Soil sand content
sed	Sediment yield
SED_{dep}	Amount of sediment deposited in the reach
SILT	Soil silt content
SOL_ALB	Soil albedo
SOL_AWC	Soil available water capacity
SOL_BD	Soil bulk density
SOL_CBN	Soil carbon content
SOL_K	Soil saturated hydraulic conductivity
SOL_ZMX	Soil maximum root depth
SPCON	Calibration coefficient
SPEXP	Calibration coefficient
$STDEV_{obs}$	Standard deviation of observed data
SW_t	Final soil water content
SW_0	Initial soil water content
USLE_K	USLE soil erodibility factor
v__	Replace change
V_{ch}	Volume of water in the channel
$V_{ch,pk}$	Peak channel velocity
w_{seep}	Water from soil profile inflowing to the vadose zone

TABLE OF CONTENTS

Page.

1 INTRODUCTION

The tropical forest at the south-eastern region of the Brazilian Amazon has been highly suppressed and replaced by crops, pasture for cattle ranching, and mining sites (FEARNSIDE, 1985; 1993; ALVAREZ-BERRÍOS; AIDE, 2015). The average annual deforestation rate in the state of Pará, for instance, was around 4,900 km^2yr^{-1}, between 1988 and 2016 (INPE, 2017). These land cover changes have impacted the climate (NOBRE et al., 1991; LAWRENCE; VANDECAR, 2015), caused habitat fragmentation (SKOLE; TUCKER, 1993; VEDOVATO at el., 2016, RENÓ et al., 2016), affected the hydrology (COSTA; FOLEY, 1997; COSTA et al., 2003; COE et al., 2009, 2011; PANDAY et al., 2015; LAMPARTER et al., 2016) and impacted water quality (ROULET et al., 2000; FARELLA et al., 2001; BIGGS et al., 2004; OESTREICHER et al., 2017).

Regarding water quality, replacing the forest with pasture, agricultural and bare soil areas, for instance, can intensify the sheet erosion process, which in turn provides larger amounts of sediment to the water bodies (EL-SWAIFY et al., 1982; LAL, 1990; LABRIÈRE et al., 2015).

Gold mining activities, in particular, have also affected the water quality, mainly by increasing sediment in the rivers, accelerating river siltation processes (FARELLA et al., 2001; TELMER et al., 2003; LOBO et al., 2015). The increase of sediment in surface waters also reduces the underwater light field, which can limit the primary production (MELACK, 1985; HILL et al., 1995; GUENTHER and BOZELLI, 2004; COSTA et al., 2017) and, consequently, disrupt the ecological balance, by affecting the food web as well as fish diversity (MOL; OUBOTER, 2004).

In the Brazilian Amazon, mining activities have been reported in several sub-basins, such as Madeira River Basin (Rondônia State), Trombetas, Xingu and Tapajós River Basins (Pará State) (PARROTTA; KNOWLES, 2001; ARAÚJO NETO, 2009; ALVAREZ-BERRÍOS; AIDE, 2015; BALZINO et al., 2015). In the Medium Tapajós basin, west of Pará state, artisanal gold mining started in the 1950 decade (BEZERRA et al., 1998), becoming the main economic activity since

then (RODRIGUES et al., 1994; SEDEME, 2012; CETEM, 2013; MAISONNAVE; PRADO, 2017).

The Tapajós River and its tributaries drain the leached Precambrian shield (GIBBS, 1967), resulting in naturally low sediment concentrations in their waters, defined as clear waters (JUNK, 1997; DEVOL; HEDGES, 2001). However, several studies have reported high sediment concentrations in Tapajós River and some of its tributaries, downstream of gold mining sites (ROULET et al., 2000; TELMER et al., 2003, 2006; COSTA et al., 2013; LOBO et al., 2015)

These studies have reported the dynamics of sediment concentrations in the Tapajós River and its tributaries, establishing a relationship between the expansion of gold mining activities and the increase of sediment concentrations (TELMER et al., 2006; COSTA et al., 2013, LOBO et al., 2015). Using remote sensing techniques, Lobo et al. (2015) estimated Total Suspended Solids (TSS) in Crepori River and related the increase of TSS to the expansion of gold mining in the basin.

These studies were based on *in situ* or/and remote sensing data which estimate TSS in the river, but do not distinguish between the proportion of sediment concentration derived from sheet erosion (diffuse source) and that produced by gold mining activities. Thus, the following question arises: from measured and estimated sediment concentration in Crepori River, what is the proportion of sediment generated by sheet erosion and what is the parcel generated by gold mining activity?

Hydrological and water quality models such as the Soil and Water Assessment Tool (SWAT) (ARNOLD et al., 1998) can help to answer this question, once they allow estimating the sediment concentration related to the replacement of the forest with pasture, bare soil and other land cover types. Moreover, the modelling approach permits the simulation of sediment concentration driven by different scenarios of land cover and management (NEITSCH et a., 2011), allowing to set the baseline of sediment concentration in pristine condition, as well as to predict the impact of land cover change on water quality (NEITSCH et al., 2011; ARNOLD et al., 2012a).

SWAT has been successfully applied on different Brazilian regions to simulate streamflow and sediment concentrations (MAEDA et al., 2009; LELIS; CALIJURI, 2010; UZEIKA et al., 2012; STRAUCH et al., 2013; LAMPARTER et al., 2016; BLAINSKI et al., 2017). However, few studies have modelled the impacts of land cover change on sediment concentrations in the Brazilian Amazonian region (BRESSIANI et al., 2015).

2 OBJECTIVES

The main objective of this study was to estimate the parcels of sediment concentration that are derived from diffuse source (sheet erosion), and that resulted from gold mining activity alone in an Amazonian Basin impacted by artisanal gold mining. By distinguishing these proportions, this study aims at better understanding the gold mining impact on sediment concentration in an Amazonian River against the impact of sheet erosion intensified by the land cover change.

Thus, in this study, SWAT was applied at the Crepori River Basin to:

i) Investigate the effects of land cover change on sediment concentrations in the Crepori River, from 2001 to 2012 and in a land cover scenario of the future decade around 2040;

ii) Investigate the baselines of sediment concentrations in a pristine condition and in a condition of complete soil exposure;

iii) Compare the results to the sediment concentration estimated by Lobo et al. (2015), to evaluate the effects of gold mining activities comparatively to the land cover change impacts on sediment concentration in the river.

3 THEORETICAL BACKGROUND

Sediment yield and transport to water bodies in humid tropical regions are naturally and mainly driven by water erosive processes on soil (EL-SWAIFY et al., 1982; LABRIÈRE et al., 2015). In the Medium Tapajós Basin, the Artisanal Gold Mining activity intensifies the sediment yield to the water resources (BEZERRA et al., 1998; TELMER et al., 2006; COSTA et al., 2013, LOBO et al., 2015). In this section, items 3.1 and 3.2 summarize the main sediment yield processes that occur in the Medium Tapajós Basin.

3.1 Soil erosion and its effects on the ecosystem

Pluvial soil erosion is highly related to the surface runoff process, which can be triggered by the high precipitation rates observed in tropical regions (EL-SWAIFY et al., 1982; LAL, 1990; LABRIÈRE et al., 2015). Surface runoff is one of the several hydrological processes that compose the water cycle, as schematized in Figure 3.1.

Figure 3.1. The water cycle.

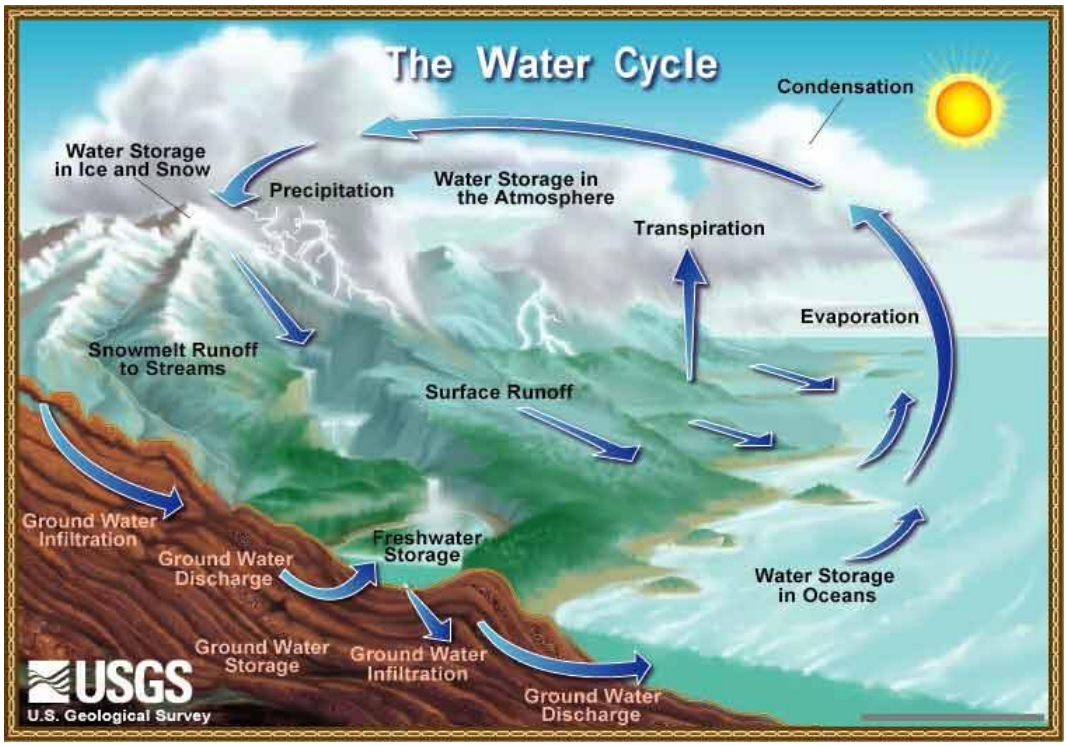

Source: United States Geological Survey (USGS)

The surface runoff results from the parcel of precipitation on the watershed which is not intercepted neither infiltrated into soil. This water is driven by gravity towards lower areas of the terrain, through tiny lines shaped according to the local micro-topography. These tiny lines, along with erosive processes and with the physical characteristics of the terrain, shape an unstable micro-drainage network, which in turn converges to the stable watershed's drainage network. Finally, the water in the watershed's drainage network flows out from the basin, towards lower regions, eventually reaching the ocean (TUCCI, 2009). The surface runoff is an important trigger of the pluvial soil erosion processes, capable of yielding sediments that may reach the water resources in a watershed. This process is closely related to the land cover characteristics, relief, soil properties and the rainfall intensity (SELBY, 1970).

Soil erosion is a naturally occurring process that performs a relatively slow removal of soil under stable natural conditions, within an assumed 'geologic norm' (TOY, 1977). According to Beasley (1972), raindrops hitting the soil is the first step in the water erosion process as these raindrops break down soil aggregates, whereas runoff detaches and transport soil particles. The particle movement resulting from raindrop splash and surface runoff is called sheet erosion.

Sheet erosion removes lighter soil particles, slowly removing thin layers of soil. Bertoni and Lombardi Neto (1990) consider this type of erosion as one of the most dangerous, since it slowly degrades the soil in large areas without being noticed and, therefore, usually no management practices are applied in time to prevent it.

Once the sediments are detached from the soil, they can be transported by the surface runoff to the water bodies of the watershed. In the channel, the streamflow can also cause channel erosion, increasing the sediment concentration in the water (ARNOLD et al., 2012a).

Apart from the impacts of sheet erosion on soil quality such as nutrient losses and deterioration of soil structure (BEASLEY, 1972, BERTONI; LOMBARDI NETO, 1990), this process also affects water resources. The increase of sediments in rivers, for instance, directly impacts physical and biotic aspects of the

environment. FAO (1965) and Beasley (1972) list the impacts of sediment discharge: on channel sedimentation, which reduces channel capacity and contributes to flooding, reduces water supplies, increases costs of maintaining navigable channels and harbours and decreases the potential for hydro-power; on filling of reservoirs, which reduces their water storage capacity and shortens their useful life.

On the biotic aspect, the increase of sediment concentration in water bodies reduces the underwater light field, which, in turn, limits phytoplankton primary production (MELACK, 1985; HILL et al., 1995; GUENTHER; BOZELLI, 2004), disrupting the ecological balance, as well as aquatic biodiversity, by affecting the food web (MOL; OUBOTER, 2004).

Selby (1970) defined a conceptual model that relates factors that cause soil erosion. These factors include climate characteristics, land surface characteristics and human modifications of the natural environment. According to Toy (1977), the human factor is included in this model due to human's capacity to alter the remaining factors, increasing or mitigating soil erosion. The climate represents the forcing variable of the erosion process, with intense precipitation events usually associated to higher erosion rates. Likewise, regarding land topography represented by slopes, high slopes are usually associated to an increase in erosion severity.

Several studies have shown human impacts on soil erosion and sediment concentration on water bodies. Greenwood et al. (2015) report 6.8 to 15.2 mm, in average, of soil removal in a 0.2 x 0.2m pasture plot in 65 days exposure to natural meteorological conditions, including rainfall events. Thus, the authors state that pasture areas are a significant sediment sources, affecting water quality of receiving streams. Moreover, agricultural areas in Maryland have removed approximately 0.15m of soil layer due to erosion and increased the sedimentation rates in reservoirs (COSTA, 1975).

In the Tapajós Basin, deforestation and agricultural areas have accelerated soil erosion (ROULET et al., 2000; FARELLA et al., 2006; OESTREICH et al., 2017) and the gold mining activity have also increased or promoted sediment yield to

the water resources. Lobo et al. (2015) estimated TSS in Crepori River, analysing a 40-year time series of remote sensing data. The authors found a clear relationship between their estimates and the increase of sediment concentration generated by gold mining activities in the basin.

Besides affecting water quality and its suitability for human consumption or use in several enterprises, sediment also transports and stores other pollutants (JULIEN, 1998). Weston et al. (2004) relate sedimentation and toxicity in water bodies to agricultural activities. The authors performed toxicity tests with midges and amphipods and found out that pesticides, used in agriculture, associated to sediments, led to extreme toxicity in some of the studied water bodies.

Highly toxic pollutants derived from anthropic activities can associate to sediments, increasing the severity of pollution in water bodies. Methylmercury, for instance, is associated with sediments in water bodies next to artisanal gold mining sites and deforested areas (OESTREICHER et al., 2017). Passos et al. (2007) and Rodrigues et al. (2017) found mercury levels in fishes of Tapajós region affected by gold mining explotation. Further, Egler et al. (2006) show that plants are also affected by methylmercury in these regions, and Faial et al. (2015) found levels of mercury in hair of riverside inhabitants of the Tapajós region.

3.2 Artisanal gold mining and soil erosion in the Medium Tapajós Basin

In the Medium Tapajós Basin, the artisanal gold mining is the main economic activity (SOUZA; VEIGA, 2009; CETEM, 2013; ALVAREZ-BERRÍOS; AIDE, 2015; MAISONNAVE; PRADO, 2017). During the 1980s, the gold mining expanded to large drainages such as the Crepori River, leading to the establishment of the 'Gold Mining Reserve' (Figure 4.1) by the Federal Government, in 1983 and the legalization of several gold mining sites (BEZERRA et al., 1998). Since then, due to the installation of rudimentary roads and airstrips, gold mining activity expanded across the basin (RODRIGUES et al., 1994).

According to ICMBio (2009), in alluvium deposits of gold mining sites, the usual technique applied is the hydraulic mining. In this technique, the process called ‘dismantle’ (referring to the dismantle of the soil in ravines located near the rivers,

where the gold is found), uses high pressure water jets for removing the soil clayey layer and leaching the gravelly horizon, where the gold is usually found (ICMBIO, 2009; WATZEN; MOL, 2013). This process generates a fluid slurry, which bares the gold along with soil particles detached in the dismantle process. This fluid is sucked into the sluice box, an equipment that uses gravity to separate the soil particles of gravel, small rocks and fine particles from the fractions containing the gold. Mercury is added in the sluice box to cling to the gold, forming the amalgam, which is heavier than the soil particles and therefore, is easier to be separated (SCHMINK; WOOD, 2010).

The resulting effluent flows to the river, carrying the soil particles and fractions of mercury (ICMBIO, 2009; WATZEN; MOL, 2013). Finally, the gold is recovered by burning out the mercury of the amalgam material, which releases volatile mercury to the atmosphere. This volatile mercury later condenses and falls on the area, contaminating both, terrestrial and water ecosystems (WATZEN; MOL; 2013). According to Schmink and Wood (2010), few precautions are taken to avoid skin contact of inhaling the toxic mercury gas resulting from this process. Retorts (condenser equipments), filters and other mercury capture devices can retain up to 95% of the evaporated mercury and significantly reduce the exposure to the toxic gas (BALZINO et al., 2015; UNEP, 2015). Nevertheless, several artisanal gold mining sites usually do not present efficient retorting processes (VEIGA et al., 2014) and handmade or overused retorts can release fractions of mercury even when the retorting system is used (BALZINO et al., 2015).

Other technique used in Amazonian gold mining sites is performed in the riverbed. In this technique, the bed material is sucked from the riverbed through floating small-scale dredges, large industrial dredges or large suction pumps into rafts (TELMER et al., 2006; CAHETÉ, 2008; ICMBIO, 2009). From the rafts, the material is conducted to the sluice box, following the same process previously described in the hydraulic technique (CAHETÉ, 2008). According to Telmer et al. (2006), the industrial large-scale dredging is the most destructive method applied for gold mining, since it combines both, the hydraulic mining using dismantle processes and the riverbed dredging. According to Bezerra et al. (1998), these techniques used in gold mining sites at Crepori basin increase soil erosion,

resulting in the increase of sediment concentrations in the river water. Finally, heavy machinery and explosives are also used to retrieve gold from deeper rocks (TELMER et al., 2006; CAHETÉ, 2008; ICMBIO, 2009)

Although the rivers in this region are classified as clear water rivers (JUNK, 1997; DEVOL; HEDGES, 2001), with sediment concentration at Tapajós River and its tributaries around 1.6 mg/L upstream of gold mining sites, values up to 500 mg/L were reported downstream of mining areas (TELMER et al., 2006; COSTA et al., 2013, LOBO et al., 2015).

Lobo et al. (2015) analysed 40 years of orbital remote sensing data records (images from Landsat satellite sensors) over Amazonian waters impacted by gold mining activities. By retrieving TSS estimates from those images, the authors reconstituted the dynamics and the evolution of TSS in those waters through time, allowing the establishment of a clear relationship between sediment concentration and the gold mining expansion in this region. TSS estimated using 1973 images were used as a baseline of TSS that would be naturally present in Crepori waters, considering that the few gold mining sites active back in that period would not represent significant sediment sources. Thus, the TSS was found to range from 5.38 mg/L, in the beginning of the time series, to 333.60 mg/L, in years with intense gold mining activities. However, this study did not distinguish the parcels of estimated TSS that were related to deforestation and natural erosive processes and the parcels of TSS related to the gold mining activity alone. The authors highlight the importance of adopting mining techniques that minimize TSS in the water, if gold mining continue to be explored in the Amazon.

It is also important to remember that aside from the impact on water quality (LOBO et al., 2015; OESTREICHER et al., 2017), the gold mining activity also contributes to the increase of deforestation rates in protected areas (ALVAREZ-BERRÍOS; AIDE, 2015), to changes in river morphology (WITTMANN; JUNK, 2016) and causes the contamination of fauna and flora with methylmercury (EGLER et al., 2006; PASSOS et al., 2007; RODRIGUES et al., 2017). Moreover, although it is an important economic activity in the Tapajós region and even though there are technologies and systems capable of minimizing its impacts, the gold mining cycle still results in negative impacts on the

communities involved, including diseases caused by the exposure to methylmercury (CASTILHOS et al., 2015; FAIAL et al., 2015; SOUZA et al., 2017), besides occupational hazards and poverty that follows the gold mining cycle (FERNANDES et al., 2014; WHO, 2016).

To promote both erosion and sediment yield control, as well as land use planning, soil management and sustainable use of land and water resources, it is important to know and understand the impacts of land cover changes on water availability and quality. In this context, hydrological models represent important tools to predict land cover impacts on water bodies, allowing the analysis of different and hypothetical scenarios, which can assist decision makers to follow procedures that promote sustainable development.

3.3 Hydrological Modelling

Physical description to explain completely and precisely a natural hydrological system is hampered by the high complexity of the processes that occur in these systems. This limitation compromises quantitative and qualitative analysis of the natural system (CHOW, 1978; TUCCI, 2005).

Thus, these systems can be studied with hydrological models, which can be understood as simplified representations of real hydrological systems (MORADKHANI; SOROOSHIAN, 2009). According to Abbott and Refsgaard (1996), mathematical hydrological models can be classified as follows:

Regarding the relationship between the parameters, representing the hydrological cycle in the modelling procedure:

a) Empirical: known as "black box", are models that are not based on physical analysis of processes associated to the watershed. Instead, they are based on time series analysis of observed data of the system's water input and output.

b) Conceptual: known as semi-empirical or "grey box", are based on empirical simplifications to represent the physical processes that occur in the watershed. In these models, physically-based structures and equations are associated to semi-empirical structures. The physical meaning,

however, is not as clear to allow parameters to be estimated by direct measurements. In this case, parameters are estimated via calibration.

c) Physically based: known as "white box", these models describe the natural system using mathematical representations of mass flux, movement, and energy. Thus, these models have a level of representation that may directly describe physical processes.

Regarding the types of parameters used in the modelling procedure:

a) Deterministic: these are models in which equal input sets always lead to the same output signal when executed in the same conditions. These do not include components with random behaviours.

b) Stochastic: these models have at least one component with random character not implicit in the inputs. Thus, the same inputs result in different outputs, even though the model is run under the same conditions.

Regarding spatial representation and or relationship between parameters:

a) Lumped: in these models, the watershed is treated as a single unit. Therefore, the variables and parameters do not present spatial relations, i.e., the real system is reduced to a single object.

b) Distributed: as opposed to lumped models, distributed models consider the spatial dependency of variables and parameters, often leading to a more realistic representation of the studied system. However, according to Tucci (2005), strictly speaking, there are no completely distributed models, once the modelling is always performed in a lumped way over the watershed, as the parameters are lumped in the limit of the spatial subdivision used in the study.

Regarding temporal dependency:

a) Static: these are models in which parameters do not vary in time.

b) Dynamic: these are models in which parameters vary in time, as the results of an iteration are inputs to the next.

Thus, hydrological models can combine different characteristics, allowing the modelling to be applied in several studies. This variety of applications has allowed studies on prediction of impacts of climate variations, land cover, land use and management on water quantity and quality (MORIASI et al., 2012).

In this context, the model Soil and Water Assessment Tool (SWAT) stands out as one of the hydrological and water quality models most used in the world (GASSMAN et al., 2014).

3.4 Soil and Water Assessment Tool (SWAT)

Developed by the Agricultural Research Service (ARS) of the United States Department of Agriculture (USDA), the Soil and Water Assessment Tool (SWAT) is a hydrological model physically based, dynamic, with a daily time step, semi-distributed, based on watershed-scale processes (ARNOLD et al., 2012a). According to Neitsch et al. (2011), the model was developed to agricultural areas, large and complex watersheds, with spatial variability of soil types, land cover and management, and allows the analysis of long time series.

The successful diffusion of SWAT is also due to detailed documents about the model, including theoretical manuals and tutorials (NEITSCH et al., 2011; ARNOLD et al., 2012b) available online (http://swatmodel.tamu.edu), as well as other publications, plug-ins for Geographic Information Systems (GIS) and the support offered by the developer team.

SWAT has been continuously developed for roughly 30 years (GASSMAN et al., 2007), and in this period, the model has been applied worldwide, demonstrating its suitability for modelling hydrology and water quality in a wide range of different environments. Several studies have demonstrated SWAT capability for delivering precise results, when modelling tropical (including Brazilian) basins for streamflow (STRAUCH et al., 2013; FUKUNAGA et al., 2015; LAMPARTER et al., 2016) and sediment (PINTO et al., 2013; CREECH et al., 2015; LUZ et al., 2016; MONTEIRO et al., 2016).

For modelling, SWAT divides the watershed into sub-basins, based on the topography. Sub-basins, in turn, are subdivided into Hydrologic Response Units

(HRU), which are regions in the sub-basins that have homogeneous land cover, soil type, and slope. According to Neitsch et al. (2011), analysis using HRU lead to more accurate results of streamflow in the main channel, once total streamflow is calculated from simulated streamflow from each HRU, considering its specific characteristics.

SWAT simulations are based on the water balance given by Equation 3.1.

$$SW_t = SW_0 + \sum_{i=1}^{t} \left(R_{day\,i} - Q_{surf\,i} - E_{a\,i} - w_{seep\,i} - Q_{gw\,i}\right) \qquad (3.1)$$

Where SW_t is the final soil water content (mm H_2O); SW_0 is the initial soil water content on day (mm H_2O); t is the time (days); R_{dayi} is the precipitation on day i (mm H_2O); Q_{surfi} is the surface runoff on day i (mm H_2O); E_{ai} is the evapotranspiration on day i (mm H_2O); w_{seepi} is the amount of water from the soil profile inflowing to the vadose zone on day i (mm H_2O); and Q_{gwi} is the base flow on day i (mm H_2O).

According to Arnold et al. (1998), the model's components to represent the sub-basins are categorized as follows:

a) Hydrology: based on the water balance (Equation 3.1), this component includes the simulation of surface runoff volume. This component considers the Curve Number procedure from the Soil Conservation Service (SCS) (USDA-SCS, 1972), which describes surface runoff as a function of the precipitation, the losses from infiltration, interception, and retention in the terrain (PEREIRA, 2008). the hydrology component also includes percolation, lateral-flow, ground-flow, transmission losses, ponds, and evapotranspiration. SWAT allows evapotranspiration to be estimated using three different methods: i) the method proposed by Hargreaves et al. (1985), that models evapotranspiration as a function of the maximum solar radiation and the air temperature; ii) the method proposed by Priestley and Taylor (1972), which considers net solar radiation and the air temperature; iii) Penman-Monteith (MONTEITH, 1965; ALLEN, 1986; ALLEN et al., 1989), which is based on solar

radiation, air temperature, wind speed and relative air humidity (ARNOLD et al., 1998).

b) Climate: this component includes precipitation, air temperature, solar radiation, wind speed and relative air humidity.

c) Sediments: this component estimates the sediment yield based on the Modified Universal Soil Loss Equation (MUSLE) (Equation 3.2) (WILLIAMS; BERNDT, 1977), which considers the soils characteristics, land cover, topography and the surface runoff (ARNOLD et al., 1998). SWAT is able to simulate the sediment concentrations at HRU level, using the runoff energy to detach and transport sediments to the river channel (NEITSCH et al., 2011). The MUSLE equation is given in Equation 3.2:

$$\mathrm{sed} = 11.8 \times \left(\mathrm{Q_{surf}} \times \mathrm{q_{peak}} \times \mathrm{area_{HRU}}\right)^{0.56} \times \mathrm{K_{USLE}} \times \mathrm{C_{USLE}} \times \mathrm{P_{USLE}} \times \mathrm{LS_{USLE}} \times \mathrm{CFRG} \quad (3.2)$$

Where *sed* is the sediment yield on a given day (tons); Q_{surf} is the surface runoff volume (mm H_2O/ha); q_{peak} is the peak runoff rate (m^3/s); $area_{hru}$ is the area of the HRU (ha); K_{USLE} is the Universal Soil Loss Equation (USLE) soil erodibility factor (0.013 metric ton m^2 h/(m^3-metric ton cm)); C_{USLE} is the USLE cover and management factor (-); P_{USLE} is the USLE support practice factor (-); LS_{USLE} is the USLE topographic factor (-) and *CFRG* is the coarse fragment factor (-).

The initial sediment concentration in the channel is then computed considering both, the sediment yield (Equation 3.2) and the volume of water in the channel (NEITSCH et al., 2011). Then, channel erosion and sediment deposition processes occuring in the stream (ARNOLD et al., 2012a) are computed to result in the actual sediment concentration in the channel.

The sediment deposition and the channel degradation are indirectly computed, by calculating the maximum amount of sediment that can be transported from a reach segment, using the Simplified Bagnold Equation (BAGNOLD, 1977), given in Equation 3.3, as follows:

$$CONC_{sed,ch,mx} = SPCON \times \left(V_{ch,pk}\right)^{SPEXP} \quad (3.3)$$

Where $CONC_{sed,ch,mx}$ is the maximum concentration of sediment that can be transported through the channel (ton/m³ or kg/L); *SPCON* is a calibration coefficient, $V_{ch,pk}$ is the peak channel velocity (m/s) calculated by SWAT, and *SPEXP* is a calibration coefficient. *SPCON* varies between 0.0001 and 0.01 and *SPEXP* varies between 1 and 1.5 (ARNOLD et al., 2012a), with the lowest values for both parameters, *SPCON* and *SPEXP*, representing high deposition rates in the channel, consequently resulting in less suspended sediment in the water.

Then, the sediment concentration in the stream in the beginning of the time step ($CONC_{sed,ch,i}$) is compared to the concentration calculated with Equation 3.3. If the initial sediment concentration is higher than the maximum concentration of sediment calculated by Equation 3.3, than deposition is the main process occurring in the stream and the net amount of sediment deposited in the channel is calculated by Equation 3.4. On the other hand, if the initial sediment concentration in the reach is lower than the maximum concentration of sediment calculated by Equation 3.3, than the channel erosion is assumed the dominant process occurring in the stream and the amount of sediment released in the stream by channel erosion is calculated by Equation 3.5.

$$SED_{dep} = \left(CONC_{sed,ch,i} - CONC_{sed,ch,mx}\right) \times V_{ch} \quad (3.4)$$

$$SED_{deg} = \left(CONC_{sed,ch,mx} - CONC_{sed,ch,i}\right) \times V_{ch} \times K_{ch} \times C_{ch} \quad (3.5)$$

Where SED_{dep} is the amount of sediment deposited in the reach (metric tons), SED_{deg} is the amount of sediment re-entrained in the reach due to channel erosion (metric tons), $CONC_{sed,ch,i}$ is the initial sediment concentration in the reach (kg/L or ton/m³), $CONC_{sed,ch,mx}$ is the maximum concentration of sediment that can be transported through the channel (kg/L or ton/m³), V_{ch} is the volume of water in the reach (m³); and K_{ch} and C_{ch} are the channel erodibility factor (-) and the channel cover factor (-), respectively, both defined on Julian and Torres (2006) or adjusted during calibration. According to Arnold et al. (2012a), both K_{ch} and C_{ch} range from 0 to 1, with 0 representing a non-erosive channel (for K_{ch}) and a channel completely protected from erosion by cover (for C_{ch}), and with 1 representing no resistance to erosion (for K_{ch} parameter) and no vegetative cover on channel (for C_{ch}). Therefore, lowest values for both K_{ch} and C_{ch} represent a low erodible

channel, whereas highest values for both parameters represent high erodible channel.

d) Soil Temperature: this variable is simulated using a function of humidity and depth, surface temperature and annual average air temperature.

e) Crop growth: crop growth is simulated by simplifications of the Erosion-Productivity Impact Calculator (EPIC) (WILLIAMS et al., 1984), which estimates the impacts of erosion on soil productivity, simulating crop growth and related processes (USDA, 1990).

f) Potential growth: based on Beer's law to estimate the solar radiation's interception, and based on Monteith approach (MONTEITH, 1977), to estimate the potential daily biomass increase. Crop growth is analysed regarding the amount of intercepted light during the period of plant growth and the efficiency with which the intercepted light is used. This approach considers the crop's leaf area index distribution, the temperature, and the water supply in the soil (MONTEITH, 1977).

g) Nutrients: Nitrogen is estimated based on the product between mean concentration, the surface runoff, lateral-flow, and percolation. Once phosphorus is associated with sediments, it is estimated as a function of unstable phosphorus concentration in the upper soil layer and the surface runoff.

h) Agricultural management: is based on sub-models that simulate crop systems, water irrigation and the use of fertilizers, pesticides, and grazing.

i) Channel and reservoir transport: this component considers the water balance, sediment, nutrients and pesticides transport.

The sub-models and routines that constitute SWAT operate using coefficients and parameters related to the input data that characterize the watershed regarding topography, drainage network, soil types, land cover and the precipitation, which is the forcing variable in the modelling. Observed streamflow, sediment, and nutrient concentration data are used for the model's calibration and validation.

3.4.1 Sensitivity Analysis, Calibration, and Validation

Physically based and distributed models, at first, requires the parameters used in the modelling to be defined solely based on field data, which makes the calibration step unnecessary. However, usually, these models are applied in scales in which it is impossible to directly define the parameters. Thus, the calibration step becomes an important and necessary phase in the modelling, to define and better adjust the parameters (REFSGAARD; STORM, 1996).

It is recommended a minimum of three years of daily precipitation data for the 'warm-up' period in the beginning of the model run (NEITSCH et al., 2011; ABBASPOUR, 2015). This period is used by SWAT to set the appropriate initial conditions, especially for soil moisture. It is also recommended 5 years of daily precipitation data and daily or monthly streamflow data for the calibration period, to adjust model parameters so as simulated variables match observed values. Finally, other 5 years of daily precipitation data and daily or monthly streamflow data are required for validation.

According to Arnold et al. (2012b), the first step for SWAT's calibration and validation is to determine the parameters that are the most influent in the modelling results. The authors explain that the sensitivity analysis determines the rate of variation of the model's output, given the variation of the input parameter values. Thus, this analysis is used to identify key parameters to be used in the calibration procedure.

To assist in the sensitivity analysis, calibration and validation of SWAT, the SWAT-CUP tool (SWAT - Calibration and Uncertainty Programs) was developed, using a semi-automatic approach (ABBASPOUR, 2015). This tool performs the sensitivity analysis using "one-at-a-time" method, in which the parameter values change one by one, and the "global" method, in which all the parameters values change simultaneously.

Each approach for sensitivity analysis leads to different results. Arnold et al. (2012b) state that the main disadvantage of "one-at-a-time" method is the fact that when a parameter is analysed, the correct value of the remaining parameters will never be known. On the other hand, the disadvantage of the "global" sensitivity

analysis is the need to perform a large number of simulations. Authors such as Oliveira (2014), consider global sensitivity analysis the most detailed procedure to know the relation between the parameters.

Once the sensitivity analysis is concluded, the model should be calibrated using the most sensitive parameters. Arnold et al. (2012b) define the calibration as a procedure to improve the model parameterization, regarding parameters that were not defined based on field analysis. According to the authors, the calibration is characterized by the careful selection of values (within realistic ranges) for the input parameters, based on a comparison between the model's output and observed data, reducing the uncertainties of the simulations.

There are basically three calibration methods: the manual method (trial and error), in which the parameter values are defined based on the analyst knowledge about the hydrological processes and about the watershed; the automatic calibration, which uses optimization algorithms to define the set of ideal parameter values that satisfies an accuracy criteria; calibration combining both methods, in which the initial values of parameters are chosen with manual calibration and then, the automatic calibration is performed (or vice-versa), this method usually leads to a more refined result (RESFGAARD; STORM, 1996)

SWAT-CUP includes the Parameter Solution (ParaSol) optimization algorithm for calibration and uncertainty analysis. ParaSol is a global, efficient and well-adapted method for calibration and uncertainty analysis of environmental and water quality models (VAN GRIENSVEN; MEIXNER, 2004, 2007).

According to Van Griensven and Meixner (2007), ParaSol calculates objective functions (OF) based on the model outputs and on observed data. Then, by running several iterations, the algorithm optimizes these OF aggregated into a global optimization criterion (GOC), by varying the parameter values within a pre-defined range given by the analyst. Thus, calibration is concluded when the set of parameters values that lead to the global optimal values of GOC is found.

3.4.2 Land Use Update Tool (LUP)

An important issue during the calibration procedure is the land cover change. As land cover changes can affect significantly the hydrological response of the basin, the observed streamflow data used in the calibration step can vary throughout the calibration period, influenced by the land cover changes (WHITE; CHAUBEY, 2005). Thus, when a single land cover is used to set up the model and for the calibration procedure, additional uncertainties can be introduced to the modelling (PAI; SARASWAT, 2011).

To overcome this issue, SWAT offers the Land Use Update Tool (LUP), which updates the land cover information during the period of simulation. Once the land cover defines the HRUs, to activate the LUP, it is required to set the updated HRU area fractions in each sub-basin as well as the date, in the simulation period, when the land cover information has to be updated. Once the land cover is updated, it remains in effect for the remainder of the simulation, until the next land cover update takes place (ARNOLD et al., 2012a). Thus, when calibrating the model that was set up using LUP, the land cover changes are taken into account in the calibration procedure, avoiding the selection of biased parameter values.

Once calibration is concluded, the model's validation is performed based on the simulated outputs of the calibrated model. Validation is the comparison of simulated results to observed data and therefore, it is a procedure that demonstrates if the model is able to make sufficiently accurate simulations of the variables (streamflow, sediments etc) (ARNOLD et al., 2012b). Thus, as long as the model's validation indicates good results, the model can be applied to understand and predict impacts of land cover and climate changes o hydrology and water quality (BONUMÁ, 2011).

3.4.3 Applications of SWAT

SWAT has been applied in several different studies, but most of them aim at streamflow and sediment modelling, analysing impacts of land cover change. This section brings some examples of SWAT application in different researches.

Applying SWAT to an urban basin in New Jersey, USA, Qiu and Wang (2014) showed that Total Suspended Sediments and Total Phosphorus were water-quality issues in the region and through the modelling simulations, the authors suggested implementing management measures to reduce both sediment and phosphorus loads in 9% and 49%, respectively.

Impacts of land cover changes in four different periods (1973, 1986, 1992 and 1997), in the Alto San Pedro basin, between USA and Mexico were evaluated using SWAT (NIE et al., 2011). It was found that urbanization led to the increase in surface runoff from 1973 to 1997, whereas the substitution of pasture areas to reforested areas for logging of Algaroba (*Prosopis juliflora*) led to a reduction of baseflow, impacting the water resources in the region.

Baker and Miller (2013) evaluated the impacts of land cover changes on streamflow in the Rift Valey, Kenya. Scenarios were simulated to represent 17 years of land cover change, generating high agreement with annual values. Simulations showed that land cover changes resulted in the increase of surface runoff and in the reduction of growndwater recharge, leading to negative impacts on the water resources and on the local communities.

Other studies use SWAT to evaluate land cover change impacts in different time and spatial scales (LIN et al., 2015), using remote sensing data (SONG et al., 2011) as well as to assess climate change effects on hydrology and water quality (MUTTIAH; WURBS, 2002; CHIEN et al., 2013; SUN et al., 2013; DEB et al., 2015).

Zhang et al. (2012) applied SWAT in the Huifa River Basin, China, calibrating the model for a streamflow series from 1956 to 1964. The calibrated model was used to rebuild the natural streamflow for the period of 1965 to 2005, and simulated results indicated that anthropic activity reduced the streamflow in the basin. Climate change effects, according to the authors, varied responding to the increase and reduction of precipitation, temperature, and solar radiation.

In Brazil, the use of SWAT model has increased throughout the last decade. Bressiani et al. (2015) state that more than 100 studies published between 1999

and 2015 used the model to answer a wide range of questions regarding land cover change and climate change effects on water resources.

As international publications, studies using SWAT in Brazilian areas generally explore the hydrological characterization of watersheds and the effect of different scenarios of land cover and soil management on streamflow and water quality (STRAUCH et al., 2013; PERAZZOLI et al., 2013; PEREIRA et al., 2014; FUKUNAGA et al., 2015).

Bressiani et al. (2015) show that the majority of studies using SWAT in Brazil applies the model in the Southeast, South and Northeast regions of the country, and only a few studies are performed in the North region, specifically in the Amazonian region. The authors explain that the low density of the hydro-meteorological network in the Amazonian region is the great challenge to the use of distributed and physically-based models.

On the other hand, the development of Remote Sensing techniques and products represent a reliable alternative to overcome *in situ* data scarcity issues, supporting the application of physically-based and distributed hydrological models in remote regions.

3.5 Remote Sensing and Hydrological Modelling

Physically based and distributed hydrological models, such as SWAT, demand a large amount of spatially-distributed and high temporal resolution data to better represent the studied area (ABBOTT et al., 1986).

However, conventional data acquisition is usually based on field sampling surveys and on a limited number of gauges unable to provide spatially distributed data. In remote areas, data availability is frequently an issue due to the lack or due to the low density of monitoring systems. In this context, data derived by remote sensing techniques represent a good alternative for complex hydrological models (SCHULTZ, 1988).

According to De Troch et al. (1996), at least five advantages of data derived by remote sensing techniques in contrast to conventional methods can be listed: i) there is no disturbance of the object or of the process being measured; ii) data are

spatially distributed; iii) data can have high spatial and/or temporal resolution; iv) data is available in digital format; v) data availability in remote and inaccessible areas.

Furthermore, some remote sensing instruments, such as orbital sensors, can provide long-term data series, allowing time-series analysis on the dynamics and evolution of hydrological key components through time, improving the understanding of the hydrological cycle and even improving model performance (KITE; PIETRONIRO, 1996; NIJZINK et al, 2017).

In hydrological studies, remotely sensed data can be applied in different levels. From the detection of items of interest (plumes in water bodies, snow etc), to deriving input data and retrieving hydrological parameters directly (topographic and land cover data, geological information and precipitation rates, for instance) (SALOMONSON, 1983).

As a wider variety of sensors and products are launched, hydrological and hydraulic studies have been benefited by applying remotely sensed data in several manners, from hydro-meteorological monitoring to broad analysis supporting leading decision makers on environmental preservation and economic activities issues (SATGÉ, 2017). In this context, several studies have used remote sensing to characterize the land cover and vegetation parameters necessary in hydrological modelling (CHEN et al., 2005; PEÑA-ARANCIBIA et al., 2016; HUNINK et al., 2017); to characterize the topography (RAGETTLI et al., 2015; MUKOLWE et al., 2016); to retrieve inputs and/or for model calibration regarding soil moisture and evapotranspiration (OTTLÉ; VIDAL-MADJAR, 1994; STRAUCH; VOLK, 2013; WANDERS et al., 2014; SILVESTRO et al., 2015; FERRANT et al., 2016); to estimate daily river discharge (BIRKINSHAW et al., 2012; DOMENEGHETTI et al., 2014) and flood extent and levels (GRIMALDI et al., 2016); to estimate lake bathymetry (ESSAYAS et al., 2014) and to analyse lake extreme events of droughts (SATGÉ et al., 2017), amongst other purposes.

Remotely sensed data is also used to derive a wide range of meteorological products, which provide valuable inputs for hydrological modelling. To mention a few, Climate Forecast System Reanalysis (CFSR), the European Centre for

Medium-Range Weather Forecasts (ECMWF) ERA-Interim products and the Modern-Era Retrospective Analysis for Research and Applications (MERRA) products have been used as input data in hydrological modelling studies in several and environmentally different watersheds, leading to the improvement of model performance, when compared to the use of conventional data sources (FUKA et al., 2013; KROGH et al., 2015; AUERBACH et al., 2016; ESSOU et al., 2017).

Precipitation estimates driven by remote sensing data are essential for large-scale hydrological modelling, especially in remote and inaccessible regions that are usually unmonitored. Since the main water input in a hydrological model is the precipitation, this variable has a crucial role in estimating streamflow, erosive processes, sediment, and nutrient transport. Thus, an accurate representation of precipitation rates, frequency and spatial variability is indispensable for the model accuracy (HSU; SOROOSHIAN, 2009).

3.6 Precipitation in Distributed Hydrological Model

Precipitation data are usually obtained by rain gauges, which along with stream gauges configure the hydro-meteorological network. In Brazil, the National Water Agency (ANA) operates the National Hydro-meteorological Network and provides hydro-meteorological data in the HIDRO database, available in the Hydrological Information System Hidro-Web (http://hidroweb.ana.gov.br).

According to WMO n°168 (1994), the hydro-meteorological network must be implemented to allow the interpolation, or spatialization of meteorological data between the gauges, permitting the estimation of sufficiently precise data in any place in the area monitored by the network.

However, due to the high spatial variability of precipitation, data recorded by rain gauges are usually representative of a small radius around the rain gauge. This is particularly observed in regions with low density of rain gauge associated with the predominance of convective rainfall (COLLISCHONN et al., 2008). Thus, it is necessary that precipitation data acquisition is made in small spatial scale and frequently, so its spatial and temporal distribution are properly represented (HUFFMAN et al., 2007).

The Tropical Rainfall Measuring Mission (TRMM) represents an appropriate alternative to overcome the challenge of spatially distributed precipitation data represented by the low-density rain gauge network in many tropical regions.

3.6.1 The Tropical Rainfall Measuring Mission (TRMM)

The Tropical Rainfall Measuring Mission (TRMM) is a joint project from the National Aeronautics and Space Agency (NASA) and the Japanese Aerospace Exploration Agency (JAXA), that launched its first satellite in November/1997, and after 17 years in orbit, the mission ended in April/2015, being replaced by the Global Precipitation Measurement (GPM). Once it was the first to use passive and active microwave instruments, and to travel on low inclination (35°) circular orbit, TRMM was the main satellite in the world for studying precipitation and storms associated with the climate processes in the tropics (NASA, 2016a).

TRMM travelled in 90 minutes its circular non-heliosynchronous orbit, in 35° tropical inclination at 350 km of altitude, which allowed data sampling in the tropics with more frequency and spatial consistency than satellites with polar orbit (NASDA, 2016; NRC, 2016). In August/2001, to save fuel and increase the mission's duration, the flight altitude was boosted from 350 km to 403 km.

Curtarelli et al. (2014) investigated the effects of the flight altitude boost on precipitation estimates of 3B43 product in central Brazil region. According to them, despite the significant increase in the root mean square error (RMSE) in the estimates after the boost, the increase on the RMSE has not impaired the application of the product in their study.

Furthermore, Collischonn et al. (2008) compared the estimates of TRMM 3B42 product for the period between 1998 and 2006 to *in situ* rain gauge records from the Tapajós Basin, in the Brazilian Amazon. According to the authors, the comparison between these data did not show noticeable changes in the estimates of the 3B42 product, even though the algorithm and the satellite flight altitude have been changed throughout the analysed time series.

TRMM had several sensors on board, such as the Clouds and the Earth's Radiant Energy System (CERES), which aimed to register the earth and clouds radiance;

the Lightning Image Sensor (LIS), designated to register the global ray distribution; and the precipitation sensors: Precipitation Radar (PR), TRMM Microwave Imager (TMI) and the Visible and Infrared Scanner (VIRS) (NASDA, 2016).

According to Kummerow et al. (1998), measurements from the TMI and PR sensors are complementary. TMI sensor measures the emittance from rainfall clouds but does not determine precisely the relative altitude of these measurements. PR sensor, on the other hand, captures specific data on the cloud's altitude, by indirect measurements of the return time of the backscattered signal. Lastly, VIRS sensor provides temperature and structure data on the top of the clouds, complementing collected data from TMI and PR.

A short description of the TRMM precipitation sensors operation is given bellow, according to NASA (2016b,c,d,e):

- TRMM Microwave Imager (TMI): the precipitation estimates from the TMI sensor are based on Planck's law, according to which the spectral radiance of a black body varies with its temperature.

  In the microwave spectral band, large open water bodies present emissivity around 0.5 (CARSEY, 1992) and, therefore, emit about half the energy specified by Planck's law to a black body at the same temperature. Therefore, to passive microwave radiometers, large water bodies are identified as areas with low energy emission. Conversely, raindrops have higher emissivity, and therefore, emit an amount of microwave radiation near that described by Planck's law. Thus, when precipitation occurs over large water bodies, there is a contrast between the low energy emitted by the surface and high energy emitted by the raindrops.

  Over dry surfaces, on the other hand, where this contrast is not clear due to the higher emissivity of the land's surface and objects on it, indirect measurements of ice quantity in the clouds are used to infer about the rain. The high-frequency microwave radiation (85.5GHz) is highly backscattered by ice from the top of the majority rainfall clouds. This backscatter reduces the microwave signal detected by the sensor over dry

surfaces, leading to the contrast. Thus, areas with low detected energy correspond to regions covered with potentially rainy clouds (NASA, 2016b).

- Precipitation Radar (PR): PR is a key instrument in TRMM. According to Jensen (2009), on the contrary of passive microwave sensors, PR allows registering precise precipitation data over dry surfaces, providing information about the rainfall that effectively hits the surface.

  This instrument detects the precipitation type, intensity (up to 0.7 mm hr^{-1}), horizontal and vertical distributions (up to 20 km of altitude) and three-dimensional profiles of precipitation structure. Combined with optical sensors, PR data improve the accuracy of precipitation estimates (NRC, 2016 and NASA, 2016c).

- Visible Infrared Scanner (VIRS): this passive sensor is sensitive to five spectral regions distributed between the visible and infrared bands (from 0.63 to 12 μm), providing data that are used as indirect precipitation index. Radiance detected by this sensor in the infrared region is used to determine the temperature of the top of the clouds, which is associated with the cloud's altitude, as the colder the cloud, the higher it should be. Finally, the high altitude of clouds is related to the convective precipitation, usual in tropical regions.

  Some high clouds, however, are not associated with precipitation, as the Cirrus clouds family. To distinguish these clouds from the ones that effectively generate precipitation, data acquired by VIRS are compared in the 10.8 and 12.0 μm wavelengths of infrared band. Nevertheless, the use of data generated by infrared radiation leads to significant errors in immediate precipitation estimates and therefore, VIRS data are combined to data from PR and TMI (NASA, 2016d).

The main characteristics of TRMM instruments are listed in Table 3.1.

Table 3.1. Main characteristics of TRMM instruments.

	Flight altitude	Precipitation Radar (PR)	TRMM Microwave Imager (TMI)	Visible/Infrared Scanner (VIRS)
Frequency/ wavelength	-	Vertical polarization: 13.8 GHz	Dual polarization: 10.65, 19.35, 37 and 85.5 GHz Vertical Polarization: 21 GHz	0.63, 1.6, 3.75, 10.8 and 12 μm
Imaging mode scan	-	Cross-track	Conical	Cross-track
Spatial Resolution	350 km	4.3 km	4.4 km in 85.5 GHz	2.2 km
	403 km	5.0 km	5.1 km in 85.5 GHz	2.4 km
Swath	350 km	215 km	760 km	720 km
	403 km	247 km	878 km	833 km

Source: Adapted from NASA (2016f).

3.6.2 The TRMM/TMPA 3B42 (V.7) Product

Although it is feasible to estimate precipitation from one type of sensor alone, the estimates become more accurate and with better spatial and temporal resolution when data from different sensors are combined (HUFFMAN et al., 2007). To combine these data, several algorithms were developed, such as the TRMM Multi-satellite Precipitation Analysis 3B42 (TMPA 3B42).

According to Huffman et al. (2007), TMPA 3B42 product combines precipitation estimates from TRMM sensors in a product of monthly accumulated values (3B31), which presents low temporal resolution due to the TRMM revisit time. To overcome this issue, precipitation estimates from Geostationary Operational Environmental System (GOES) are adjusted based on 3B31 product, resulting in a product with a spatial resolution of 0.25° x 0.25° and temporal resolution of 3 hours, named 3B42 RT (Real Time). 3B42 RT estimates are corrected to monthly total precipitation values registered by gauges from the Global Precipitation Climatological Centre (GPCC), in a 1° x 1° grid, resulting in the 3B42 product. Although this correction is made in a 1° x 1° grid, the 3B42 product maintains the 0.25° x 0.25° spatial resolution.

According to Zulkafli et al. (2014), the version 7 of the 3B42 algorithm has significant lower bias and better spatial representation of the precipitation than the version 6. Moreover, the authors stress that the use of 3B42 V.7 product leads to

better performance in hydrological models when modelling streamflow, reducing the differences between simulated and observed data.

4 MATERIALS AND METHODS

This study was conducted using SWAT.v.2012 implemented in the open source Geographic Information System QuantumGIS (QGIS) (QGIS, 2016), via QSWAT.1.3 plug-in (DILE et al., 2016), SWATEditor_2012.10.19 (SWAT, 2016) and SWAT Calibration and Uncertainty Programs (SWAT-CUP) (ABBASPOUR, 2015).

4.1 Study Area

Crepori River Basin (Figure 4.1a) is located at Pará State/Brazil, and drains approximately 13,600 km² at the medium Tapajós basin, in the south centre of the Brazilian Amazon. The region has a tropical humid climate with a short dry season, with average temperatures between 22°C and 26°C, average annual precipitation between 2000 and 2250 mm, and Ami climate, according to Köppen classification (IBAMA, 2004; ICMBio, 2010). The rainy season occurs between October and May (INMET, 2017) and, dividing the water level regime into two periods, in average, the river's low-water level season occurs between June and December, whereas the high-water level season occurs between January and May (ANA, 2016a, b) (Figure 4.1b). Figure 4.1 presents the study area, the precipitation and water level regimes related to the pink gauge (Figure 4.1a).

Figure 4.1. Study area. (a) Crepori Basin location. (b) Precipitation and water-level regimes in Crepori Basin.

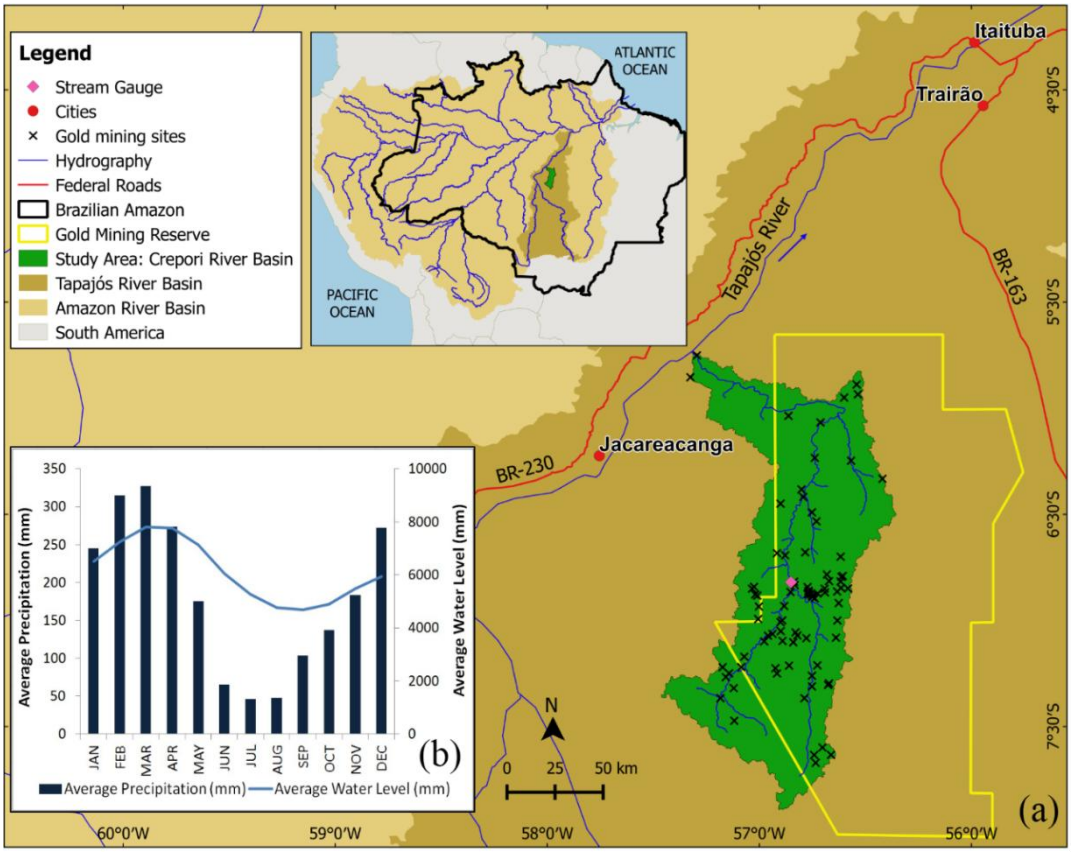

4.2 Summary of Methods

The following flowchart (Figure 4.2) summarizes the steps taken in this work, starting with the input data selection, pre-processing and defining the parameters (model set up); the first model run; sensitivity analysis, calibration and validation; simulation of scenarios and analysis of the results.

Figure 4.2. Flowchart showing the main steps of the study.

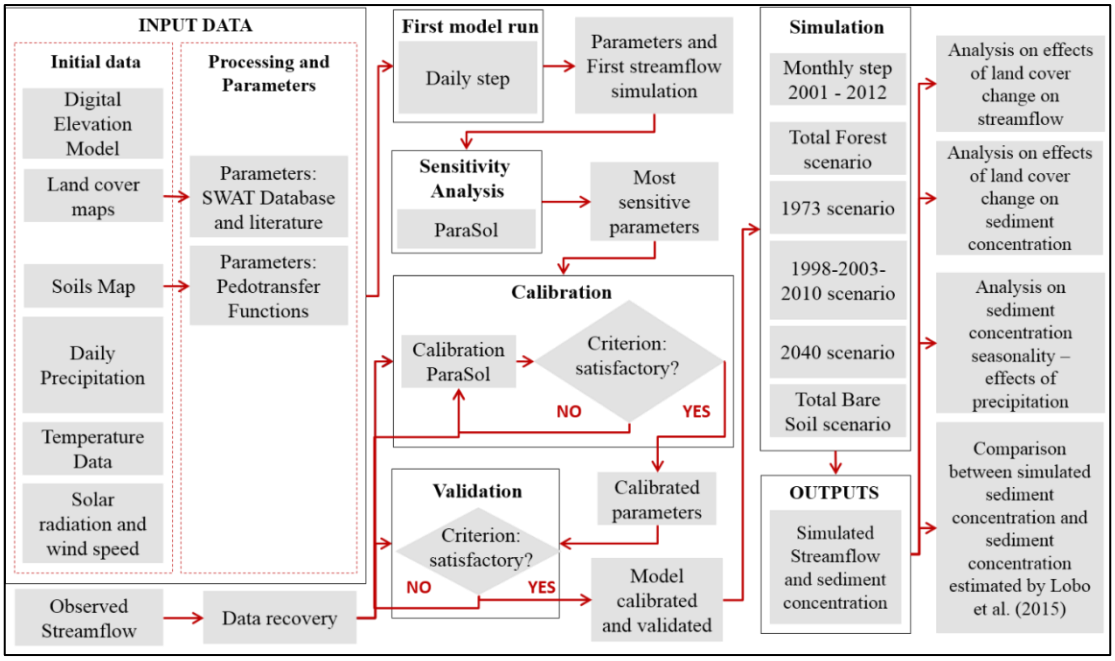

Source: produced by the author.

4.3 SWAT Input Data

The model's main input data regards to soil type, land cover, topography and weather of the study area. Table 4.1 summarizes the main characteristics of these input data used in this work.

Table 4.1. SWAT main input data.

SWAT INPUT DATA	Spatial Resolution/Scale	Source
Digital Elevation Model	1 arc second (~30 m)	SRTM (USGS, 2016)
Land Cover Maps (years: 1973, 1998, 2003 and 2010)	30 m	Classification of Landsat5/TM Images (USGS, 2017) Lobo et al. (2015)
Soil Types Map	1:250,000	IBGE (2016)
Daily Precipitation (1998 - 2012 period)	0.25° (~30 km)	TRMM 3B42 Daily v.7 (NASA, 2016g)
Daily Temperature (1998 - 2012 period)	0.70° (~80 km)	ERA Interim Daily Product (ECMWF, 2017)
Daily solar radiation (1998 - 2012 period) Daily wind speed (1998 - 2012 period)	0.25° (~30 km)	NCEP/CFSR (GLOBAL WEATHER DATA, 2016)

4.3.1 Topographic data

A Digital Elevation Model (DEM) is used to define the watershed as well as its topographic characteristics, such as elevation, slopes, slope lengths and the drainage network.

In this study, the DEM provided by the Shuttle Radar Topography Mission (SRTM), with a spatial resolution of 1 arc-second (approximately 30 m) (http://earthexplorer.usgs.gov/) was used as the source of topographic information to run SWAT. The Terrain Analysis Using Digital Elevation Models (TauDEM) (http://hydrology.usu.edu/taudem/taudem2.0/taudem.html) tool included in QSWAT plugin was used to derive a hydrologically consistent DEM and perform relief analysis. Figure 4.3 shows the slopes (Figure 4.3a), elevation (Figure 4.3b), the Crepori watershed and the river network derived from the DEM.

Figure 4.3. Topography and river network of Crepori Basin. Slopes (a) and Elevation (b).

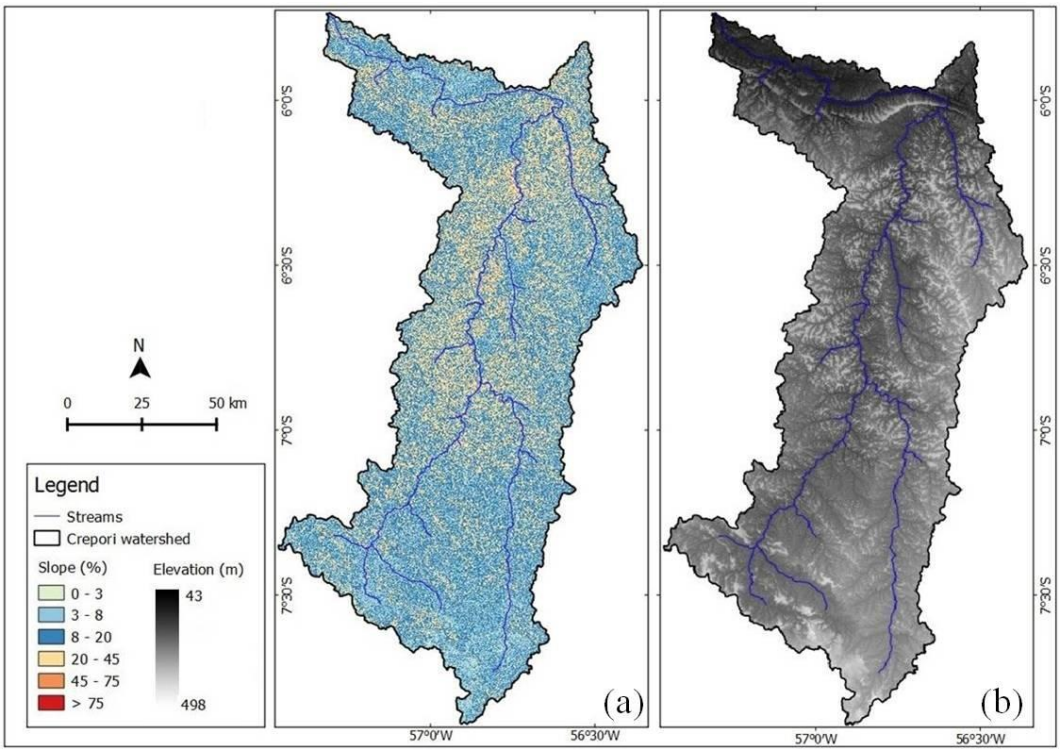

4.3.2 Land cover scenarios

In the period between 1998 and 2012, Crepori basin presented the highest accumulated deforestation rates (up to 1,34% of the basin was deforested) in the years of 1998, 2003 and 2010 (INPE, 2017). Thus, the years of 1998, 2003 and 2010 were defined as land cover scenarios to be updated during the period of simulations (1998 to 2012) using SWAT Land Use Update Tool.

All mapped-scenarios were built using artisanal gold mining areas detected by Lobo et al. (2016) and land cover classes of 'Forest', 'Non-forest' and 'Water', detected by Maximum Likelihood (SCHOWENGERDT, 1983; CÂMARA et al., 1992) classification of Landsat5/TM surface reflectance images (bands 3, 4 and NDVI) and manual editions. In order to model only the impact of land cover changes on water resources, artisanal gold mining sites were classified as 'Bare soil' ("barren" in SWATv.2012 database) for all scenarios used in this study.

Since there were no high spatial resolution images available for this region to perform validation of the classifications, the land cover maps of 1998, 2003 and 2010 were compared to the same Landsat5/TM images used in the classification procedure. All classifications led to overall accuracies higher than 88%, and significant Kappa index higher than 0.85, which was considered good for this study. The confusion matrix generated in the validation of the land cover maps are presented on Appendix A (Tables A.1, A.2 and A.3).

Since there were few gold mining sites in Crepori basin back in 1973, Lobo et al. (2015) used suspended sediment estimates in 1973 as the baseline in their study. Therefore, the present study included the 1973 scenario in the simulations and used Lobo et al. (2015) estimates of TSS for 1973 as a reference. This process is an attempt to overcome the lack of *in situ* data for calibration and validation of sediment simulations, giving a standard for assessing the model's performance in relation to sediment simulations.

To evaluate the impacts of deforestation on water resources at Crepori Basin in the future, a land cover scenario was built for 2040. To build this scenario, the deforestation rates observed for the period between 1998 and 2010 (for both land cover changes: from forest to pasture and from forest to bare soil areas) were

extrapolated for the next 30 years. Firstly, the land cover changes rates for the classes of ‘Forest’, ‘Non-forest’ and ‘Bare Soil’ were calculated for the period between 1998 to 2010 and then, were scaled for one year, as shown in Appendix A, Table A.4. The areas of 'Forest', 'Non-forest' and 'Bare Soil' were computed for the 2040 scenario by multiplying the annual land cover change rates (Appendix A, Tabel A.4) by the areas detected in the land cover map of 2010 and by the length of the period between 2040 and 2010 (30 years). Then, the features corresponding to 'Forest', 'Non-forest' and 'Bare Soil' in the 2010 land cover map were buffered until their areas corresponded to the computed area of these land cover classes for the scenario of 2040.

Finally, to set maximum and minimum baselines of sediment concentration for the simulations, two hypothetical scenarios were built; i) Crepori watershed covered with forest (Total Forest scenario); ii) Crepori watershed transformed to bare soil (Total Bare Soil scenario).

The area of each land cover type at Crepori basin for all scenarios are summarized in Table 4.2, and the maps are shown in Figures 4.4, 4.5 and 4.6.

Table 4.2. Percentages of land cover types at Crepori river basin for each scenario.

Scenario Land Cover	**Total Forest**	**1973**	**1998**	**2003**	**2010**	**2040**	**Total Bare Soil**
Forest	99.47	99.42	98.49	97.15	96.65	92.19	0
Non-forest	0	0.004	0.67	1.67	1.97	5.55	0
Bare Soil	0	0.05	0.44	0.65	0.91	1.78	99.47
Water surface	0.53	0.53	0.41	0.53	0.48	0.48	0.53

Figure 4.4. Land cover scenarios: Total Forest and 1973.

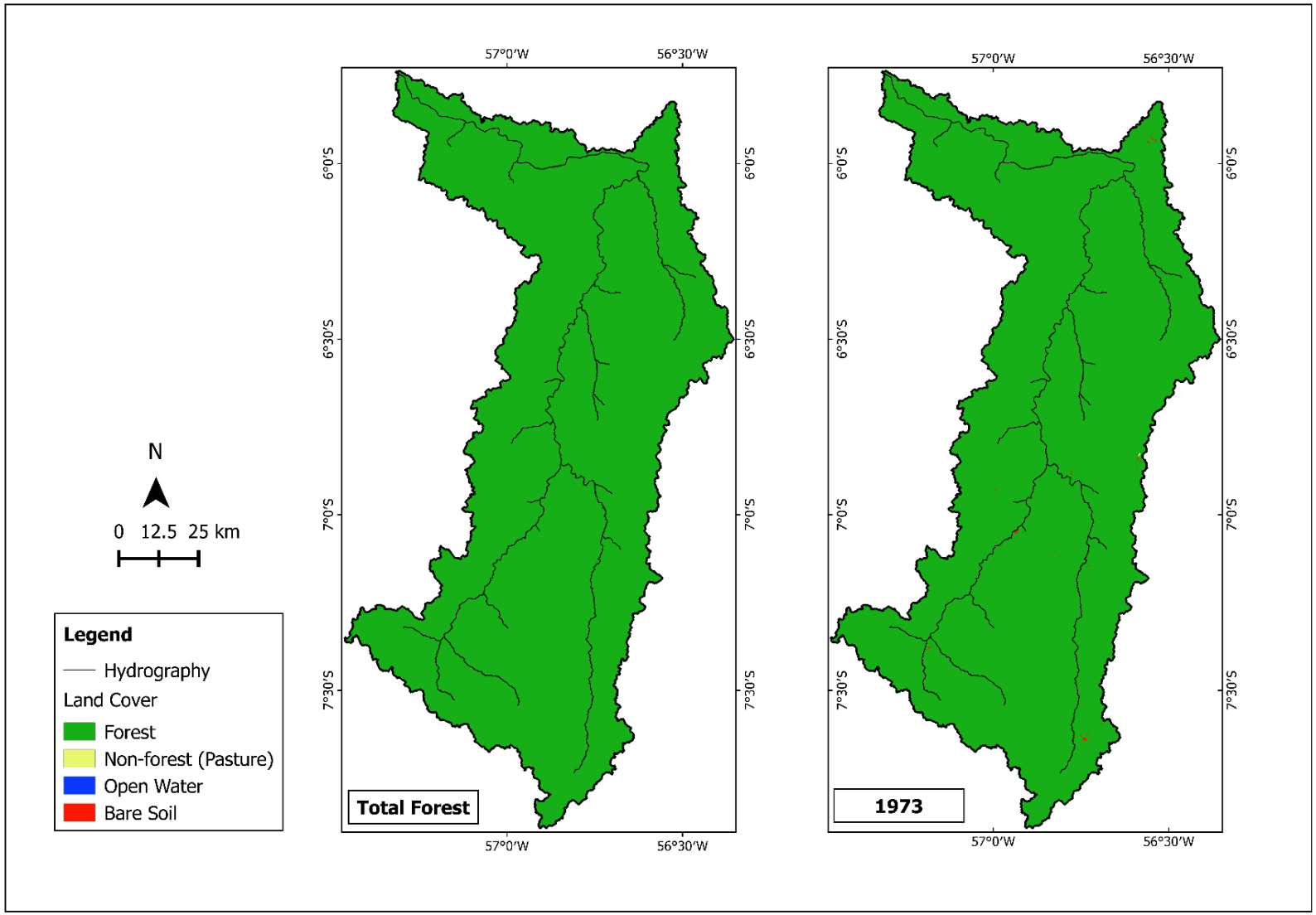

Figure 4.5. Land cover scenarios: 1998 and 2003

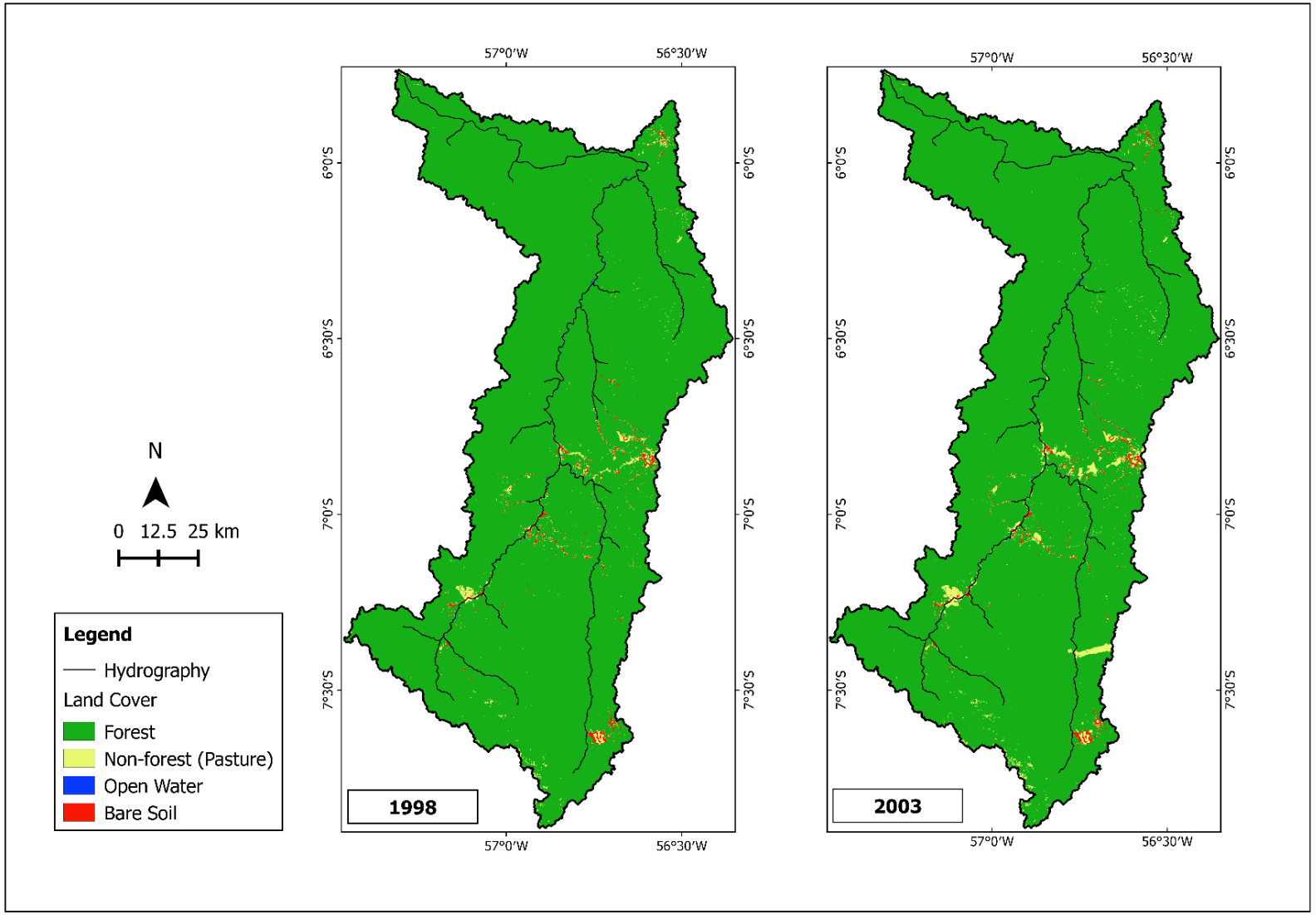

Figure 4.6. Land cover scenarios: 2010, 2040 and Total Bare Soil

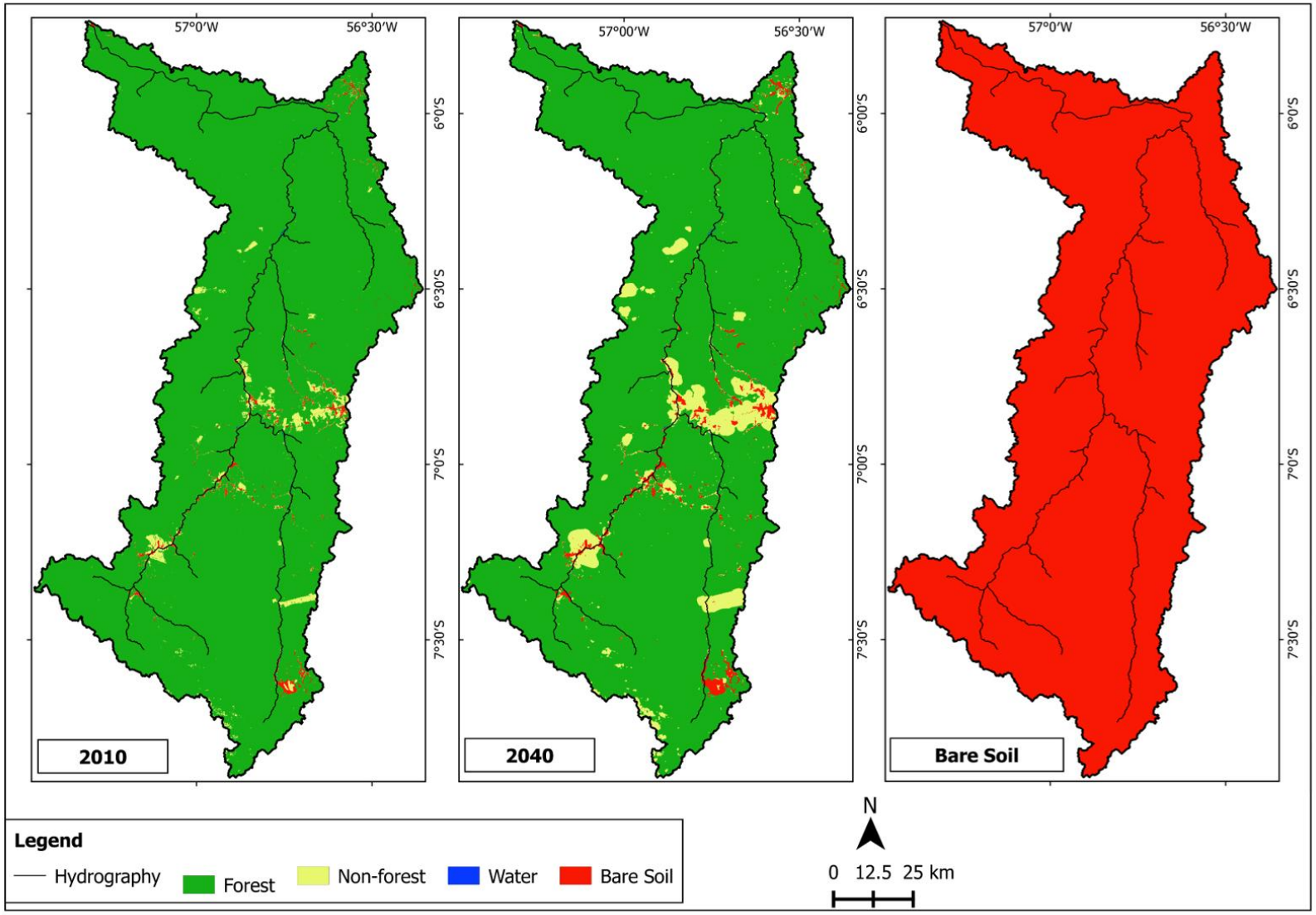

4.3.2.1 Vegetation parameters

Parameters regarding vegetation's physical and physiological characteristics are required to model the interactions between vegetation and water, especially the evapotranspiration process. SWAT has a database with recommended vegetation parameter values for several vegetation types and crops.

From SWATv.2012 database, 'Pasture' was chosen to represent the 'Non-forest' land cover class for all mapped scenarios, while 'Forest Evergreen' was chosen to represent the 'Forest' land cover class. Evapotranspiration was computed according to Hargreaves et al. (1985). The initial values of parameters of Non-forest and Forest classes are shown in Appendix B (Table B.1).

4.3.3 Soil data and parameterization

Soil physicochemical data and parameters are used to characterize the soil and then, to model water movement through the soil layers as well as to model the sediment yield.

The 1:250,000 pedological map of Brazilian Legal Amazon (IBGE, 2016) (Figure 4.7) was used along with soil physicochemical data, such as the number and the depth of soil layers (NLAYERS), rock (ROCK) and carbon content (SOL_CBN), as well as soil texture (SAND, SILT and CLAY), retrieved from RADAMBRASIL (BRAZIL, 1975), EMBRAPA (EMBRAPA/SNLCS, 1984; EMBRAPA/FAO, 1991) and DNPEA/MA (BRASIL, 1973) databases shown in Appendix C (Table C.1 and Table C.2). Since there were very few information about the soils in Crepori basin, it was assumed that the same types of soils from regions near the basin would have similar physicochemical properties.

The classification of soil hydrological groups made by Sartori et al. (2005) was used to define the parameter (HYDGRP) of Crepori soils. Maximum root depths (SOL_ZMX) were based on Quesada et al. (2011), and the albedo (SOL_ALB) was estimated according to the relation proposed by Post et al. (2000), whereas the USLE erodibility parameter (USLE_K) was calculated according to Williams (1995), as recommended by Arnold et al. (2012a). These parameters values are listed in Appendix C (Table C.3).

Pedotransfer functions were applied for estimating soil saturated hydraulic conductivity (SOL_K) (AHUJA et al., 1984; TOMASELLA; HODNETT, 1997), soil bulk density (SOL_BD) (TOMASELLA; HODNETT, 1998) and available water capacity (SOL_AWC) (VAN GENUCHTEN, 1980; TOMASELLA et al., 2000). Initial soil parameter values estimated by pedotransfer functions are shown in Appendix C (Table C.4).

Figure 4.7. Pedological map of Crepori basin.

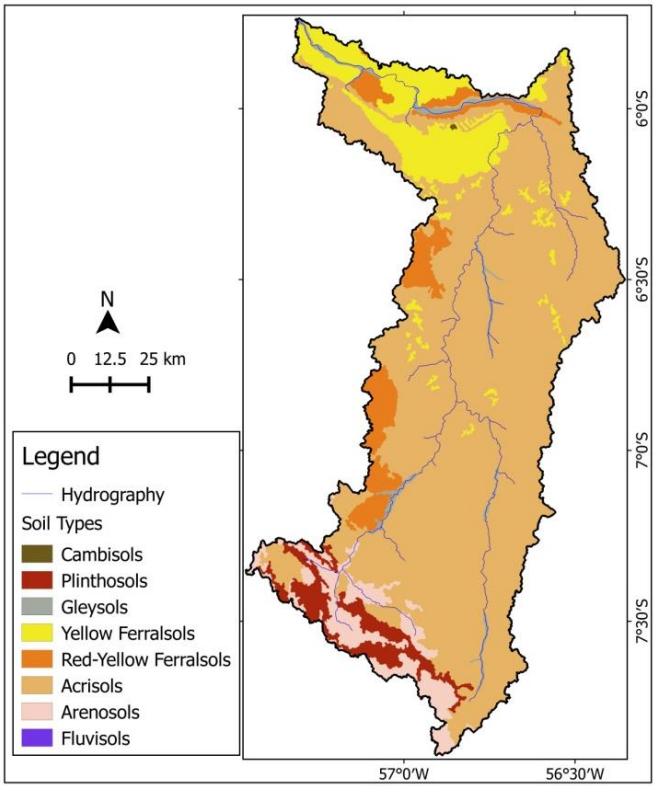

Estimated values of soil parameters shown in Appendix C (Table C.4) were compared to values reported in the literature for similar soils from Amazonian or tropical regions. Similar values were found for Soil Bulk Density (CORREA, 1984; TOMASELLA; HODNETT, 1996; TOMASELLA; HODNETT, 2004), Available Water Capacity (TOMASELLA; HODNETT, 2004), Soil Albedo (FORMAGGIO et al., 1996; OLIVEIRA et al., 2013; SILVA et al, 2014) and USLE erodibility factor (RANZANI, 1980; TAGLIARI, 2009; ENCINAS, 2011). Some of the Soil Saturated Hydraulic Conductivity estimated values were higher than those expected for Amazonian soils (which tends to range from 10 to 1.000mm/h) (TOMASELLA; HODNETT, 2004; FAJARDO et al, 2010;

FIGUEIREDO et al, 2016). However, as the pedotransfer function used in this step was derived for Amazonian soils and considering that these values will be better adjusted during the calibration step, the estimates were maintained as an initial guess of the Saturated Hydraulic Conductivity parameter.

4.3.4 Daily precipitation and temperature data

Due to the scarcity of weather stations and the lack of *in situ* data records, precipitation estimates from TRMM 3B42 Daily v.7 product and ERA Interim Daily temperature data for the period between 1998 and 2012 were used. ERA Interim and TRMM data were cross-referenced to data from weather stations located in or near the basin (ANA, 2016b; INMET, 2017).

TRMM 3B42 Daily v.7 data were cross-referenced to data from the ANA rain gauge located at 6°28'12"S, 56°28'12"W, in the Crepori basin. To evaluate the representativeness of TRMM rainfall product, the following metrics were used:

- The coefficient of correlation (r), which indicates the agreement between observed and estimated precipitation. This coefficient is calculated as shown in Equation 4.1:

$$r = \frac{\sum_{i=1}^{n}(P_{obs,i}-\overline{P}_{obs})\times(P_{est,i}-\bar{P}_{est})}{\sqrt{\sum_{i=1}^{n}\left(P_{obs,i}-\bar{P}_{obs}\right)^2\times\sum_{i=1}^{n}\left(P_{est,i}-\bar{P}_{est}\right)^2}} \quad (4.1)$$

- The bias, which indicates the over or underestimation trends in the estimated precipitation series. Bias is calculated with Equation 4.2 as follows:

$$bias = \frac{\sum_{i=1}^{n}(P_{est,i}-P_{obs,i})}{\sum_{i=1}^{n}P_{obs,i}} \quad (4.2)$$

- The RMSE-Observations Standard Deviation Ratio (RSR), which standardizes the Root Mean Squared Error (RMSE) to the Standard Deviation of the observed precipitation series. The RSR for the precipitation series is calculated as shown in Equation 4.3:

$$RSR = \frac{RMSE}{STDEV_{obs}} = \frac{\sqrt{\sum_{i=1}^{n}(P_{obs,i} - P_{est,i})^2}}{\sqrt{\sum_{i=1}^{n}(P_{obs,i} - \overline{P}_{obs})^2}} \quad (4.3)$$

Where $P_{obs,i}$ is the observed precipitation in month i; $P_{est,i}$ is the precipitation estimated by TRMM product in month i; $\bar{P}_{obs}$ is the average observed precipitation; $\bar{P}_{est}$ is the average estimated precipitation. All metrics presented are dimensionless. Figure 4.8 shows the comparison of monthly precipitation from both sources and Table 4.3 shows the values calculated for each metric used.

Figure 4.8. TRMM and INMET rain gauge monthly precipitation data.

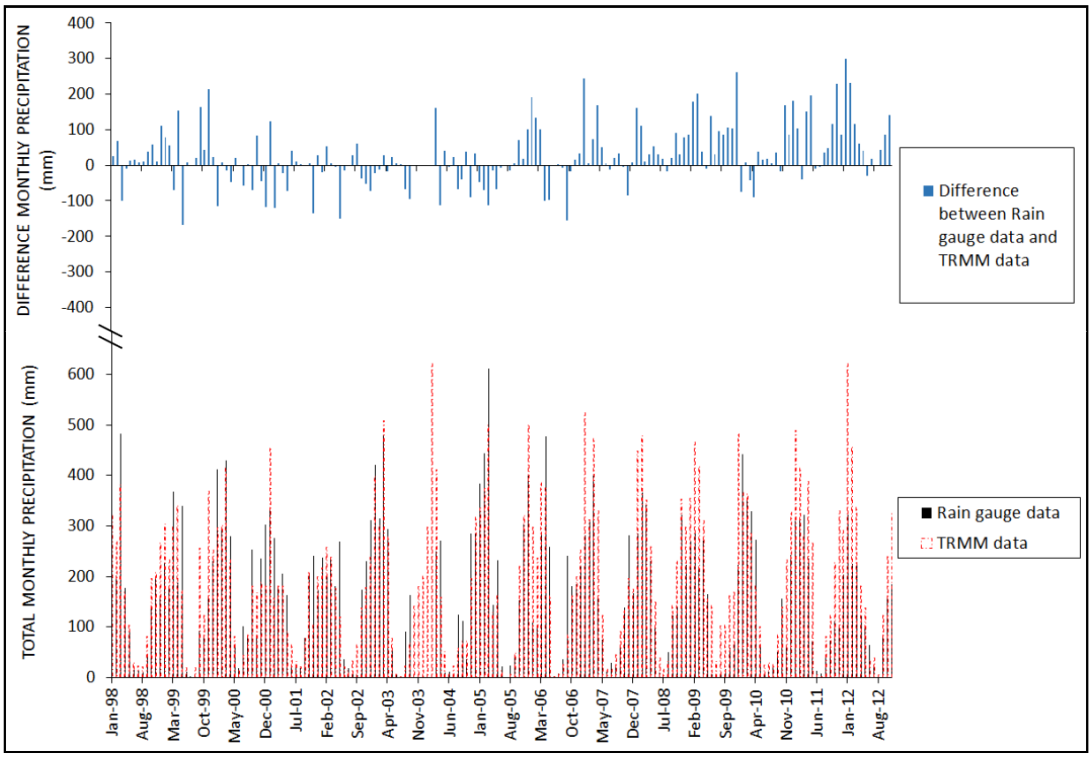

Table 4.3. Calculated metrics for precipitation data cross-referencing.

r	bias	RSR
0.82	0.16	0.67

Although it is possible to find discrepancies between precipitation estimated by TRMM product and that measured at the rain gauge, no systematic deviation between these datasets was observed (Figure 4.8).

The coefficient of correlation can be considered relatively high and both, bias and RSR are considered low (Table 4.3). The positive value calculated for the bias metric indicates that TRMM product tends to overestimate the precipitation in relation to the rain gauge data. From Figure 4.8, it is possible to notice that this overestimation is more frequent in the last years of the series.

The differences in the values of precipitation provided by these datasets can be attributed to the different spatial scale of TRMM and the rain gauge, to the disparities on the time considered to account the days in both sources, and to the uncertainties in the measurements, estimates and recordings performed in both, the rain gauge and the TRMM algorithm. Therefore, given the high spatial and temporal variability of this variable (precipitation), considering those sources of uncertainties in both datasets and in the data comparison and considering that no systematic deviations were found, no bias correction was applied to this data. Furthermore, the calculated metrics show that TRMM TMPA 3B42 v.7 product is well representing the precipitation over the study area.

Finally, since performing the modelling procedure in a monthly time step can smooth the differences between the datasets, and given that the analysis in this study will be conducted by comparing different land cover scenarios, the differences observed between the two precipitation data sources are considered insufficient to jeopardize the analysis in this study.

ERA Interim daily temperature data were cross-referenced to daily temperature records from an INMET station located at Itaituba city (4°16'48"S, 55°58'48"W) (Figure 4.1), the nearest station with available temperature data. Thus, for this cross-referencing analysis, ERA Interim daily temperature data for that location were used.

It was verified that ERA Interim data were, in average, systematically overestimating the minimum temperatures from 1998 to 2000 in 1.58°C (Figure 4.9). Therefore, a bias correction of -1.58°C was applied to the dataset for this period (Figure 4.9). ERA Interim data were also underestimating the maximum daily temperatures in 7.58°C, in average, for the entire series (Figure 4.10). Thus, a bias correction of +7.58°C was applied to the maximum temperatures (Figure

4.10). Figures 4.9 and 4.10 show ERA Interim and INMET datasets for maximum and minimum temperatures and the bias-corrected ERA Interim data. Although this analysis was performed for Itaituba temperature datasets, it was assumed that the bias in ERA Interim data was the same for the Crepori basin. Thus, for ERA Interim data corresponding to Crepori basin, the same bias corrections were applied.

Figure 4.9. INMET and ERA Interim daily minimum temperatures and the bias-corrected ERA Interim data.

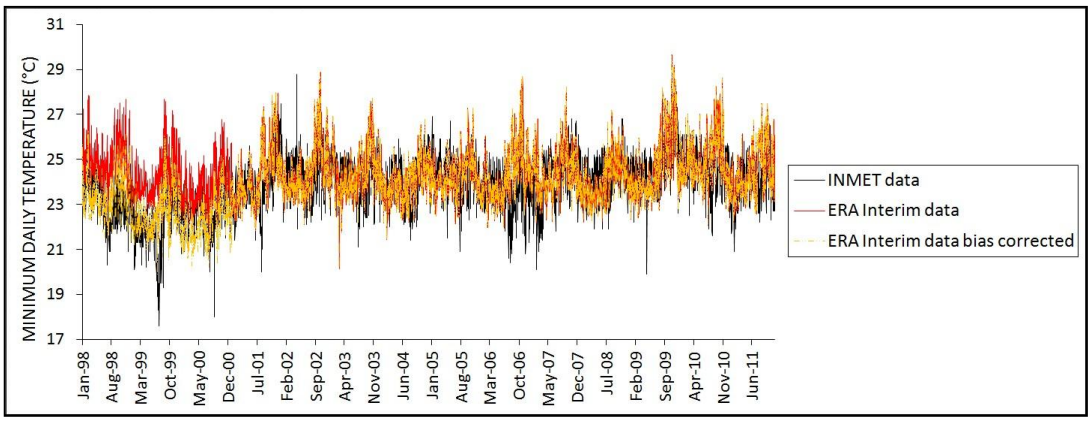

Figure 4.10. INMET and ERA Interim daily maximum temperatures and the bias-corrected ERA Interim data.

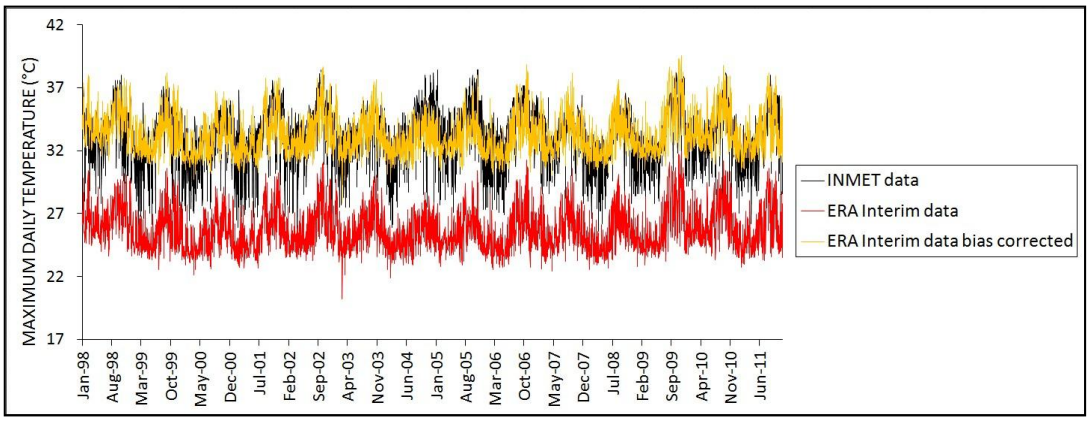

4.3.5 Sediment parameters

SWAT calculates surface runoff (Q_{surf}) and peak discharge (q_{peak}) based on the curve number procedure and on precipitation data (USDA-SCS, 1972; NEITSCH et al., 2011). The USLE topographic parameter, LS_{USLE}, is calculated based on

slopes and slope lengths retrieved from the input DEM (Figure 4.3) (NEITSCH et al., 2011).

CFRG values are calculated by SWAT, based on rock content presented in Appendix C (Table C.2) and K_{USLE} (USLE_K parameter) values, as previously mentioned, were estimated according to Williams (1995), based on soil texture shown in Appendix C (Table C.3). C_{USLE} values available at SWAT.v.2012 database were used for each land cover (Table 4.4), whereas P_{USLE} value was set to 1 for all land cover types, representing the condition of no support practices being applied on the watershed.

Table 4.4. C_{USLE} values used from SWAT.v.2012 database.

Land Cover	**C_{USLE} value (-)**
Forest (FRSE)	0.001
Non-forest (PAST)	0.003
Bare Soil (BARR)	0.2

4.4 Streamflow Observed Data for Calibration and Validation

The daily streamflow data needed to calibrate and validate the model were retrieved from records of the streamflow gauge number 17610000 (Creporizão - 6°49'12"S, 56°51'0"W) (Figure 4.1), operated by ANA and available online (HidroWeb - http://www.snirh.gov.br/hidroweb/) (ANA, 2016a).

The streamflow gauge records have a data series of 7 years (from 2002 to 2008) of daily streamflow and of daily water-level data, and 4 years with only daily water-level data. Table 4.5 summarizes the data available in the ANA Creporizão gauge records.

Table 4.5. Data available from ANA Creporizão streamflow gauge records.

	2002	2003	2004	2005	2006	2007	2008	2009	2010	2011	2012	2013
JAN		H/Q		H/Q	H/Q	H/Q	H/Q	H/Q	H	H	H	H
FEB	H/Q	H/Q	H/Q	H/Q	H/Q	H/Q	H/Q	H/Q	H	H	H	H
MAR	H/Q	H/Q	H/Q	H/Q	H/Q	H/Q	H/Q	H/Q	H	H	H	H
APR	H/Q	H/Q	H/Q	H/Q	H/Q	H/Q	H/Q	H	H	H	H	
MAY	H/Q	H/Q	H/Q	H/Q	H/Q	H/Q	H/Q	H	H	H	H	
JUN	H/Q	H/Q	H/Q	H/Q	H/Q	H/Q	H/Q	H	H	H	H	
JUL		H/Q	H/Q	H/Q	H/Q	H/Q	H/Q	H	H	H	H	
AUG		H/Q	H/Q	H/Q	H/Q	H/Q	H/Q	H	H	H	H	
SEP	H/Q	H/Q	H/Q	H/Q	H/Q	H/Q	H/Q	H	H	H	H	
OCT	H/Q		H/Q		H/Q	H/Q	H/Q	H	H	H	H	
NOV	H/Q		H/Q	H/Q	H/Q	H/Q	H/Q	H	H	H	H	
DEC	H/Q		H/Q	H/Q	H/Q	H/Q	H/Q	H	H	H	H	

H/Q = Water Level (cm) and Streamflow (m³/s) data available		= Data verified by ANA
H = Only Water Level (cm) data available		= Data not verified by ANA

Since there were streamflow data missing in the series between 1998 and 2012, it was necessary to complete the series, by retrieving the equation used to convert water-level values to streamflow values, also called 'rating curve' (TUCCI, 1993). As recommended by Collischonn and Dornelles (2013), the power equation type (Equation 4.4) was used to represent the relation between water-level and discharge.

$$Q = a(H - h)^b \tag{4.4}$$

Where Q is the discharge (m³/s); H is the water level (m); h is the water level to which discharge is zero (m); a and b are parameters representing the channel shape. The parameters a, b and h can be adjusted using the least squares method.

In order to avoid the rating curve to be biased by uncertainty in water-level or uncertainty in discharge data, only data previously verified by ANA were used in this process. Moreover, once the water-level and discharge values vary significantly between low and high values in the series, it was necessary to split the dataset into two groups of water-level data: one series with the lowest (from 4.10 to 7.335 m) and one series with the highest (up from 7.34 to 9.95 m) water-

level values. Thus, two rating curves were retrieved, one for each group of data series. This procedure aimed at reducing the relative deviations between the observed data values and the values calculated from the rating curves (COLLISCHONN; DORNELLES, 2013).

The rating curves retrieved (Figures 4.11 and 4.12) presented relative errors (difference between the value given by the rating curve and that recorded for the gauge) 0 and 0.98% and between 0 and 0.97% for the data series with values from 4.10 to 7.335 m, and from 7.34 to 9.95 m, respectively.

Figure 4.11. Rating curve retrieved for low water level (from 4.10 to 7.34m).

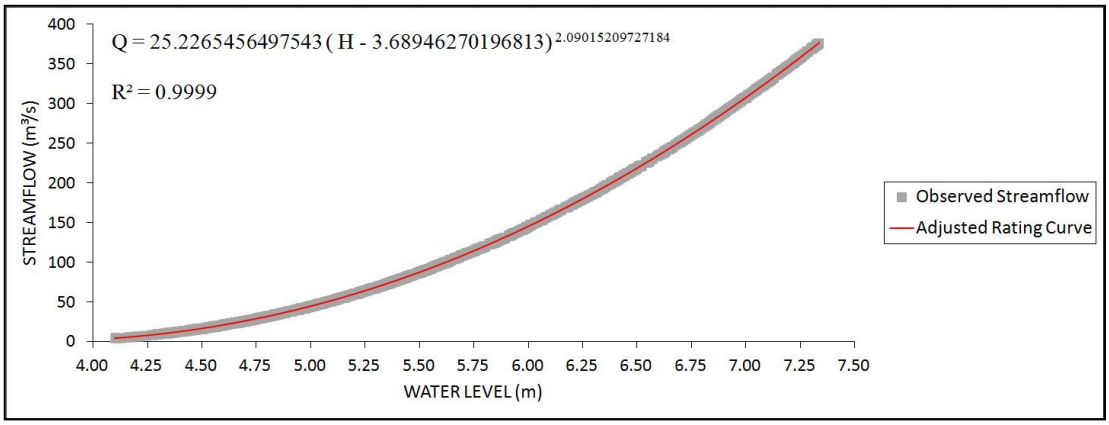

Figure 4.12. Rating curve retrieved for high water level (from 7.34 to 9.95m).

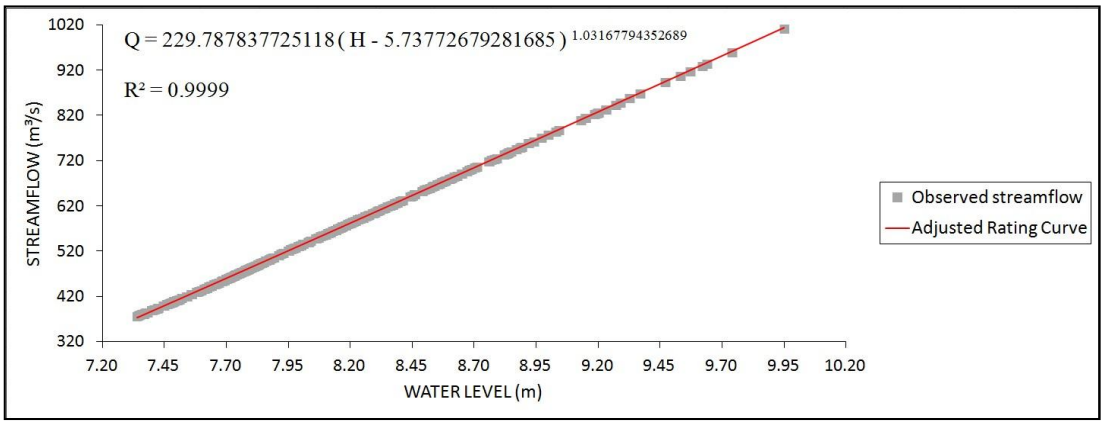

Then, using the retrieved rating curves, the discharge dataset was reconstituted (Figure 4.13).

Figure 4.13. Reconstituted streamflow daily dataset.

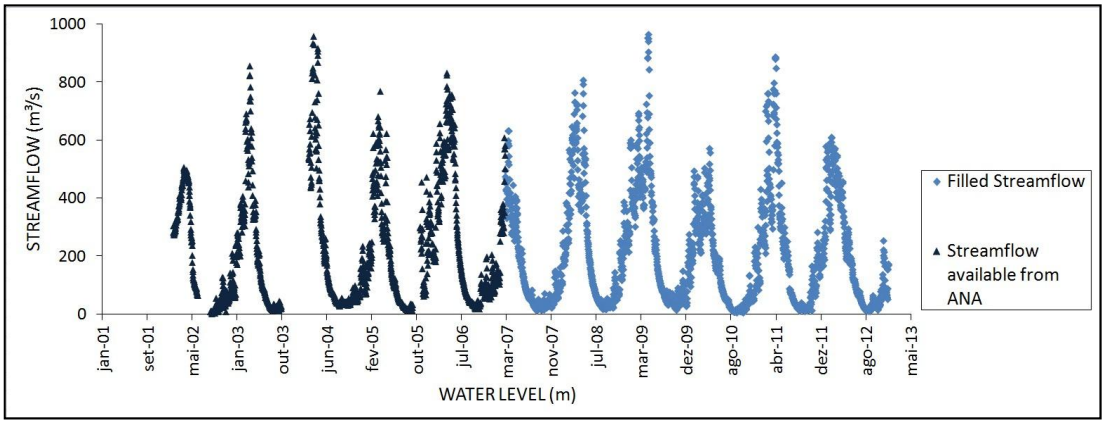

4.5 Precipitation and Streamflow Series for Model Warm-Up, Calibration and Validation

Precipitation data for the first three years (1998, 1999 and 2000) were used for model warm-up, whereas the remaining twelve years of precipitation data (2001-2012) were used, along with streamflow data, for the model calibration and validation (Figure 4.14). Figure 4.14 shows the monthly precipitation accumulated for the region of Crepori Basin upstream the stream gauge and the division of the series for model warm up, calibration and validation.

Figure 4.14. Monthly precipitation and streamflow data for warm-up, calibration and validation periods.

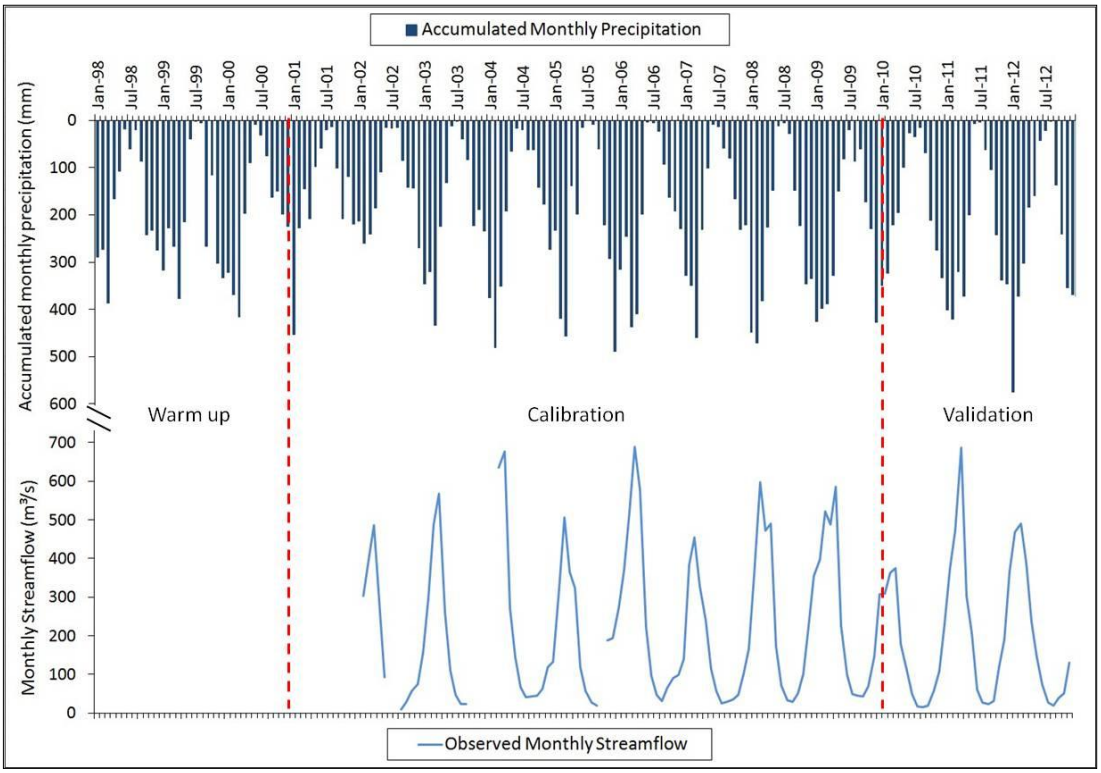

4.6 Model Setup, Sensitivity Analysis, Calibration, Validation and Performance Assessment

The model was set up by writing the input data to SWAT's database. In this step, the Land Use Update Tool was activated to include the land cover information for the scenarios of 1998, 2003 and 2010, with the update dates set respectively to 01/01/1998, 01/01/2003 and 01/01/2010.

4.6.1 First model run and manual calibration

The model was run without performing any calibration, and using the SWATCheck1.2 tool (implemented in SWATEditor_2012.10.19), the average annual values and proportions of evapotranspiration, streamflow and lateral flow were compared to values reported in the literature as well as to the observed streamflow values. In this step, it was noticed that the proportion of the average evapotranspiration to the average annual precipitation was not reasonably corresponding to the references (evapotranspiration represents around 54% of

precipitation volume) (SHUTTLEWORTH, 1988; MALHI et al., 2002; TOMASELLA et al., 2008; CUARTAS et al., 2012). Moreover, the simulated streamflow was highly different from the observed streamflow, and the proportion of lateral flow to the streamflow was not corresponding to the proportion reported by Lamparter et al. (2016) (around 80%) for the Jamanxim basin, which is next to Crepori and was assumed to have similar groundwater dynamics.

Therefore, before performing the sensitivity analysis and the automatic calibration, a manual calibration (trial and error) was performed, to better adjust the average water balance to the references.

In this procedure, parameters whose values directly impact evapotranspiration, streamflow and groundwater (NEITSCH et al., 2011) were manually changed within the limits of their physical meaning available in SWATv.2012 database and suggested by Neitsch et al. (2011).

To better adjust the model to evapotranspiration, vegetation parameter values available in the literature (LAURENT; RUELLAND, 2010; STRAUCH; VOLK, 2013) and at the Large Scale Biosphere-Atmosphere Experiment in Amazonia (LBA) project database (WILLIAMS et al., 2012; COSTA; COHEN, 2013) replaced their initial values. All the parameters included in this step, as well as their values, are shown in Appendix B (Table B.1, Table B.2 and Table B.3).

The parameter subjected to the largest changes, before water balance components were adjusted, was the Saturated Hydraulic Conductivity (SOL_K). As previously mentioned, the values estimated for SOL_K via pedotransfer functions were not corresponding to several values reported in the literature (TOMASELLA; HODNETT, 2004; FAJARDO et al, 2010; FIGUEIREDO et al, 2016). Thus, in the manual calibration, this parameter was changed in higher proportions than others. By significantly reducing SOL_K values, the average annual water balance presented components with more reliable values and proportions, when compared to the references (SHUTTLEWORTH, 1988; MALHI et al., 2002; TOMASELLA et al., 2008; CUARTAS et al., 2012; LAMPARTER et al., 2016).

4.6.2 Sensitivity analysis

Sensitivity analysis was performed using the SWAT-CUP platform and the global sensitivity analysis method (ABBASPOUR, 2015) as recommended by Oliveira (2014).

To preserve the spatial dependency of spatial-dependent parameters, 'relative change' (r__) method, which changes the parameter value proportionally to its initial value (ABBASPOUR, 2015) was set during the automatic calibration procedure. The 'replace' (v__) method was used for both parameters with no spatial dependency and parameters for which initial value was not available on literature, measurements or estimates. The range of variation for the parameter's values was defined based on the limits given by Neitsch et al. (2011), to ensure their physical meaning.

For including parameters in the sensitivity analysis, listed in Appendix D (Table D.3), the following criteria were applied: i) uncertainty in parameter values definition, during the parameterization step, ii) based on previous studies (STRAUCH et al., 2012; FUKUNAGA et al., 2015; LAMPARTER et al., 2016), which indicate, for instance, that groundwater parameters are usually sensitive in the SWAT modelling of Brazilian watersheds; iii) based on the author's observations, from the manual calibration step, regarding the parameters' effects on the behaviour of modelling results. The most sensitive parameters defined in this procedure are ranked in Table 4.6.

Table 4.6. Ranking of the most sensitive parameters.

RANK #*	PARAMETER CODE	DESCRIPTION
1	GWQMN.gw	Threshold depth water in the shallow aquifer required for return flow to occur (mm H_2O)
2	ALPHA_BNK.rte	Baseflow alpha factor for bank storage (days)
3	GW_DELAY.gw	Groundwater delay time (days)
4	ALPHA_BF.gw	Baseflow alpha factor (1/days)
5	SOL_AWC(2).sol_____PAST**	Available water capacity of the soil layer (mm H_2O/mm soil)
6	SOL_AWC(1).sol_____PAST**	
7	SOL_AWC(3).sol_____FRSE**	
8	CN2.mgt____LV__FRSE***	Initial SCS runoff curve number for moisture condition II (-)
9	REVAPMN.gw____FRSE	Threshold depth of water in the shallow aquifer for "revap" or percolation to the deep aquifer to occur (mm H_2O)
10	CN2.mgt____FF__FRSE***	Initial SCS runoff curve number for moisture condition II (-)
11	SOL_K(3).sol_____FRSE	Saturated hydraulic conductivity (mm/h)
12	CN2.mgt____LV__PAST***	Initial SCS runoff curve number for moisture condition II (-)
13	SOL_BD(1).sol_____PAST**	Moist bulk density (Mg/m^3 or g/cm^3)
14	CH_K2.rte	Effective hydraulic conductivity in main channel alluvium (mm/h)

*Parameters ordered from the most sensitive (#1) to the last sensitive (#14).
**PAST and FRSE refer to the land covers: 'Pasture' and 'Forest Evergreen', in the SWATv.2012 database and the numbers in the parentheses refer to the soil layer number.
*** LV and FF refer to the soil types: Red-yellow Ferralsols and Plinthosols.

4.6.3 Automatic calibration

The most sensitive parameters were then included in the automatic calibration, using ParaSol method, implemented in SWAT-CUP platform. Table 4.7 shows the method used for changing the parameter values, the range of values' variation and the parameter's initial values.

Table 4.7. Parameters and ranges for calibration.

METHOD FOR VALUE CHANGE	PARAMETER CODE	INITIAL VALUE	MINIMUM VALUE	MAXIMUM VALUE
Replace	GWQMN.gw	1000	0	5000
Replace	ALPHA_BNK.rte	0	0	1
Replace	GW_DELAY.gw	31	1	450
Replace	ALPHA_BF.gw	0.048	0	1
Relative Change	SOL_AWC(2).sol_____PAST	Variable*	-0.03	0.05
Relative Change	SOL_AWC(1).sol_____PAST	Variable*	-0.03	0.05
Relative Change	SOL_AWC(3).sol_____FRSE	Variable*	-0.03	0.05
Replace	CN2.mgt____LV__FRSE	30	30	68
Relative Change	REVAPMN.gw____FRSE	614	-1	1.19
Replace	CN2.mgt____FF__FRSE	77	77	79
Relative Change	SOL_K(3).sol_____FRSE	Variable*	-0.05	0.1
Replace	CN2.mgt____LV__PAST	30	30	68
Relative Change	SOL_BD(1).sol_____PAST	Variable*	-0.05	0.05
Replace	CH_K2.rte	0	0	130

*Different initial value for each soil type. For all initial values of soil parameters, refer to Appendixes C and D (Table C.3 and Table D.2).

The set of the best parameter values adjusted during the calibration was then applied to SWAT and the model was run for the validation period.

Calibration and validation of sediment concentrations were not possible due to two main issues. The first was the lack of daily sediment concentration records available for the Crepori River. The second is that even if sediment concentration records were available, these measurements would be biased by the sediment yielded by gold mining. Once SWAT does not model gold mining, and this study focus in sediment concentrations caused by land cover changes, the model could not be calibrated or validated using direct measurements of sediment concentrations at the Crepori River.

However, as an attempt to assess sediment concentration simulated by the model, these simulated values were compared to those reported in published studies (TELMER et al., 2006; COSTA et al., 2013; LOBO et al. 2015).

4.6.4 Validation and model performance assessment

The following metrics (MORIASI et al., 2007) were used to validate the modelling (comparing simulated to observed streamflow for the validation period) and to evaluate the model performance in the entire series:

- The coefficient of determination (R^2) - interpreted as the proportion of the variance in the dependent variable that is predictable from the independent variable, and is defined as shown in Equation 4.5.

$$R^2 = 1 - \frac{\left[\sum_{i=1}^{n}(Q_{obs,i}-\overline{Q}_{obs})(Q_{sim,i}-\overline{Q}_{sim})\right]^2}{\sum_{i=1}^{n}(Q_{obs,i}-\overline{Q}_{obs})^2 \sum_{i=1}^{n}(Q_{sim,i}-\overline{Q}_{sim})^2} \quad (4.5)$$

- Nash-Sutcliffe Coefficient of Efficiency (NSE) (NASH; SUTCLIFFE, 1970) - which determines the relative magnitude of residual variance compared to the variance of observed data, reflecting the overall fit of a hydrograph (MORIASI et al., 2007). This statistics ranges from -∞ to 1, with NSE = 1 indicating a perfect model fit, NSE = 0 indicating that the model is accurate as the mean of observed data, and NSE < 0, indicating that the average of the observed values is a better predictor than the model. NSE is defined by Equation 4.6.

$$NSE = 1 - \frac{\sum_{i=1}^{n}(Q_{obs,i}-Q_{sim,i})^2}{\sum_{i=1}^{n}(Q_{obs,i}-\overline{Q}_{obs})^2} \quad (4.6)$$

- Percent Bias (PBIAS) (GUPTA et al., 1999), which indicates the average trending of the model to over or underestimate the simulated values. Therefore, the optimum value of PBIAS is 0%, when the model, in average, is predicting the variable with no bias. PBIAS is defined by Equation 4.7.

$$PBIAS = 100 \times \frac{\sum_{i=1}^{n}(Q_{obs,i}-Q_{sim,i})}{\sum_{i=1}^{n} Q_{obs,i}} \quad (4.7)$$

- RMSE-Observations Standard Deviation Ratio (RSR) (SINGH et al., 2005), which standardizes RMSE using the observations standard deviation. The optimum value of RSR is 0, indicating that the model is perfectly predicting the variable (RMSE = 0), to a large positive value, indicating poor model performance, with large RMSE. The RSR is defined according to Equation 4.8.

$$RSR = \frac{RMSE}{STDEV_{obs}} = \frac{\sqrt{\sum_{i=1}^{n}(Q_{obs,i}-Q_{sim,i})^2}}{\sqrt{\sum_{i=1}^{n}(Q_{obs,i}-\overline{Q}_{obs})^2}} \quad (4.8)$$

In Equations 4.5, 4.6, 4.7 and 4.8, R^2 is the Coefficient of Determination, *NSE* is the Nash-Sutcliffe Coefficient of Efficiency, *PBIAS* is the Percent Bias, *RSR* is the RMSE-Observations Standard Deviation Ratio; n is the number of observed data, $Q_{obs,i}$ is the observed streamflow on day or month i, $\overline{Q}_{obs}$ is the average observed streamflow, $Q_{sim,i}$ is the streamflow simulated on day or month i and $\overline{Q}_{sim}$ is the average simulated streamflow.

These statistics were calculated separately for the calibration (2001 to 2009) and the validation period (2010 to 2012), and then, for the entire series (2001 to 2012). To evaluate the model performance, and consider the model calibrated and validated, the calculated statistics values were compared to the reference values suggested by Moriasi et al. (2007) (Table 4.8). Thus, if the statistics values were below the 'Satisfactory' rate (Table 4.8), the calibration procedure was repeated, followed by a new validation. When the statistics values were above the 'Satisfactory' rate, the model was considered calibrated and validated, and ready to simulate the scenarios.

Table 4.8. Statistics recommended by Moriasi et al. (2007) for streamflow model performance assessment on a monthly time step.

Performance rating	**RSR**	**NSE**	**PBIAS**
Very good	$0.00 \leq RSR \leq 0.50$	$0.75 \leq NSE \leq 1.00$	$PBIAS \leq \pm 15\%$
Good	$0.50 \leq RSR \leq 0.60$	$0.65 \leq NSE \leq 0.75$	$\pm 15\% \leq PBIAS \leq \pm 30\%$
Satisfactory	$0.60 \leq RSR \leq 0.70$	$0.50 \leq NSE \leq 0.65$	$\pm 30\% \leq PBIAS \leq \pm 55\%$
Unsatisfactory	$RSR \geq 0.70$	$NSE \leq 0.5$	$PBIAS \geq \pm 55\%$

The non-parametric statistic 'Locally Weighted Scatterplot Smoothing' (LOWESS) (CLEVELAND, 1981) was applied to the differences between observed and simulated streamflow for the series from 2001 to 2012 to detect model trends in relation to under and overestimation. LOWESS is a relatively robust method for graphical analysis that can detect and indicate overall trends in the simulated data series, giving insights on physical explanations for the trends. According to Cleveland (1979), LOWESS uses robust locally weighted regression to smooth a scatterplot (x_i, y_i), (i=1,2,...). The fitted value is a polynomial fit to the data using least squares (x_k, y_k), and the weight of (x_i, y_i) is large for xi close to x_k. When applied to the simulated streamflow over the entire time series, LOWESS can smooth the small-scale time trends, highlighting the overall model trends.

4.7 Simulation of Scenarios and Comparison Between SWAT-Simulated Sediment Concentration and TSS Estimated by Lobo et al. (2015)

After calibration and validation for streamflow, the model was run using the land cover scenarios to simulate both streamflow and sediment concentration.

Once the scenarios of 1998, 2003 and 2010 were included in the model set up, using the Land Use Update Tool, the simulations of streamflow and sediment concentrations for these scenarios were performed at the same model run. Therefore, in this document, these scenarios will be referred to as 1998-2003-2010.

Sediment concentration simulated by SWAT was then compared to TSS estimated by Lobo et al. (2015). For low slopes regions, like Crepori basin, bed load is usually low in relation to suspended load (up to 1%) (DUNNE et al., 1998, STRASSER et al., 2004) and therefore, in this study, TSS and sediment concentration are assumed to be comparable for the study area.

5 RESULTS AND DISCUSSION

5.1 Calibration

As result of manual calibration, the model simulated average annual evapotranspiration as approximately 54% of precipitation, which is in agreement with rates reported in the literature for forested areas in this region (SHUTTLEWORTH, 1988; MALHI et al., 2002; TOMASELLA et al., 2008; CUARTAS et al., 2012). Also, total flow was computed as mainly generated by lateral flow, which is corroborated by the study of Lamparter et al. (2016) at Jamanxim River basin, located next to Crepori basin.

The result from automatic calibration, performed on a monthly basis, using all sensitive parameters is shown in Table 5.1.

Table 5.1. Parameters used in the automatic calibration and their best-calibrated values.

PARAMETER CODE	DESCRIPTION	CALIBRATED VALUE
ALPHA_BF	Baseflow alpha factor (1/days)	0.58
ALPHA_BNK	Baseflow alpha factor for bank storage (days)	0.051
CH_K2	Effective hydraulic conductivity in main channel alluvium (mm/h)	39.37
CN2_LV_PAST** CN2_FF_FRSE** CN2_LV_FRSE**	Initial SCS runoff curve number for moisture condition II	56.29 78.25 33.08
GW_DELAY	Groundwater delay time (days)	8.21
GWQMN	Threshold depth water in the shallow aquifer required for return flow to occur (mm H_2O)	198.48
REVAPMN_FRSE*	Threshold depth of water in the shallow aquifer for "revap" or percolation to the deep aquifer to occur (mm H2O)	572.85
SOL_AWC (1)_PAST* SOL_AWC (2)_PAST* SOL_AWC (3)_FRSE*	Available water capacity of the soil layer (mm H_2O/mm soil)	1.018*** 1.004*** 1.005***
SOL_BD (1)_PAST*	Moist bulk density (Mg/m³ or g/cm³)	0.982***
SOL_K (3)_FRSE*	Saturated hydraulic conductivity (mm/h)	1.008***

*Numbers (1, 2, 3) refer to the soil layer number, while the codes FRSE and PAST refer to the land covers from SWATv.2012 database 'Forest Evergreen' and 'Pasture', respectively.
**Codes LV and FF refer to the soil types: Red Yellow Latosol and Plintosols, respectively.
***Calibrated values to be multiplied by the initial parameter values.

Calibrated soil parameters values were in accordance with values recorded in the literature: Saturated Hydraulic Conductivity (TOMASELLA; HODNETT, 2004; FAJARDO et al, 2010; FIGUEIREDO et al, 2016); Soil Bulk Density (CORREA, 1984; TOMASELLA; HODNETT, 1996; TOMASELLA; HODNETT, 2004); Available Water Capacity (TOMASELLA; HODNETT, 2004), whereas the remaining calibrated parameters values were all within the range of physical meaning, given by Neitsch et al. (2011).

As previously stated, calibration and validation for sediment concentrations were not possible in this study. Nevertheless, comparison with reference sediment concentration (TELMER et al., 2006; COSTA et al., 2013; LOBO et al. 2015), further presented in Section 5.3, shows that the model was reasonably simulating sediment concentrations.

5.2 Validation and Model Performance Assessment

Streamflow simulated using the best set of calibrated parameter values, compared to observed streamflow is shown in Figure 5.1.

Figure 5.1. Simulated to observed streamflow.

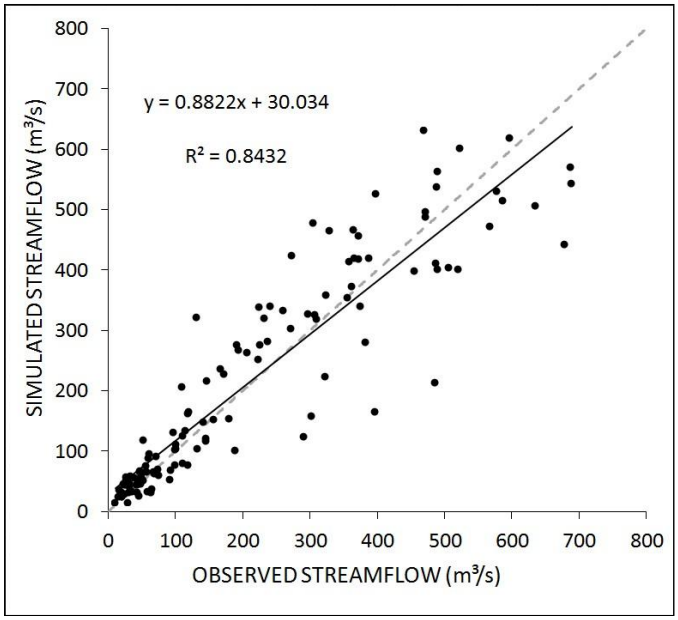

Statistics of performance calculated for the calibration and validation periods and for the entire series are shown in Table 5.2.

Table 5.2. Calibration and validation statistics.

	R^2	NSE	Classification	RSR	Classification	PBIAS (%)	Classification
Calibration period	0.84	0.84	Very good	0.40	Very good	3.56	Very good
Validation period	0.84	0.84		0.40		-18.46	Good
Entire series	0.86	0.84		0.40		-2.44	Very good

All model performance statistics, for the calibration (2001 to 2009), validation (2010 to 2012) and the entire period (2001 to 2012) fell within the recommended (MORIASI et al., 2007) thresholds (Table 4.8) indicating that the model was well calibrated and validated.

Finally, the LOWESS curve calculated for the relative differences between observed and simulated streamflow is plotted in Figure 5.2.

Figure 5.2. Relative differences between observed and simulated streamflow and the LOWESS curve.

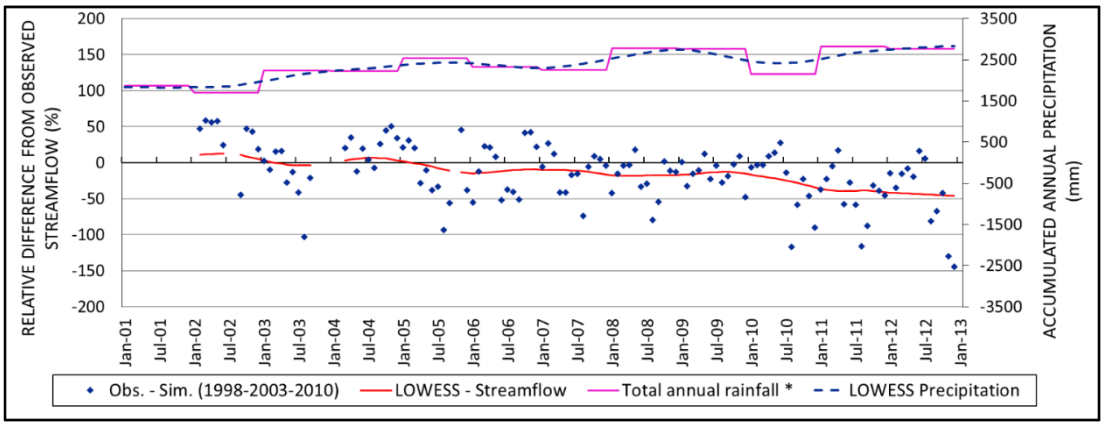

*Accumulated annual precipitation and LOWESS Precipitation are plotted on the secondary scale.

The LOWESS curve indicates that the model tends to underestimate streamflow in the beginning of the series (positive LOWESS) and to overestimate the streamflow in the end of the series (negative LOWESS).

It is not possible to establish a clear relation between the detected model trend and the land cover change, once no marked changes are observed in LOWESS curve on the land cover change dates (01/01/2003, 01/01/2010). On the other hand, annually accumulated precipitation trending seems to follow the trending detected in the LOWESS curve. As in the beginning of the series (2001 and 2002), annual accumulated precipitation was lower than in other years, simulated streamflow was also lower (positive streamflow LOWESS). Moving on to the end of the series, annual accumulated precipitation increased and was higher in the years of 2008, 2009, 2011 and 2012, when simulated streamflow was also higher (negative streamflow LOWESS). Thus, precipitation trending may be associated to the model trending.

This analysis suggests that precipitation data used in this study may be biased, leading to a precipitation increase throughout the series. However, as stated in section 4.3.4, no systematic error was detected when comparing precipitation estimates to *in situ* records.

Lastly, the model trend detected with LOWESS was assumed insufficient to jeopardize the study, since the trending seems to be related to precipitation data and does not seem to be associated with the land cover changes. Therefore, the detected trend in the model does not impact the analysis on the effects of land cover changes on sediment concentration in Crepori River, since the precipitation series that forces the simulations is the same for all land cover scenarios simulations. Furthermore, although there are large absolute values of relative difference throughout the series, the error index (PBIAS) used to assess the predictions' average relative deviations was considered 'good' for the validation period (the same period with the largest relative differences plotted in Figure 5.2) and 'very good' for the entire series simulations. Nevertheless, the detected trend will be considered in the results analysis of this study, as necessary.

5.3 Simulation of Scenarios and Comparison Between SWAT-Simulated Sediment Concentration and TSS Estimated by Lobo et al. (2015)

After calibration and validation, the model was run for the scenarios of 1998-2003-2010, 1973, 2040, Total Forest and Total Bare Soil. Figure 5.3 shows the precipitation data used and the simulated hydrographs.

Figure 5.3. Precipitation and streamflow: Accumulated annual precipitation data plotted in the secondary scale, and Hydrographs of observed and simulated streamflow.

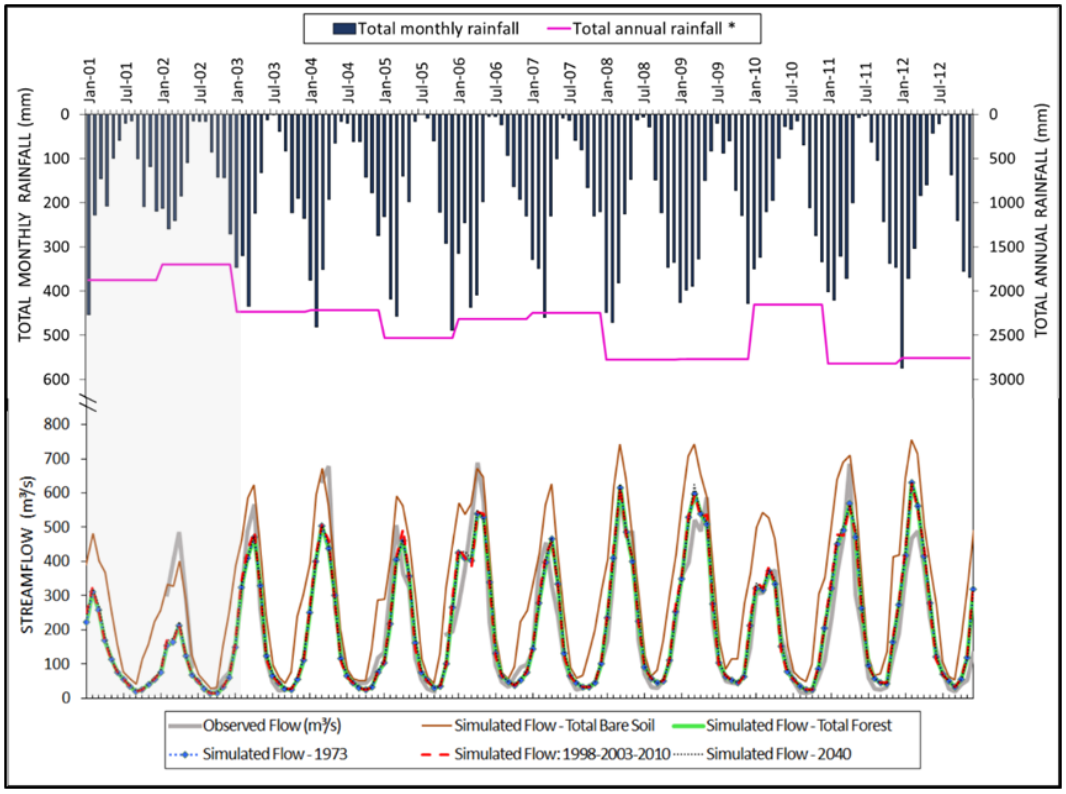

*Accumulated annual precipitation is plotted on the secondary scale.

In Figure 5.4, the percent differences between the streamflow simulated for the scenario of 1998-2003-2010 and the streamflow simulated for the scenarios of Total Forest, 1973, 2040 and Total Bare Soil are plotted.

Figure 5.4. Percent differences between streamflow simulated for the 1998-2003-2010 scenario and that simulated for the remaining scenarios.

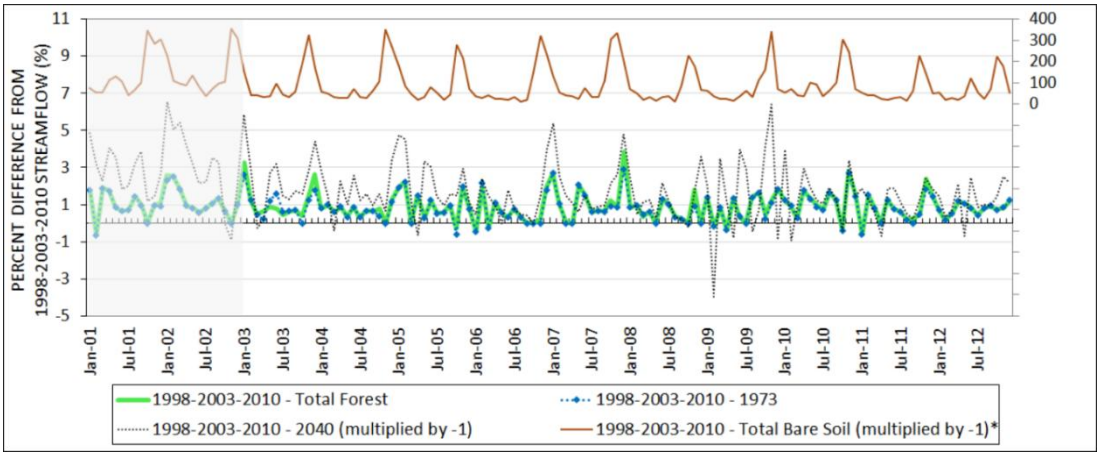

*Percent difference between streamflow simulated for 1998-2003-2010 scenario and Total Bare Soil scenario is plotted on the secondary scale.

Streamflow simulated for the scenario used during the calibration (1998-2003-2010), as well as for the 1973, 2040 and Total Forest scenarios were lower than the observed values for the first two years of simulations: 2001 and 2002 (Figure 5.3). As previously mentioned, SWAT requires a warm-up period to set the proper initial conditions for the simulations. The mismatch between observed and simulated streamflow, as well as the fact that the lowest peak values of simulated streamflow for the entire series and for all scenarios occurred in the first two years of the simulations (2001 and 2002), suggests that the length of the warm-up period used might not have been long enough for setting the appropriate initial conditions for the modelling. On the other hand, accumulated precipitation for 2001 and 2002 were lower than the accumulated precipitation of the remaining years of the series (Figures 5.2 and 5.3), what could also explain the low values of streamflow simulations for those years. Moreover, other sources of uncertainties on both, precipitation and streamflow data must be taken into account. Once the results simulated for 2001 and 2002 could be influenced by these issues, these first two years of simulations (2001 and 2002 – the faded area of the graph in Figures 5.3, 5.4, 5.5 and 5.6) were not included in the following analysis.

The hydrographs (Figure 5.3) show that the scenarios of Total Forest, 1973 and 1998-2003-2010 and 2040 generated similar streamflow results. Considering the trending detected in the model, simulation for the 1998-2003-2010 scenario does

not show a significant change in the streamflow pattern throughout the series, which can be explained by the small change in land cover area in this period, when compared to the entire watershed area (approximately 3% of Crepori basin area suffered land cover changes from 1998 to 2012). This suggests that for the scale of the modelling performed in this study, the land cover changes on Crepori river basin from 1998 to 2012 were not sufficient to influence the total streamflow.

However, in a more extreme deforestation scenario, the land cover changes effectively affected water discharge. Total Bare Soil hydrographs (Figure 5.3) show that the simulated streamflow is higher than observed streamflow for this scenario on both, dry and wet periods. In Figure 5.4 it is possible to notice that the reduction of forested areas tends to increase the streamflow (positive percent differences). This can be explained by the fact that with less forested areas, interception is reduced and water infiltration in the soil is also impaired. Thus, more water is available for the runoff process, which can quickly increase streamflow. The increase of streamflow in the 2040 and Total Bare Soil scenario concur with trending of increase in water discharge due to deforestation, detected in published studies (COSTA el at., 2003; COE et al., 2009; 2011; LIMA et al., 2014; PANDAY et al., 2015; DIAS et al., 2015; SOUZA-FILHO et al., 2016), demonstrating the influence of the forest cover on the water discharge.

The effect of the land cover change is more evident in the simulations of sediment concentration, as each scenario led to noticeably different results (Figure 5.5).

Figure 5.5. Simulated, estimated and measured sediment concentrations distribution over the period from 2001 to 2012.

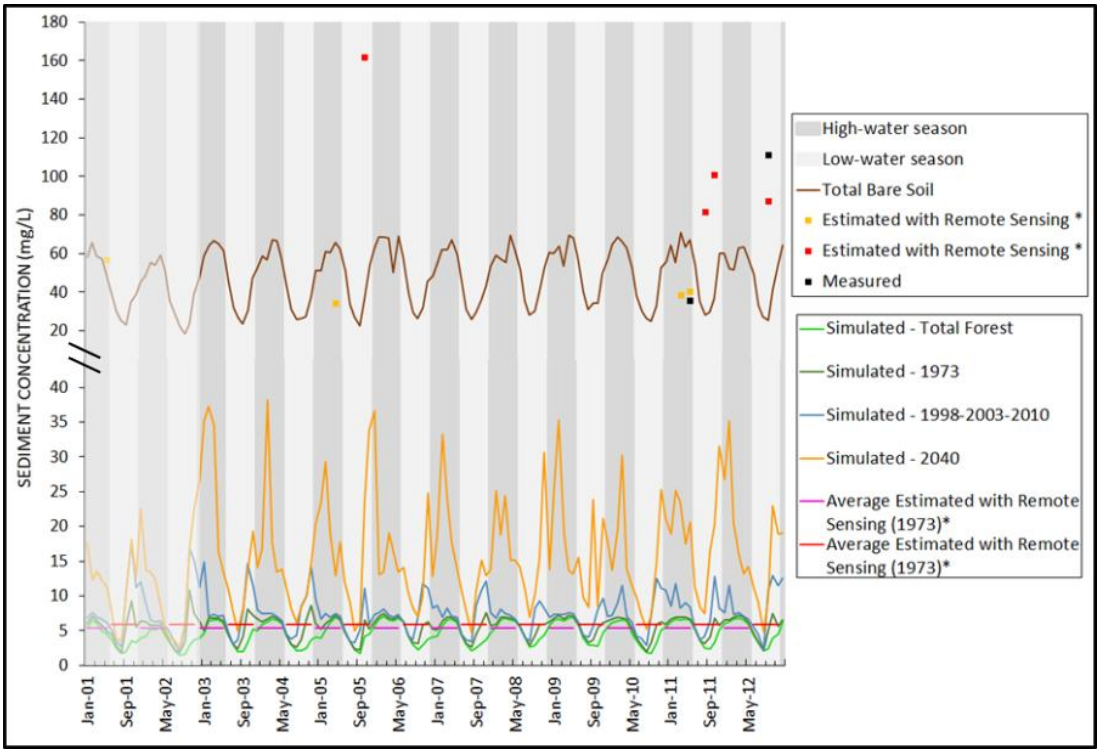

* Sediment concentrations measured or estimated by Lobo et al. (2015).
"Total Bare Soil", “Estimated with Remote Sensing” and “Measured” are plotted in the secondary scale.

The value of 0.06 was used for channel erodibility factor (CH_COV1) and 1 was used for channel cover factor (CH_COV2), whereas the values of 0.0001 and 1 were used for parameters related to deposition processes in the river (SPCON and SPEXP, respectively). These parameter values are related to low sediment concentration in the water, representing channels with good resistance to erosion and low values of maximum sediment that can be transported by the stream (ARNOLD et al., 2012a).

These parameter values were not adjusted under a calibration procedure considering long time series of *in situ* sediment concentration data and therefore, they represent a source of uncertainty in the model. Nevertheless, they were assumed to be appropriate for this study, since the Crepori River have the natural character of waters with low sediment concentration, classified as a clear water river (GIBBS, 1967; JUNK, 1997; DEVOL; HEDGES, 2001), presenting rocks and gravel as the main materials of its bank and riverbed (ICMBio, 2009), and

because sediment concentration simulated for 1973 scenario using these parameter values were similar to those estimated by Lobo et al. (2015) for the same year.

Simulated sediment concentration increased from the Total Forest towards the 1973, 1998-2003-2010, 2040 and Total Bare Soil scenarios.

For the 1973 scenario, the simulated sediment concentration varied between 2.0 mg/L and 8.6 mg/L, with averages of 6.3 and 4.7 mg/L for the high and low-water level season, respectively. For this same year, using remote sensing techniques, Lobo et al. (2015) estimated sediment concentration of 5.38 and 5.93mg/L for the high and low-water season, respectively. The differences between simulated and estimated sediment concentrations for 1973 can be explained by the fact that sediment concentration simulation in the 1973 scenario was performed using precipitation data from the period from 1998 to 2012, whereas, when using remote sensing techniques, Lobo et al. (2015) estimated sediment concentration driven by the actual precipitation from 1973. Moreover, although in 1973 there were only a few and small gold mining sites at Crepori, the activities from these sites could be already impacting water quality.

Lastly, it is also worth stating that sediment concentration estimated by Lobo et al. (2015) for 1973 were retrieved using images generated by the Landsat Multispectral Scanner System (MSS) sensor, whose radiometric features such as coarse radiometric resolution (6 bit) and wide spectral bands (minimum of 100 nm) (NASA, 2017) are known to cause larger uncertainties to the estimates of water optically active components (CURRAN; NOVO, 1988).

Despite the differences between simulated sediment concentration and those estimated by Lobo et al. (2015), in average, these values are of comparable magnitudes. Thus, it is reasonable to assume that the model simulates sediment concentration satisfactorily, disregarding the gold mining effects.

Simulation of Total Forest scenario generated sediment concentrations ranging from 1.7 mg/L to 7.1 mg/L. Even though the Total Forest is a hypothetical scenario that does not include native sparse vegetation (Open Ombrophilous Forest) detected at Crepori basin (ICMBIO, 2010), sediment concentration

derived from this scenario concur with background concentration found by Costa et al. (2013) and Telmer et al. (2006) (1.60 and ~7 mg/L) in the Tapajós river, upstream sediment plumes caused by gold mining sites. Lastly, the sediment concentration simulated for the scenarios of 1973 and Total Forest concur with the fact that in pristine conditions, the waters in this region have low sediment concentration, once it is located at the Precambrian shield, characterized by old and highly leached rocks (GIBBS, 1967).

In the 1998-2003-2010 scenario, sediment concentrations varied from 2.3 to 14.9 mg/L, whereas in the 2040 scenario the variation was between 4.7 and 38.2 mg/L and in the Total Bare Soil scenario, sediment concentration reached 22.6 to 70.9 mg/L.

Overall, the reduction of 2.82% on forest covered area (from 99.47% of the watershed in the Total Forest scenario to 96.65% of the watershed in 1998-2003-2010 scenario) was sufficient to increase the minimum and maximum simulated sediment concentration by 32.95% (from 1.7 mg/L to 2.3 mg/L) and 111.05% (from 7.1mg/L to 14.9 mg/L), respectively. In the 2040 scenario, the reduction of 7.28% of forest covered area (from 99.47% in the Total Forest scenario to 92.19 in the 2040 scenario) led to an increase in minimum and maximum sediment concentrations of 2.7-fold (from 1.7 mg/L to 4.7 mg/L) and 5.4-fold (from 7.1 mg/L to 38.2 mg/L) respectively. With the maximum reduction on forest coverage, the scenario of Total Bare Soil led to an increase of 13-fold (from 1.7 mg/L to 22.6 mg/L) and 10-fold (from 7.1 mg/L to 70.9 mg/L), in the minimum and maximum values, respectively.

In general, the increase in bare soil area leads to the increase in sediment concentration, due to the increased erosion of the landscape (DUNNE; LEOPOLD, 1978; BRUIJNZEEL, 1990). However, this relation is limited by the watershed characteristics, such as slopes and soil type, represented in Equation 3.2.

Regarding seasonality, sediment concentration peaks are observed during the low-water season for the scenarios of 1998-2003-2010 and 1973 (Figure 5.5). These peaks usually occur in the months of October and November, when the rainy

season starts but the water level in the river is still low. To better understand the occurrence of these peaks, Figure 5.6 illustrates the water and sediment yield and the sediment concentration for each scenario.

Figure 5.6. Sediment and water yield and the sediment concentration for each scenario.

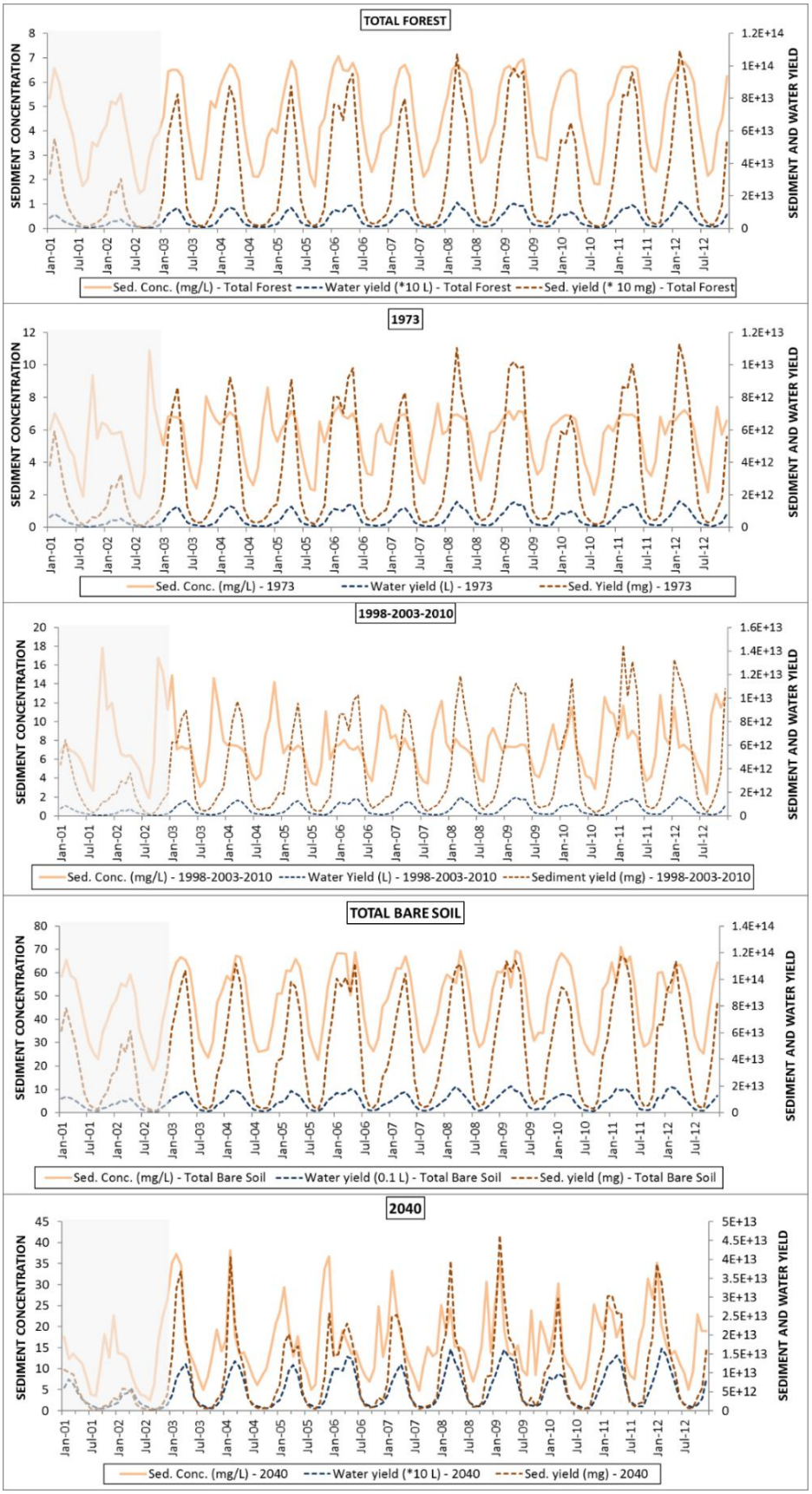

Since the soil erosion caused by precipitation modulates sediment yield, when the rainy season starts (around October and November), sediment yield increases. As the water level, and therefore, the water volume, in the river is still low in October and November, the higher amount of sediment yield combined with the low volume of water in the river results in high sediment concentration in this period (Figure 5.6).

Although in the high-water season precipitation rates are higher, leading to higher sediment yield, sediment concentration is lower than these peaks due to the higher volume of water in the river. Conversely, the peaks of sediment concentration in the low-water seasons are not observed in the scenarios of Total Forest and Total Bare Soil (Figure 5.5).

Because the Total Forest scenario presents all the basin's soil covered by the forest, even though the precipitation rates start to increase at the end of the low-water season, the precipitation rates in this period are not sufficient to significantly increase erosion and consequently, the sediment yield. In the high-water season, however, sediment concentration increases as a result of higher precipitation rates leading to relatively higher levels of erosion.

For the 2040 and for the Total Bare Soil scenarios, the resulting sediment concentration is a more direct response to the precipitation rates, since in these scenarios the bare soil areas are larger and considering that these areas are very near the river. Thus, even though the precipitation rates start to increase the sediment yield at the end of the low-water season, the sediment yield in the high-water season is even higher (Figure 5.6). Thus, the sediment concentration peaks occur during the high-water season. For the remaining months of the low-water season, sediment concentration is lower than in high-water season for all scenarios (Figure 5.5). Moreover, disregarding the peaks of sediment concentration in the low-water season, all scenarios led to high sediment concentration during the months of the high-water level, and low sediment concentration in most of low-water level months (Figure 5.5).

This overall dynamic is exactly the opposite of estimated sediment concentration dynamic caused by gold mining activities (BEZERRA et al., 1998; LOBO et al.,

2015). According to the authors, higher sediment concentrations occur during the low-water season due to the intensification of gold mining activities. As SWAT was applied without simulating the gold mining activities, the seasonality of simulated sediment concentration is a response to the precipitation rates combined with the land cover in each scenario.

Simulated sediment concentration for the scenarios of 1998-2003-2010 and Total Bare Soil are compared to Lobo et al. (2015) results in Table 5.3.

Table 5.3. Comparison between sediment concentrations simulated from 1998-2003-2010 and Total Bare Soil scenario and those estimated by Lobo et al. (2015).

	Simulated Sediment Concentrations (mg/L)			**Estimated Sediment Concentrations* (mg/L)**
	1998-2003-2010 Scenario	**2040**	**Total Bare Soil**	**1997-2012 Period**
Average (high water period)	7.6	19	59.4	52.64
Average (low water period)	7	14	37.1	117.44
Maximum	14.9	38.2	70.9	231.29
Minimum	2.3	4.7	22.6	34.2
	Simulated to Estimated Sediment Concentrations Ratio (%)			
Average (high water period)	14	36	113	-
Average (low water period)	6	12	32	-
Maximum	6	17	31	-
Minimum	7	14	66	-
Maximum % of Bare Soil area at the watershed	0.91	1.78	100	-

* Estimates from Lobo et al. (2015).

Sediment concentration simulated in the scenarios of 1998-2003-2010, 2040 and Total Bare Soil were lower than the concentration estimated by Lobo et al. (2015) (Table 5.3), for both high and low-water seasons. The only exception is for the

Total Bare Soil scenario results on the high-water season (Table 5.3), where the ratio between simulated and estimated sediment concentration is 113%, which means that sediment concentration simulated by the model is 13% higher than the concentration estimated by Lobo et al. (2015). Although this result shows Total Bare Soil scenario leading to higher sediment concentration than that sediment concentration estimated by Lobo et al. (2015), it is worth noting that in the Total Bare Soil scenario, 100% of the Crepori basin is without any soil cover, whereas the proportion of bare soil area at the Crepori basin for the period when Lobo et al. (2015) conducted the estimates was about 0.91% (Table 5.3).

The comparison between simulations of 1998-2003-2010 scenario and sediment concentration estimated by Lobo et al. (2015) indicate that in average, 14% of the sediment concentration estimated by Lobo et al. (2015) for high water season was caused by the land cover changes, whereas this proportion was of 6%, in average, for the low water period. Finally, the simulation results for the 2040 scenario compared to the sediment concentration estimated by Lobo et al. (2015) shows that even the steady increase in bare soil areas for the next 30 years would result in less sediment concentration in Crepori River than that already measured or estimated, if gold mining activity is not considered. This indicate the severity of gold mining techniques impacts on the water resources.

Disregarding seasonality, both 1998-2003-2010, 2040 and Total Bare Soil scenarios led to simulated sediment concentrations lower than concentrations estimated and measured by Lobo et al. (2015), demonstrating that the effects of gold mining activities on the Crepori river water quality may be greater than the impacts of complete soil exposure in the basin.

6 FINAL CONSIDERATIONS AND CONCLUSIONS

SWAT was shown to be a feasible tool to successfully simulate streamflow (NSE = 0.84, PBIAS = -2.44%, RSR = 0.40) and sediment concentrations in Crepori River basin, delivering good results. Even though the model could not be calibrated for sediment concentration, the comparison between sediment concentration simulated in this work and those estimated by Lobo et al. (2015) indicates that the model can reasonably simulate this variable.

This study shows that from 2001 to 2012, the land cover change (~3% of Crepori Basin area) caused only a noticeable impact on water quality whereas no impact was perceived in the streamflow regime. Sediment concentration gradually increased, following the increase of deforested areas.

The simulated baseline of sediment concentration in pristine condition demonstrates the clear-water character of Crepori River, with sediment concentration ranging from 1.7 to 7.1 mg/L, whereas the simulated sediment concentration in the condition of complete soil exposure indicates that the upper limit of sediment concentration in Crepori basin due to land cover change would be up to 70.9 mg/L.

From the comparison between simulated sediment concentration and Lobo et al. (2015) results, this study shows that in average, 14% of sediment concentration estimated in Crepori River in the high-water season was generated by sheet erosion, whereas this proportion is of 6% in low-water season, when gold mining activities are intensified. Furthermore, it can be concluded that gold mining activities may be already causing a higher impact on Crepori River water quality than the hypothetical scenario of complete soil exposure considered in this study. And finally, this study indicates that the techniques used in gold mining are the main responsible for the large increase in sediment concentration in Crepori River, since even the steady increase of bare soil areas, in the 2040 scenario, is not sufficient to equal the sediment concentration that have been already measured or estimated in the River.

To improve the reliability of this work regarding sediment simulations, further studies, such as modelling sediment yielded only by gold mining activity, and

considering the uncertainties involved in the simulations are still needed. Enhancement of the *in situ* system for monitoring meteorological, hydrological and water quality variables in the study area are also necessary to improve reliability of further analysis. Data provided by the announced new soil survey effort, the Brazilian National Soil Program"Programa Nacional de Solos do Brasil" (PronaSolos) (POLIDORO et al., 2016) should also be considered in further modelling studies as this new soil dataset might improve both hydrological and water quality modelling.

By using data directly or indirectly derived from remote sensing as inputs in SWAT, this study demonstrates the importance and feasibility of remote sensing to overcome data scarcity in poorly-monitored regions. Thus, the combination of distributed and conceptual hydrological model with GIS and remote sensing data represent a feasible tool for understanding and evaluating the impacts of land cover changes on water resources in the Amazonian region.

Finally, the use of recently-released remote sensing and reanalysis products and data are recommended in further studies as their different spatial and temporal resolutions as well as more accurate estimates, can improve modelling performance in data-scarce regions.

REFERENCES

ABBASPOUR, K.C. **SWAT-CUP:** SWAT calibration and uncertainty programs - a user manual. Dübendorf, Switzerland: Eawag, 2015. 103p.

ABBOTT, M.B.; BATHURST, J.C.; CUNGE, J.A.; O'CONNELL, P.E.; RASMUSSEN, J. An introduction to the European Hydrological System - Systeme Hydrologique Europeen, "SHE", 2: structure of a physically-based, distributed modelling system. **Journal of Hydrology**. v.87, n.1-2, p. 67-77, 1986.

ABBOTT, M.B.; REFSGAARD, J.C. **Distributed hydrological modelling**. Dordrecht, Netherlands: Kluwer Academic Publishers, 1996. v.22, 336p. ISBN: 0-7923-4042-6.

AHUJA, I.R.; NANEY, J.W.; GREEN, R.E.; NIELSEN, D.R. Macroporosity to characterize spatial variability of hydraulic conductivity and effects of land management. **Soil Science Society of America Journal**. v. 48, p. 699-702, 1984.

ALLEN, R.G. A Penman for all seasons. **Journal of Irrigation and Drainage Engineering**. ASCE, v.112, n.4, p. 348-368, 1986.

ALLEN, R.G. JENSEN, M.E.; WRIGHT, J.L.; BURMAN, R.D. Operational estimates of evapotranspiration. **Agronomy Journal**. v.81, p. 650-662, 1989.

ALVAREZ-BERRÍOS, N.L.; AIDE, T.M. Global demand for gold is another threat for tropical forests. **Environmental Research Letters**. v.10, n.1, 2015.

AGÊNCIA NACIONAL DE ÁGUAS (ANA). **Daily streamflow database**. Available at [http://www.snirh.gov.br/hidroweb/]. Accessed in Apr/2016a.

AGÊNCIA NACIONAL DE ÁGUAS (ANA). **Daily precipitation database**. Available at [http://www.snirh.gov.br/hidroweb/]. Accessed in Apr/2016b.

ARAÚJO NETO, H. **Perfil do ouro**. Brasília: Ministério de Minas e Energia, 2009.

ARNOLD, J.G.; SRINIVASAN, R.; MUTTIAH, R.S.; WILLIAMS, J.R. Large area hydrologic modeling and assessment part I: model development. **Journal of American Water Resources Association**. v.34, n.1, p.73-89,1998.

ARNOLD, J.G.; KINIRY, J.R.; SRINIVASAN, R.; WILLIAMS, J.R.; HANEY, E.B.; NEITSCH, S.L. **Soil and water assessment tool:** input/output documentation. Version 2012. 2012a.

ARNOLD, J. G.; MORIASI, D. N.; GASSMAN, P. W.; ABBASPOUR, K.C.; WHITE, M.J.; SRINIVASAN, R.; SANTHI, C.; HARMEL, R.D.; van GRIENSVEN, A.; van LIEW, M.W.; KANNAN, N.; JHA, M.K. Swat: model use, calibration, and validation. **Transactions of the ASABE. 2012 American Society of Agricultural and Biological Engineers**. v. 55, p.1491–1508, 2012b. ISSN: 2151-0032.

AUERBACH, D.A.; EASTON, Z.M.; WALTER, M.T.; FLECKER, A.S.; FUKA, D.R. Evaluating weather observations and the Climate Forecast System Reanalysis as input for hydrologic modelling in the tropics. **Hydrological Processes**. v.30, n.19, p.3466-3477, 2016.

BAGNOLD, R.A. Bedload transport in natural rivers. **Water Resources Research**. v.13, p.303-312, 1977.

BAKER, T.J.; MILLER, S.N. Using the Soil and Water Assessment Tool (SWAT) to assess land use impact on water resources in an East African watershed. **Journal of Hydrology**. v. 486, p. 100-111, 2013.

BALZINO, M.; SECCATORE, J.; MARIN, T.; TOMI, G.; VEIGA, M.M. Gold losses and mercury recovery in artisanal gold mining on the Madeira River, Brazil. **Journal of Cleaner Production**. v.102, p. 370-377, 2015.

BEASLEY, R.P. **Erosion and sediment pollution control**. The Iowa State University Press, 1972. p.320.

BERTONI, J.; LOMBARDI NETO, F. **Conservação do solo**. 3. ed. Ícone,1990. p. 355.

BEZERRA, O.; VERÍSSIMO, A.; UHL, C. **Impactos da garimpagem de ouro na Amazônia Oriental**. Belém/PA: Imazon, 1998.

BIGGS, T.W.; DUNNE, T.; MARTINELLI, L.A. Natural controls and human impacts on stream nutrient concentrations in a deforested region of the Brazilian Amazon basin. **Biogeochemistry**. v.68, n.2.p.227-257, 2004.

BIRKINSHAW, S.J.; MOORE, P.; KILSBY, C.G.; O'DONNELL, G.M.; HARDY, A.J.; BERRY, P.A.M. Daily discharge estimation at ungauged river sites using remote sensing. **Hydrological Processes**. v.28, n.3, p.1043-1054, 2014.

BLAINSKI, E.; PORRAS, E.A.A.; GARBOSSA, L.H.P.; PINHEIRO, A. **Simulation of land use scenarios in the Camboriú River Basin using the SWAT model**. RBRH, 2017. v. 22.

BONUMÁ, N.B. **Modelagem do escoamento da produção de sedimentos e da transferência de fósforo em bacia rural no sul do Brasil**. Doctoral Thesis (Soil Sciences) – Federal University of Santa Maria, 2011.

BRASIL. Ministry of Agriculture. Pedological Research Division. **Levantamento de reconhecimento de solos de uma área prioritária da Rodovia Transamazônica entre Altamira e Itaituba**. Rio de Janeiro. Brasil, 1973. Technical report, n.34.

BRASIL. National Department of Mineral Production. Projeto RADAM**. Folha SB.21 Tapajós;** geologia, geomorfologia, solos, vegetação e uso potencial da terra. Rio de Janeiro, Brasil, 1975. v.7, 418p.

BRESSIANI, D.A.; GASSMAN, P.W.; FERNANDES, J.G.; GARBOSSA, L.H.P.; SRINIVASAN, R.; BONUMÁ, N.B.; MENDIONDO, E.M. Review of Soil and Water Assessment Tool (SWAT) applications in Brazil: Challenges and prospects. **International Journal of Agricultural and Biological Engineering**. v.8, n.3, p. 9-35, 2015.

BRUIJNZEEL, L.A. **Hydrology of moist tropical forests and effects of conversion: a state of knowledge review**. Paris: UNESCO, 1990.

CÂMARA, G., SOUZA, R.C.M., FREITAS, U.M., CASANOVA, M.A. SPRING: Processamento de imagens e dados georreferenciados. In: SIMPÓSIO BRASILEIRO DE COMPUTAÇÃO GRÁFICA E PROCESSAMENTO DE IMAGENS, 5., 1992, Águas de Lindoia, BR. **Anais...** São José dos Campos: INPE, 1992. p. 233-242. IBI: <6qtX3pFwXQZ3r59YD6/GP2PJ>. (INPE-6792-PRE/3165). Disponível em: <http://urlib.net/6qtX3pFwXQZ3r59YD6/GP2PJ>.

CARSEY, F.D. **Microwave remote sensing of sea ice**. American Geophysical Union, 1992.

CASTILHOS, Z.; RODRIGUES-FILHO, S.; CESAR, R.; RODRIGUES, A.P.; VILLAS-BÔAS, R.; DE JESUS, I.; LIMA, M.; FAIAL, K.; MIRANDA, A.; BRABO, E.; BEINHOFF, C.; SANTOS, E. Human exposure and risk assessment associated with mercury contamination in artisanal gold mining areas in the Brazilian Amazon. **Environmental Science and Pollution Research**. v.22, n.15, p. 11255-11264, 2015.

CENTRO DE TECNOLOGIA MINERAL (CETEM). **Décadas de garimpagem de ouro causam danos socioambientais na Província do Tapajós (PA)**. Verbete. 2013. Available in <http://verbetes.cetem.gov.br/verbetes/ExibeVerbete.aspx?verid=143>. Accessed in Jun/2017.

CAHETÉ, F.S. A Extração do Ouro na Amazônia e Implicações para o Meio Ambiente. **Novos Cadernos NAEA**, v.1, n.2. 2008

CHAHINE, M.T. The hydrological cycle and its influence on climate. **Nature**, v.359, n. 6394, p. 373-380, 1992.

CHEN, J.M.; CHEN, X.; JU, W.; GENG, X. Distributed hydrological model for mapping evapotranspiration using remote sensing inputs. **Journal of Hydrology**. v.305, n.1-4, p. 15-39, 2005.

CHIEW, F.H.S. Estimation of rainfall elasticity of streamflow in Australia. **Hydrological Sciences Journal.** v. 51, n. 4, p. 613-625, 2006.

CHOW, V.T. **Advances in hydroscience**. New York: Academic Press, Inc. v.11, p.437. ISBN: 0-12-021811-9.1978.

CLEVELAND, W.S. LOWESS: a program for smoothing scatterplots by robust locally weighted regression. **The American Statistician**. v.35, n.1, 1981.

CLEVELAND, W.S. Robust locally weighted regression and smoothing scatterplots. **Journal of the American Statistical Association**. v.74, p. 829-836, 1979.

COE, M.T.; COSTA, M.H.; SOARES-FILHO, B.S. The influence of historical and potential future deforestation on the stream flow on the Amazon River - land surface processes and atmospheric feedbacks. **Journal of Hydrology**. v.369, p. 165-174, 2009.

COE, M.T.; LATRUBESSE, E.M.; FERREIRA, M.E.; AMSLER, M.L. The effects of deforestation and climate variability on the streamflow of the Araguaia River, Brazil. **Biogeochemistry**. v.105, n.1, p. 119-131, 2011.

COLLISCHONN, B.; COLLISCHONN, W.; TUCCI, C.E.M. Daily hydrological modeling in the Amazon basin using TRMM rainfall estimates. **Journal of Hydrology**. v.360, p.207-2016. 2008.

COLLISCHONN, W.; DORNELLES, F. **Hidrologia para engenharia e ciências ambientais**. Porto Alegre: Associação Brasileira de Recursos Hídricos (ABRH), p. 336, 2013.

CORREA, J.C. Características físico-hídricas dos solos latossolo amarelo, podzólico vermelho-amarelo e podzol hidromórfico do estado do Amazonas. **Pesquisa Agropecuária Brasileira**. v.19, n.3, p. 347-360, 1984.

COSTA, J.E. Effects of agriculture on erosion and sedimentation in the Piedmont Province, Maryland. **Geological Society of America Bulletin**. v.86, n.9, p. 1284-1286, 1975.

COSTA, M.H.; BOTTA, A.; CARDILLE, J.A. Effects of large-scale changes in land cover on the discharge of the Tocantins River, Southeastern Amazonia. **Journal of Hydrology**. v.283, p. 206-217, 2003.

COSTA, M.H.; COHEN, W. **LBA-ECO CD-15 LAI and productivity data, km 67, Tapajós National Forest:** 2003 -2004. Dataset. Available online [http://daac.ornl.gov] from Oak Ridge National Laboratory Distributed Active Archive Centre, Oak Ridge, Tennessee, USA. 2013.

COSTA, M.H.; FOLEY, J.A. Water balance of the Amazon Basin: dependence on vegetation cover and canopy conductance. **Journal of Geophysical Research: Atmospheres**. v.102, n.D20, p.23973-23989, 1997.

COSTA, M.; LOBO, F.L.; TELMER, K.; NOVO, E.M.L.M. Effects of small-scale gold mining tailings on the underwater light field in the Tapajós River Basin, Brazilian Amazon. **Remote Sensing**. v.9, n.8, p.22-23. 2017.

COSTA, M.P.F.; NOVO, E.M.L.M.; TELMER, K.H. Spatial and temporal variability of light attenuation in large rivers of the Amazon. **Hydrobiologia**. v.702, n.1.p.171-190, 2013.

CREECH, C.T.; SIQUEIRA, R.B.; SELEGEAN, J.P.; MILLER, C. Anthropogenic impacts to the sediment budget of São Francisco River navigation

channel using SWAT. **International Journal of Agricultural and Biological Engineering**. v.8, n.3, p. 140-157, 2015.

CUARTAS, L. A.; TOMASELLA, J.; NOBRE, A.D.; NOBRE, C.A.; HODNETT, M.G.; WATERLOO, M.J.; OLIVEIRA, S.M.; von RANDOW, R.C.; TRANCOSO, R.;FERREIRA, M. Distributed Hydrological modelling of a Micro-scale rainforest watershed in Amazonia: Model evaluation and advances in calibration using the new HAND terrain model. **Journal of Hydrology**. v.462-463, p. 15-27, 2012.

CURRAN, P.J.; NOVO, E.M.L.M. The relationship between suspended sediment concentration and remotely sensed spectral radiance: a review. **Journal of Coastal Research**. v.4, n.3, p.351-368, 1988.

CURTARELLI, M.P.; RENNÓ, C.D.; ALCÂNTARA, E.H. Evaluation of the Tropical Rainfall Measuring Mission 3B43 product over an inland area in Brazil and the effects of satellite boost on rainfall estimates. **Journal of Applied Remote Sensing**. v.8, n.1, p. 083589-083589, 2014.

DEB, D.; BUTCHER, J.; SRINIVASAN, R. Projected hydrologic changes under mid-21st century climatic conditions in a sub-arctic watershed. **Water Resources Management**. v. 29, p. 1467-1487, 2015.

DEE, D.P.; BALMASEDA, M.; BALSAMO, G.; ENGELEN, R.; SIMMONS, A.J.; THÉPAUT, J.-N. Towards a Consistent Reanalysis of the Climate System. Bull. **American Meteorological Society**, 95, n.8, p. 1235-1248, 2014.

DE TROCH, F.P.; TROCH, P.A.; SU, Z. and LIN, D.S. Application of remote sensing for hydrological modelling. **In**: ABBOTT, M.B. & REFSGAARD, J.C. (eds). **Distributed Hydrological Modelling**. Cap.9. Dordrecht, Netherlands: Kluwer Academic Publishers. v.22, 336p. ISBN: 0-7923-4042-6, 1996.

DEVOL, A.H.; HEDGES, J.I. Organic matter and nutrients in the mainstem Amazon River.p.275-306**.** In: McClain, M.E.; VICTORIA, R.L.; RICHEY, J.E. (eds). **The Biogeochemistry of the Amazon Basin**. Oxford University Press. p.365, 2001.

DIAS, L.C.P.; MACEDO, M.N.; COSTA, M.H.; COE, M.T.; NEILL, C. Effects of land cover change on evapotranspiration and streamflow of small catchments in the Upper Xingu River Basin, Central Brazil. **Journal of Hydrology: Regional Studies**. v.4, part B, p.108-122, 2015.

DILE, Y.T.; DAGGUPATI, P.; GEORGE, C.; SRINIVASAN, R.; ARNOLD, J. Introducing a new open source GIS user interface for the SWAT model. **Environmental Modelling & Software**. v.85, p.129-138, 2016.

DOMENEGHETTI, A.; TARPANELLI, A.; BROCCA, L.; BARBETTA, S.; MORAMARCO, T.; CASTELLARIN, A.; BRATH, A. The use of remote sensing-derived water surface data for hydraulic model calibration. **Remote Sensing of Environment**. v.149, p.130-141, 2014.

DUAN, Q.; GUPTA, V.K.; SOROOSHIAN, S. Effective and efficient global optimization for conceptual rainfall-runoff model. **Water Resources Research**. v.28, p. 1015-1031, 1992.

DUNNE, T.; LEOPOLD, L.B. Water in environmental planning. **W.H. Freeman and Company, New York**. 1978.

DUNNE, T.; MERTES, L.A.K.; MEADE, R.J.; RICHEY, J.E. Exchanges of sediment between the floodplain and channel of the Amazon River in Brazil. **Geological Society of America Bulletin**. v.110, p. 450-467, 1998.

EUROPEAN CENTRE FOR MEDIUM-RANGE WEATHER FORECASTS (ECMWF). **Era Interim Daily Database**. Available at [http://apps.ecmwf.int/datasets/data/interim-full-daily/levtype=sfc/]. Accessed in Feb/2017.

EGLER, S.G.; RODRIGUES-FILHO, S.; VILLAS-BÔAS, R.C.; BEINHOFF, C. Evaluation of mercury pollution in cultivated and wild plants from two small communities of the Tapajós gold mining reserve, Pará State, Brazil. **Science of the Total Environment**. v.368, n.1, p.424-433, 2006.

EL-SWAIFY, S.A.; DANGLER, E.W.; ARMSTRONG, C.L. Soil erosion by water in the tropics. Research Extension Series. **University of Hawaii**. Honolulu, Hawaii. p.173. ISSN: 0271-9916, 1982.

EMPRESA BRASILEIRA DE AGROPECUÁRIA (EMBRAPA/FAO). **Caracterização físico hídrica dos principais solos da Amazônia Legal:** Volume I – Estado do Pará. Belém/PA, Brasil, 1991. Technical Report.

EMPRESA BRASILEIRA DE AGROPECUÁRIA (EMBRAPA/SNLCS). **Levantamento de reconhecimento de solos e aptidão agrícola das terras do Polo Carajás Estado do Pará**. Rio de Janeiro, Brasil, 1984. Research Bulletin n° 29.

ENCINAS, O.C. **Avaliação de processos erosivos na base de operações geólogo Pedro de Moura – Coari, AM**. Master Thesis. Agriculture in the Humid Tropic. Instituto Nacional de Pesquisas da Amazônia. 2011.

ESSAYAS, A.K.; WILLIAM, P.D.; ASSEFA, M.M.; TAMMO, S.S. Bathymetry, lake area and volume mapping: a remote-sensing perspective. In: Nile River Basin. **Springer International Publishing**. p. 253-267, 2014.

ESSOU, G.R.C.; BRISSETTE, F.; LUCAS-PICHER, P. The use of reanalysis and gridded observations as weather input data for a hydrological model: comparison of performances of simulated river flows based on the density of weather stations. **Journal of Hydrometeorology**. v18, n.2, p.497-513, 2017.

FAIAL, K.; DEUS, R.; DEUS, S.; NEVES, R.; JESUS, I.; SANTOS, E.; ALVES, C.N.; BRASIL, D. Mercury levels assessment in hair of riverside inhabitants of the Tapajós River, Pará State, Amazon, Brazil: fish consumption as a possible route of exposure. **Journal of Trace Elements in Medicine and Biology**. v.30, p.66-76, 2015.

FAJARDO, J.D.V.; FERREIRA, S.J.F.; MIRANDA, S.A.F.; MARQUES FILHO, A.O. Caracterísicas hidrológicas do solo saturado na Reserva Florestal Adolpho Ducke – Amazônia Central. **Revista Árvore**, v. 34, n. 4, p. 677-684, 2010.

FOOD AND AGRICULTURE ORGANIZATION OF THE UNITED NATIONS (FAO). **Soil erosion by water:** some measures for its control on cultivated lands. FAO. Rome, Italy. p. 284. ISBN 92-5-100474-9, 1965.

FARELLA, N.; LUCOTTE, M.; DAVIDSON, R.; DAIGLE, S. Mercury release from deforested soils triggered by base cation enrichment. **Science of The Total Environment**. v.368, n.1, p.19-29, 2006.

FARELLA, N.; LUCOTTE, M.; LOUCHOUARN, P.; ROULET, M. Deforestation modifying terrestrial organic transport in the Rio Tapajós, Brazilian Amazon. **Organic Geochemestry**. v.32, n.12, p. 1443-1458, 2001.

FEARNSIDE, P.M. Agriculture in Amazonia.. In: PRANCE, G.T.; LOVEJOY, T.E. (eds) **Key environments**: Amazonia.. Oxford, UK.: Pergamon Press, 1985. p. 393-418.

FEARNSIDE, P.M. Deforestation in Brazilian Amazonia: the effect of population and land tenure. **Ambio-Journal of Human Environment Research and Management**. v.22, n.8, p. 537-545, 1993.

FERNANDES, F.R.C.; ALAMINO, R.D.C.J.; ARAÚJO, E.R. **Recursos minerais e comunidade: impactos humanos, socioambientais e econômicos**. CETEM/MCTI. Rio de Janeiro, Brazil. 2014.

FERRANT, S.; BUSTILLO, V.; BUREL, E.; SALMON-MONVIOLA, J.; CLAVERIE, M.; JAROSZ, N.; YIN, T.; RIVALLAND, V.; DEDIEU, G.; DEMAREZ, V.; CESCHIA, E.; PROBST, A.; AL-BITAR, A.; KERR, Y.; PROBST, J.L.; DURAND, P.; GASCOIN, A. Extracting soil water holding capacity parameters of a distributed agro-hydrological model from high resolution optical satellite observations series. **Remote Sensing**. v.8, n.2, p.154, 2016.

FIGUEIREDO, L.F.; ALMEIDA, F.T.; ULIANA, E.M.; CASAVECCHIA, B.C.; NOGUEIRA, F.A.S. Avaliação da condutividade hidráulica saturada, em solos de diferentes classes texturais em uma bacia hidrográfica da Amazônia. In: CONGRESSO BRASILEIRO DE ENGENHARIA AGRÍCOLA – CONBEA, 45., 2016, Florianópolis-SC, Brasil. **Anais...** São Paulo: SBEA, 2016.

FISCH, G.; MARENGO, J.A.; NOBRE, C.A. Clima da Amazônia. **Climanálise: Boletim de monitoramento e análise climática**. Edição comemorativa de 10 anos. Cap. 3. Available in : < http://climanalise.cptec.inpe.br/~rclimanl/boletim/cliesp10a/fish.html> . Accessed in Feb/2016.

FORMAGGIO, A.R.; EPIPHANIO, J.C.N.; VALERIANO, M.M.; OLIVEIRA, J.B. Comportamento espectral (450-2450nm) de solos tropicais de São Paulo. **Revista Brasileira de Ciência do Solo**. Campinas, Brasil, v. 20, p. 467-474. 1996.

FUKA, D.R.; WALTER, M.T.; MACALISTER, C.; DEGAETANO, A.T.; STEENHUIS, T.S.; EASTON, Z.M. Using the Climate Forecast System Reanalysis as weather input data for watershed models. **Hydrological Processes**. v.28, n.22, p.5613-5623, 2014.

FUKUNAGA, D.C.; CECÍLIO, R.A.; ZANETTI, S.S.; OLIVEIRA, L. T.; CAIADO, M.A.C. Application of the SWAT hydrologic model to a tropical watershed at Brazil. **Catena**. v.125, p. 206-213, 2015.

GASSMAN, P.W.; REYES, M.R.; GREEN, C.H.; ARNOLD, J.G. The Soil and Water Assessment Tool: historical development, applications, and future research directions. Transactions of the ASABE. **American Society of Agricultural and Biological Engineers**. v.50, n.4, p. 1211-1250, 2007

GASSMAN, P. W.; SADEGHI, A. M.; SRINIVASAN, R. Applications of the SWAT Model Special Section: Overview and Insights. **Journal of Environmental Quality**, p. 1–8, 2014.

GIBBS, R.J. The Geochemistry of the Amazon River System: Part I. The Factors that Control the Salinity and the Composition and Concentration of the Suspended Solids. **Geological Society of America Bulletin**. v.78, n.10, p. 1203-1232, 1967.

GLOBAL WEATHER DATA. **Global Weather Data for SWAT**. https://globalweather.tamu.edu/. Accessed in Feb/2016.

GREENWOOD, P.; WALLING, D.; QUINE, TIMOTHY. The role of livestock-poached pasture as a sediment source. **EGU General Assembly Conference Abstracts**. v.17, 2015.

GRIMALDI, S.; LI, Y.; PAUWELS, V.R.N.; WALKER, J.P. Remote sensing-derived water extent and level to constrain hydraulic flood forecasting models: opportunities and challenges. **Surveys in Geophysics**. v.37, n.5, p.977-1034, 2016.

GUENTHER, M.; BOZELLI, R. Effects of Inorganic Turbidity on the Phytoplankton of an Amazonian Lake Impacted by Bauxite Tailings. **Hydrobiologia**. v.511, n.1, p. 151-159, 2004.

GUERRA, A.J.T. O início do processo erosivo. In: GUERRA, A.J.T.; SILVA, A.S.; BOTELHO, R.G.M. (orgs). **Erosão e conservação dos solos**: conceitos e aplicações. Ed.4. Rio de Janeiro**:** Bertrand Brasil. Cap. 1, p. 17-50, 2009.

GUPTA, H.V.; SOROOSHIAN, S.; YAPO, P.O. Status of automatic calibration for hydrologic models: Comparison with multilevel expert calibration. **Journal of Hydrologic Engineering**. v4, n.2, p. 135-143,1999.

HARGREAVES, G.L.; HARGREAVES, G.H.; RILEY, J.P. Agricultural benefits for Senegal River Basin. **Journal of Irrigation and Drainage Engineering**. v.111, n.2, p. 113-124, 1985.

HILL, W.R.; RYON, M. G.; SCHILLING, E.M. Light Limitation in a Stream Ecosystem: Responses by Primary Producers and Consumers. **Ecology**. v.76, n.4, p. 1297-1309, 1995.

HSU, K.L. & SOROOSHIAN, S. Satellite-based precipitation measurement using PERSIANN system. In: SOROOSHIAN, S.; HSU, K.L.; COPPOLA, E.; TOMASSETI, B.; VERDECCHIA, M.; VISCONTI, G. (eds). **Hydrological modeling and the water cycle:** coupling the atmospheric and hydrological models. v. 63. Springer Science & Business Media, 2009. p. 27-48. ISBN: 978-3-540-77842-4.

HUFFMAN, G.J.; ADLER, R.F.; BOLVIN, D.T./ GU, G.; NELKIN, E.J.; BOWMAN, K.P.; HONG, Y.; STOCKER, E.F.; WOLFF, D.B. The TRMM multisatellite precipitation analysis (TMPA): quasi-global, multiyear, combined-sensor precipitation estimates at fine scales. **Journal of Hydrometeorology**. v.8, p. 38-55, 2007.

HUNINK, J.E.; EEKHOUT, J.P.C.; DE VENTE, J.; CONTERAS, S.; DROOGERS, P.; BAILLE, A. Hydrological modelling using satellite-based crop coefficients: a comparison of methods at the basin scale. **Remote Sensing**. v.9, n.2, p.174, 2017.

BRAZILIAN INSTITUTE OF ENVIRONMENT AND RENEWABLE NATURAL RESOURCES (IBAMA). **Floresta Nacional do Tapajós -** plano de manejo. Brasília: IBAMA, Belterra. p.373, 2004.

BRAZILIAN INSTITUTE OF GEOGRAPHY AND STATISTICS (IBGE). **Mapa pedológico da Amazonia Legal 1:250.000**. Available in ftp://geoftp.ibge.gov.br/informacoes_ambientais/pedologia/vetores/escala_250_mil/amazonia_legal/. 2016. Accessed in Feb/2016.

CHICO MENDES INSTITUTE FOR BIODIVERSITY CONSERVATION (ICMBIO). **Plano de Manejo das Florestas Nacionais do Crepori, Jamanxim e Amana, Localizadas no Estado do Pará.** Product 4.1: Crepori FLONA Physical Environment Report. Curitiba, Brasil. 2009.

CHICO MENDES INSTITUTE FOR BIODIVERSITY CONSERVATION (ICMBIO). **Plano de manejo da Floresta Nacional do Crepori, Localizada no Estado do Pará**. Executive Report. Curitiba/PR, Brasil. 2010.

BRAZILIAN NATIONAL INSTITUTE OF METEOROLOGY (INMET). **Banco de dados meteorológicos para ensino e pesquisa**. Available in [http://www.inmet.gov.br/portal/index.php?r=bdmep/bdmep]. Accessed in Feb/2017.

BRAZILIAN NATIONAL INSTITUTE FOR SPACE RESEARCH (INPE). **PRODES Project**. http://www.obt.inpe.br/prodes/index.php. Accessed in 01/2017.

JENSEN, J.R. **Sensoriamento remoto do ambiente:** uma perspectiva em recursos terrestres/translated by José Carlos Epiphanio *et al*. São José dos Campos, SP, Brasil. 2009.

JULIAN, J.P.; TORRES, R. Hydraulic erosion of cohesive river banks. **Geomorphology**. v.76, p.193-206. 2006.

JULIEN, P. Y. **Erosion and sedimentation**. 1. ed. Cambridge University Press, 1998. 280p. ISBN 0-521-44237-0.

JUNK, W. J. General aspects of floodplain ecology with special reference to Amazonian floodplains. In: Junk, W. J. (ed.). **The Central Amazon Floodplain.** Berlin: Springer, 1997. p. 3-20.

KITE, G.W.; PIETRONIRO, A. Remote sensing applications in hydrological modelling. **Hydrological Sciences Journal**. v.41, n.4, p.563-591, 1996.

KROGH, S.A.; POMEROY, J.W.; MCPHEE, J. Physically based mountain hydrological modelling using reanalysis data in Patagonia. **Journal of Hydrometeorology**. v.16, p.172-193, 2015.

KUMMEROW, C.; BARNES, W.; KOZU, T.; SHIUE, J.; SIMPSON, J. The Tropical Rainfall Measuring Mission (TRMM) Sensor Package. **Journal of Atmospheric and Oceanic Technology**. v.15, p. 809-817, 1998.

LABRIÈRE, N.; LOCATELLI, B.; LAUMONIER, Y.; FREYCON, V.; BERNOUX, M. Soil erosion in the humid tropics: a systematic quantitative review. **Agriculture, Ecosystems and Environment**. v.203, p. 127-139, 2015.

LAL, R. **Soil erosion in the tropics:** principles and management. McGraw-Hill Inc., 1990.

LAMPARTER, G.; NOBREGA, R.L.B.; KOVACS, K.; AMORIM, R.S.; GEROLD, G. Modelling hydrological impacts of agricultural expansion in two macro-catchments in Southern Amazonia, Brazil. **Regional Environmental Change**. p. 1-13, 2016.

LAURENT, F.; RUELLAND, D. Modélisation à base physique de la variabilité hydroclimatique à l'échelle d'un grand bassin versant tropical. In: IAHS Publ. (Ed). **Global change:** facing risks and threats to water resources. Fez, Morocco, France. 2010. p. 474-484.

LAWRENCE, D.; VANDECAR, K. Effects of tropical deforestation on climate and agriculture. **Nature Climate Change**. v.5, n.1, p. 27-36, 2015.

LELIS, T.A.; CALIJURI, M.L. Modelagem hidrossedimentológica de bacia hidrográfica na região sudeste do Brasil, usando o SWAT. **Revista Ambiente & Água**. v.5, n.2, p.158-174, 2010.

LIMA, L.S.; COE, M.T.; SOARES-FILHO, B.S.; CUADRA, S.V.; DIAS, L.C.P.; COSTA, M.H.; LIMA, L.S.; RODRIGUES, H.O. Feedbacks between deforestation, climate, and hydrology in the Southwestern Amazon: implications for the provision of ecosystem services. **Landscape Ecology**. v.29, n.2, p. 261-274, 2014.

LIN, B.; CHEN, X.; YAO, H.; CHEN, Y.; LIU, M.; GAO, L.; JAMES, A. Analysis of landuse change impacts on catchment runoff using different time indicators based on SWAT model. **Ecological Indicators**. v. 58, p. 55-63, 2015.

LOBO, F.L.; COSTA, M.P.F.; NOVO, E.M.L.M. Time-series analysis of Landsat-MSS/TM/OLI images over Amazonian waters impacted by gold mining activities. **Remote Sensing of Environment**. v.157, p. 170-184, 2015.

LOBO, F.L.; COSTA, M.P.F.; NOVO, E.M.L.M.; TELMER, K. Distribution of Artisanal and Small-Scale Gold Mining in the Tapajós River Basin (Brazilian Amazon) over the Past 40 Years and Relationship with Water Siltation. **Remote Sensing**, v.8, n.7, 579, 2016.

LUZ, M.P.; BEEVERS, L.C.; CUTHBERTSON, A.J.S.; MEDERO, G.M.; DIAS, V.S.; NASCIMENTO, D.T.F. The mitigation potential of buffer strips for reservoir sediment yields: the Itumbiara hydroelectric power plant in Brazil. **Water**. v.8, n.11, p.489, 2016.

MAEDA, E.E.; FORMAGGIO, A.R.; SHIMABUKURO, Y.E.; KALEITA, A.L. Impacts of agricultural expansion on surface runoff: a case study of a river basin in the Brazilian Legal Amazon. **International Journal of Geoinformatics**. v.5, n.3, 2009.

MAISONNAVE, F.; PRADO, A. Megagarimpo ilegal provoca 'febre do ouro' e divide índios no Pará. **Folha de São Paulo: Folha Digital**. JUN/2017. Ambiente. Available in <http://www1.folha.uol.com.br/ambiente/2017/06/1891796-megagarimpo-ilegal-provoca-febre-do-ouro-e-divide-indios-no-para.shtml>. Accessed in Jun/2017.

MALHI, Y.; PEGORARO, E.; NOBRE, A.D.; PEREIRA, M.G.P.; GRACE, J.; CULF, A.D.; CLEMENT, R. Energy and water dynamics of a central Amazonian rain forest. **Journal of Geophysical Research: Atmospheres**. v.107, D20, n.861, 2002.

MELACK, J. M. Interactions of detrital particulates and plankton. **Hydrobiologia**. v.125, n.1. p. 209-220, 1985.

MOL, J.H.; OUBOTER, P.E. Downstream effects of erosion from small-scale gold mining on the instream habitat and fish community of a small neotropical rainforest stream. **Conservation Biology**. v.18, p.201-214, 2004.

MONTEIRO, J.A.F.; KAMALI, B.; SRINIVASAN, R.; ABBASPOUR, K.; GÜCKER, B. Modelling the effect of riparian vegetation restoration on sediment transport in a human-impacted Brazilian catchment. **Ecohydrology**. v.9, n.7, p.1289-1303, 2016.

MONTEITH, J.L. Evaporation and the environment. In: FOGG, G. E (ed.) **The state and movement of water in living organisms.** London, UK: Cambridge University Press, 1965. P. 205-234. 19th Symposia of the Society for Experimental Biology.

MONTEITH, J.L. Climate and the efficiency of crop production in Britain. **Philosophical Transactions of the Royal Society of London**, Ser. B. v.281, p.277-329, 1977.

MORADKHANI, H.; SOROOSHIAN, S. General Review of Rainfall-Runoff Modelling: Model Calibration, Data Assimilation, and Uncertainty Analysis. In: SOROOSHIAN, S.; HSU, K.L.; COPPOLA, E.; TOMASSETTI, B.; VERDECCHIA, M.; VISCONTI, G. (eds). **Hydrological modelling and the water cycle:** coupling the atmospheric and hydrological models. Springer Science & Business Media, 2009.. v.63, p.1-24. ISBN: 978-3-540-77842-4.

MORIASI, D.N.; ARNOLD, J.G.; van LIEW, M.W.; BINGNER, R.L.; HARMEL, R.D.; VEITH, T.L. Model evaluation guidelines for systematic quantification of accuracy in watershed simulations. **Transactions of the ASABE**. v.50, n.3, p.885-900, 2007.

MORIASI, D.N.; WILSON, B.N.; DOUGLAS-MANKIN, K.R.; ARNOLD, J.G.; GOUDA, P.H . Hydrologic and Water Quality Models: Use, Calibration, and Validation. In: Transactions of the ASABE. **2012 American Society of Agricultural and Biological Engineers**. V.55, n.4, p. 1241-1247.ISSN: 2151-0032. 2012.

MUKOLWE, M.M.; YAN, K.; DI BALDASSARRE, G.; SOLOMATINE, D.P. Testing new sources of topographic data for flood propagation modelling under structural, parameter and observational uncertainty. **Hydrological Sciences Journal**. v.61, n.9, p. 1707-1715, 2016.

MUTTIAH, R.S.; WURBS, R.A. Scale-dependent soil and climate variability effects on watershed water balance of the SWAT model. **Journal of Hydrology**. v. 256, p. 264-285, 2002.

AMERICAN NATIONAL AERONAUTICS AND SPACE ADMINISTRATION (NASA). **Tropical Rainfall Measuring Mission – TRMM:** senior review proposal. NASA. 2007. Available in:< http://pmm.nasa.gov/sites/default/files/document_files/TRMMSenRevProp_v1.2.pdf>. Accessed in 18/01/2016a.

AMERICAN NATIONAL AERONAUTICS AND SPACE ADMINISTRATION (NASA). Iniciativa: BRAUN, S.A.; PIERCE, H.F. **NASA Facts:** TRMM instruments **–** TRMM microwave imager. 29/06/2011. Available in: < http://trmm.gsfc.nasa.gov/overview_dir/tmi.html> . Accessed in 21/01/2016b.

AMERICAN NATIONAL AERONAUTICS AND SPACE ADMINISTRATION (NASA). Iniciativa: BRAUN, S.A.; PIERCE, H.F**. NASA Facts: TRMM Instruments –** precipitation radar. 29/06/2011. Available in: <http://trmm.gsfc.nasa.gov/overview_dir/pr.html>. Accessed in 21/01/2016c.

AMERICAN NATIONAL AERONAUTICS AND SPACE ADMINISTRATION (NASA). Iniciativa: BRAUN, S.A.; PIERCE, H.F. **NASA Facts: TRMM Instruments –** visible and infrared scanner. 29/06/2011. Available in: < http://trmm.gsfc.nasa.gov/overview_dir/virs.html>. Accessed in 21/01/2016d.

AMERICAN NATIONAL AERONAUTICS AND SPACE ADMINISTRATION (NASA). Iniciativa: KEMPLER, S.; HEGDE, M. **Mirador:** data access made simple – product description. 06/10/2015. Available in: <http://mirador.gsfc.nasa.gov/collections/TRMM_3B42__007.shtml >. Accessed in 21/01/2016e.

AMERICAN NATIONAL AERONAUTICS AND SPACE ADMINISTRATION (NASA). **TRMM Data from the Goddard Earth Sciences (GES) DISC DAAC:** Tropical Rainfall Measuring Mission (TRMM). NASA. 2002. Available in:< http://ntrs.nasa.gov/archive/nasa/casi.ntrs.nasa.gov/20040045305.pdf>. Accessed in 18/01/2016f.

AMERICAN NATIONAL AERONAUTICS AND SPACE ADMINISTRATION (NASA). **TRMM 3B42 Daily v.7 pro**duct. Available in <https://disc.sci.gsfc.nasa.gov/SSW/#keywords=>. Accessed in Feb/2016g.

AMERICAN NATIONAL AERONAUTICS AND SPACE ADMINISTRATION (NASA). **Landsat Science:** the multispectral scanner system. Available in <https://landsat.gsfc.nasa.gov/the-multispectral-scanner-system/>. Accessed in May/2017.

NATIONAL SPACE DEVELOPMENT AGENCY OF JAPAN (NASDA). **TRMM data users handbook**. NASDA – Earth Observation Center. 2001. Available in:< http://www.eorc.jaxa.jp/TRMM/document/text/handbook_e.pdf>. Accessed: Jan/2016.

NASH, J.E.; SUTCLIFFE, J.V. River flow forecasting through conceptual models: Part 1. A discussion of principles. **Journal of Hydrology**. v10, n.3, p. 282-290, 1970.

NEITSCH, S. L.; ARNOLD, J. G.; KINIRY, J. R.; WILLIAMS, J. R. **Soil & water assessment tool -** theoretical documentation version 2009. Texas Water Resources Institute, TR-406, p.647, 2011.

NIE, W.; YUAN, Y.; KEPNER, W.; NASH, M.S.; JACKSON, M.; ERICKSON, C. Assessing impacts of landuse and landcover changes on hydrology for the upper San Pedro watershed. **Journal of Hydrology**. v. 407, p. 105-114, 2011.

NIJZINK, R.C.; ALMEIDA, S.; PECHLIVANIDIS, I.; CAPELL, R.; GUSTAFSSON, D.; ARHEIMER, B.; FREER, J.; HAN, D.; WAGENER, T.; SLEZIAK, P.; PARAJKA, J.; SAVENIJE, H.; HRACHOWITZ, M. The added value of remote sensing products in constraining hydrological models. EGU General Assembly, 19., 2017, Vienna, Austria. **Proceedings…** Vienna: EGU, 2017.

NOBRE, C.A.; SELLERS, P.J.; SHUKLA, J. Amazonian deforestation and regional climate change. **Journal of Climate**. v.4, n.10, p.957-988, 1991.

AMERICAN NATIONAL RESEARCH COUNCIL (NRC). National Academies Interim Report, 2006: assessment of the benefits of extending the tropical measuring mission: a perspective from the research and operations communities. Committee on the Future of the Tropical Rainfall Measuring Mission, National

Research Council. p. 116. ISBN: 0-309-66357-1. 2006. Available in: <www.nap.edu/catalog/11195.html>. Accessed in Jan/2016.

OESTREICHER, J.S.; LUCOTTE, M.; MOINGT, M.; BÉLANGER, É.; ROZON, C.; DAVIDSON, R.; MERTENS, F.; ROMAÑA, C.A. Environmental and anthropogenic factors influencing mercury dynamics during the past century in floodplain lakes of the Tapajós River, Brazilian Amazon. **Archives of Environmental Contamination and Toxicology**. v.72, n.1, p.11-30, 2017.

OLIVEIRA, G.; MORAES, E.C.; SHIMABUKURO, Y.E.; RUDORFF, B.F.T.; ALVALÁ, R.C.S.; SANTOS, T.V. Avaliação do albedo em diferentes tipos de uso e cobertura da terra no sudoeste da Amazônia. ***Anais XVI SBSR***. Foz do Iguaçu, Brasil. 2013.

OLIVEIRA, L.T. **Aplicação do modelo SWAT para simular vazões em uma bacia hidrográfica em Aracruz, ES**. Masters Thesis (Masters in Forestry Sciences). Federal University of Espírito Santo. 2014.

OTTLÉ, C.; VIDAL-MADJAR, D. Assimilation of soil moisture inferred from infrared remote sensing in a hydrological model over the HAPEX-MOBILHY region. **Journal of Hydrology**. v.158, n.3-4, p.241-264, 1994.

PANDAY, P.K.; COE, M.T.; MACEDO, M.N.; LEFEBVRE, P.; CASTANHO, A.D.A. Deforestation offsets water balance changes due to climate variability in the Xingu River in eastern Amazonia. **Journal of Hydrology**. v.523, p. 822-829, 2015.

PAI, N.; SARASWAT, D. SWAT2009_LUC: A tool to activate the land use change module in SWAT 2009. **Transactions of the ASABE**. v.54, n.5, p. 1649-1658, 2011.

PARROTTAS, J.A.; KNOWLES, O.H. Restoring tropical forests on lands mined for bauxite: examples from the Brazilian Amazon. **Ecological Engineering**. v.17, n.2-3, p. 219-239, 2001.

PASSOS, C.J.; MERGLER, D.; LEMIRE, M.; FILLION, M.; GUIMARÃES, J.R. Fish consumption and bioindicators of inorganic mercury exposure. **Science of the Total Environment**. v.373, n.1, p.68-76, 2007.

PEÑA-ARANCIBIA, J.L.; MAINUDDIN, M.; KIRBY, J.M.; CHIEW, F.H.S.; MCVICAR, T.R.; VAZE, J. Assessing irrigated agriculture's surface water and groundwater consumption by combining satellite remote sensing and hydrologic modelling. **Science of The Total Environment**. v.542, Part A, p. 372-382, 2016.

PERAZZOLI, M.; PINHEIRO, A.; KAUFMANN, V. Efeitos de cenários de uso do solo sobre o regime hídrico e produção de sedimentos na bacia do Ribeirão Concórdia – SC. **Revista Árvore**. v.37, n.5, p. 859-869, 2013.

PEREIRA, L.M. **Modelagem hidrológica dinâmica distribuída para estimativa do escoamento superficial em uma microbacia urbana**. Dissertação (Mestrado em Sensoriamento Remoto) – Instituto Nacional de Pesquisas Espaciais, São José dos Campos, 2008.

PEREIRA, D.R.; ALMEIDA, A.Q.; MARTINEZ, M.A.; ROSA, D.R.Q. Impacts of deforestation on water balance components of a watershed on the brazilian east coast. **Revista Brasileira de Ciência do Solo**. v.38, p. 1350-1358, 2014.

PINEDA, L. A. C. **Estudo observacional e de modelagem hidrológica de uma micro-bacia em floresta não perturbada na Amazônia central**. 2008. 241 p. (INPE-15317-TDI/1361). Tese (Doutorado em Meteorologia) - Instituto Nacional de Pesquisas Espaciais, São José dos Campos, 2008. Disponível em: <http://urlib.net/8JMKD3MGPBW/32HCQ62>.

PINTO, D.B.F.; DA SILVA, A.M.; BESKOW, S.; DE MELLO, C.R.; COELHO, G. Application of the Soil and Water Assessment Tool (SWAT) for sediment transport simulation at a headwater watershed in Minas Gerais state, Brazil. **Transactions of the ASABE**. v.56, n.2, p.697-709, 2013.

POLIDORO, J.C.; MENDONÇA-SANTOS, M.L.; LUMBRERAS, J.F.; COELHO, M.R.; CARVALHO FILHO, A.; MOTTA, P.E.F.; CARVALHO JUNIOR, W.; ARAUJO FILHO, J.C.; CURCIO, G.R.; CORREIA, J.R.; MARTINS, E.; SPERA, S.T.; OLIVEIRA, S.R.M.; BOLFE, E.L.; MANZATTO, C.V.; TOSTO, S.G.; VENTURIERI, A.; SA, I.B.; OLIVEIRA, V.A.; SHINZATO, E.; ANJOS, L.H.C.; VALLADARES, G.S.; RIBEIRO, J.L.; MEDEIROS, P.S.C.; MOREIRA, F.M.S.; SILVA, L.S.L.; SEQUINATTO, L.; AGLIO, M.L.D.; DART, R.O. **Programa Nacional de Solos do Brasil (PronaSolos).** EMBRAPA Solos, 2016.. p.54. ISSN 1517-2627.

POST, D.F.; FIMBRES, A.; MATTHIAS, A.D.; SANO, E.E.; ACCIOLY, L.; BATCHILY, A.K.; FERREIRA, L.G. Predicting soil albedo from soil color and spectral reflectance data. **Soil Science Society American Journal**. v. 64, p. 1027-1034, 2000.

PRIESTLEY, C.F.B.; TAYLOR, R.J. On the assessment of surface heat flux and evaporation using large-scale parameters. **Monthly Weather Review**. v.100, p. 81-92, 1973.

QGIS. QGIS Development Team 2014. **QGIS Geographic Information System.** Open Source Geospatial Foundation. Available in <http://qgis.osgeo.org>. Accessed in FEB/2016.

QIU, Z.; WANG, L. Hydrological and water quality assessment in a subburban watershed with mixed land uses using SWAT model. **Journal of Hydrologic Engineering**. v. 19, n. 4, p. 816-827, 2014.

QUESADA, C.A.; LLOYD, J.; ANDERSON, L.O.; FYLLAS, N.M.; SCHWARZ, M.; CZIMEZICK, C.I. Soils of Amazonia with particular reference to the RAINFOR sites. **Biogeosciences**. v.8, p. 1415-1440, 2011.

RAGETTLI, S.; PELLICCIOTTI, F.; IMMERZEEL, W.W.; MILES, E.S.; PETERSEN, L.; HEYNEN, M.; SHEA, J.M.; STUMM, D.; JOSHI, S.; SHRESTHA, A. Unravelling the hydrology of a Himalayan catchment through integration of high resolution in situ data and remote sensing with an advanced simulation model. **Advances in Water Resources**. v.78, p. 94-111, 2015.

RANZANI, G. Erodibilidade de alguns solos do estado do Amazonas. **Acta Amazonica**, Manaus. V.10, n.2, p. 263-269, 1980.

REFSGAARD, J.C.; STORM, B. Construction, calibration and validation of hydrological models. In: ABBOTT, M.B.; REFSGAARD, J.C. (eds.). **Distributed hydrological modelling**..Dordrecht, Netherlands: Kluwer Academic Publishers. v.22, Cap.3, 1996. ISBN: 0-7923-4042-6.

RENÓ, V.; NOVO, E.; ESCADA, M. Forest fragmentation in the lower Amazon floodplain: implications for biodiversity and ecosystem service provision to riverine populations. **Remote Sensing**. v.8, p. 886, 2016.

RODRIGUES, R. M.; MASCARENHAS, A. F. S.; ICHIHARA, A. H.; SOUZA, T. M. C.; BIDONE, E. D.; BELLIA, V.; HAGON, S.; SILVA, A. R. B.; BRAGA, J. B. P.; STILIANIDI FILHO, B. **Estudo dos impactos ambientais decorrentes do extrativismo mineral e poluição mercurial no Tapajós –** pré-diagnóstico. Rio de Janeiro, Cetem/CNPq, 1994.

RODRIGUES, A.P.C.; MACIEL, P.; SILVA, L.C. Chronic effects of methylmercury on Astronotus ocellatus, an Amazonian fish species. **Journal of Aquatic Pollution and Toxicology**. v.1, p.2, 2017.

ROULET, M.; LUCOTTE, M.; CANUEL, R.; FARELLA, N.; COURCELLES, M.; GUIMARÃES, J.-R.D.; MERGLER, D.; AMORIM, M. Increase in mercury contamination recorded in lacustrine sediments following deforestation in the central Amazon. **Chemical Geology**. v.165, n.3-4, p. 243-266, 2000.

SALOMONSON, V.V. Water resources assessment. **In:** Manual of Remote Sensing. Ed. COLWELL, J. **American Society of Photogrammetry and Remote Sensing**. p.1497-1570, 1983.

SARTORI, A.; LOMBARDI NETO, F.; GENOVEZ, A.M. Classificação hidrológica de solos brasileiros para a estimativa da chuva excedente com o método do serviço de conservação do solo dos estados unidos. Parte I: classificação. **Revista Brasileira de Recursos Hídricos**. v. 10, n. 4, p.05-18, 2005.

SATGÉ, F.C. **Recursos hídricos do altiplano andino**: contribuição do sensoriamento remoto. 2017. 213 f., il. Tese (Doutorado em Geociências Aplicadas)—Universidade de Brasília, Brasília, 2017.

SATGÉ, F.C.; ESPINOZA, R.; ZOLÁ, R.P.; ROIG, H.; TIMOUK, F.; MOLINA, J.; GARNIER, J.; CALMANT, S.; SEYLER, F.; BONNET, M.P. Role of climate variability and human activity on Poopó Lake droughts between 1990 and 2015 assessed using remote sensing data. **Remote Sensing**. v.9, n.3, p.218, 2017.

SCHMINK, M.; CHARLES, H.W. **Contested frontiers in Amazonia**. Columbia University Press, 2010.

SCHOWENGERDT, R.A. **Techniques for image processing and classification in remote sensing.** . New York: Academic Press,1983.

SCHULTZ, G.A. Remote sensing in hydrology. **Journal of Hydrology**. v.100, n.1-3, p.239-265, 1988.

SECRETARIA DE ESTADO DE DESENVOLVIMENTO ECONÔMICO, MINERAÇÃO E ENERGIA (SEDEME/PA). **Plano de Mineração do Estado do Pará 2013-2030.** Relato da 3ª Oficina: Atividades Garimpeiras no Estado do Pará. Jun/2012. Available in <http://sedeme.com.br/portal/download/oficinas/3-oficina-atividades-garimpeiras.pdf>. Accessed in Jun/2017.

SELBY, M.J. **Slopes and slope processes**. Hamilton, New Zeland: New Zeland Geographical Society, 1970.

SHI, P.; MA, X.; HOU, Y.; LI, Q.; ZHANG, Z.; QU, S.; CHEN, C.; CAI, T.; FANG, X. Effects of land use and climate change on hydrological processes in the upstream of Huai River, China. **Water Resources Management**. v. 21, p. 1263-1278, 2013.

SHUTTLEWORTH, W.J. Evaporation from Amazonian Rainforest. Proceedings of the Royal Society of London, Series B, **Biological Sciences**. v. 233, n.1272, p. 321-346, 1988.

SILVA, A.K.L.; CRESTANA, S.; SOUZA, A.M.L.; VENTURIERI, A.; NUNES, H.G.G.C.; SANTOS, J.T.S.; GALHARTE, C.A. SWAT applications in eastern Amazonia: A case study of the Acará Mirim and Bujaru river basin in State of Pará, Brazil. In: INTERNATIONAL SWAT CONFERENCE, 2014, Porto de Galinhas-PE, Brasil. **Proceedings...** 2014.

SILVEIRA, A.L.L. da. Ciclo hidrológico e bacia hidrográfica. In: TUCCI, C.E.M. (org). **Hidrologia**: ciência e aplicação. 20. ed.. Porto Alegre: UFRGS, Cap. 2, p.35-40, 2009.

SILVESTRO, F.; GABELLANI, S.; RUDARI, R.; DELOGU, F.; LAIOLO, P.; BONI, G. Uncertainty reduction and parameter estimation of a distributed hydrological model with ground and remote-sensing data. **Hydrology and Earth System Science**. v.19, p. 1727-1751, 2015.

SINGH, J.; KNAPP, H.V.; ARNOLD, J.G.; DEMISSIE, M. Hydrological modelling of the Iroquois River watershed using HSPF and SWAT. **Journal of the American Water Resources Association**. v.41, n.2, p.343-360, 2005.

SONG, X.; DUAN, Z.; KONO, Y.; WANG, M. Integration of remotely sensed C factor into SWAT for modelling sediment yield. **Hydrological Processes**. v. 25, p. 3387-3398, 2011.

SKOLE, D.; TUCKER, C. Tropical deforestation and habitat fragmentation in the Amazon: satellite data from 1978 to 1988. **Science**. v.260, p.1905-1910, 1993.

SOUZA, E.S.; TEIXEIRA, R.A.; COSTA, H.S.C.; OLIVEIRA, F.J.; MELO, L.C.A.; FAIAL, K.C.F.; FERNANDES, A.R. Assessment of risk to human health from simultaneous exposure to multiple contaminants in an artisanal gold mine in Serra Pelada, Pará, Brazil. **Science of the Total Environment**. v.576, p.682-695, 2017.

SOUZA-FILHO, P.W.M.; SOUZA, E.B.; SILVA JUNIOR, R.O.; NASCIMENTO JR, W.R.; MENDONÇA, B.R.V.; GUIMARÃES, J.T.F.; DALL'AGNOL, R.; SIQUEIRA, J.O. Four decades of land-cover, land-use and hydroclimatology changes in the Itacaiúnas River watershed, southeastern Amazon. **Journal of Environmental Management**. v.167, p. 175-184, 2016.

STRASSER, M.A.; VINZON, S.B.; MASCARENHAS, F.C.B. Transporte de sedimentos de arraste no Rio Amazonas. In: Surface hydrology and water chemistry. LBA SCIENTIFIC CONFERENCE, 3., Brasília,Brazil. **Anais…** 2004.

STRAUCH, M.; BERNHOFER, C.; KOIDE, S.; VOLK, M.; LORZ, C.; MAKESCHIN, F. Using precipitation data ensemble for uncertainty analysis in SWAT streamflow simulation. **Journal of Hydrology**. v.414, p. 413-424, 2012.

STRAUCH, M.; VOLK, M. SWAT plant growth modification for improved modelling of perennial vegetation in the tropics. **Ecological Modelling**. 269, p. 98-112, 2013.

STRAUCH, M.; LIMA, J.E.F.W.; VOLK, M.; LORZ, C.; MAKESCHIN, F. The impact of best management practices on simulated streamflow and sediment load in a central Brazilian catchment. **Journal of Environmental Management**. v.127, p.S24-S36, 2013.

SUN, R.; ZHANG, X.; SUN, Y.; ZHENG, D.; FRAEDRICH, K. SWAT-based streamflow estimation and its responses to climate change in the Kadongjia River watershed, Southern Tibet. **Journal of Hydrometeorology**. v.14, p. 1571-1586, 2013.

SWAT. Soil and Water Assessment Tool. **SWATEditor_2012.10.19**. Available in <http://swat.tamu.edu/software/qswat/>. Accessed in Feb/2016.

TAGLIARI, P.D. **Perdas de solo e mercúrio em diferentes usos e manejos da terra na região do Baixo Tapajós**. 2009. xv, 116 f., il. Dissertação (Mestrado em Ciências Florestais)-Universidade de Brasília, Brasília, 2009.

TELMER, K.; COSTA, M.; ANGÉLICA, R.S.; ARAÚJO, E.S.; MAURICE, Y. Mining induced emissions of sediment and mercury in the Tapajós River Basin Pará, Brazilian Amazon, 1985-1998, determined from the Ground and from Space. In: VILLAS BOAS, R. C.; BEINHOFT, C.; SILVA, A. R. (eds.). **Mercury in the Tapajós Basin**. 2. ed. Rio de Janeiro: GEF/UNIDO/CYTED/CETEM/IMAAC publication, 2003.

TELMER, K.; COSTA, M.; ANGÉLICA, R.S.; ARAUJO, E.S.; MAURICE, Y. The source and fate of sediment and mercury in the Tapajós River, Pará, Brazilian Amazon: Ground and space-based evidence. **Journal of Environmental Management**, v. 81, n.2, p.101-113, 2006.

TOBIN, K.J.; BENNETT, M.E. Temporal analysis of Soil and Water Assessment Tool (SWAT) performance based on remotely sensed precipitation products. **Hydrological Processes**. v. 27, p. 505-514, 2013.

TOMASELLA, J.; HODNETT, M.G. Soil hydraulic properties and van Genuchten parameters for an oxisol under pasture in central Amazonia. In: GASH, J.H.C.; NOBRE, C.A.; ROBERTS, J.M.; VICTORIA, R.L. (eds). **Amazonian Deforestation and Climate**. John Wiley, Chichester, UK, p. 101-124, 1996.

TOMASELLA, J.; HODNETT, M.G. Estimating unsaturated hydraulic conductivity of Brazilian soils using soil-water retention data. **Soil Science**. v.162, n.10, p. 703-712, 1997.

TOMASELLA, J.; HODNETT, M.G. Estimating soil water retention characteristics from limited data in Brazilian Amazonia. **Soil Science**. v. 16 3, n.3, p. 190-202, 1998.

TOMASELLA, J.; HODNETT, M.G.; ROSSATO, L. Pedotransfer functions for Brazilian soils. **Soil Science Society of America Journal**. v. 61, p. 327-338, 2000.

TOMASELLA, J.; HODNETT, M.G. Pedotransfer functions for tropical soils. **Developments in Soil Science**. v.30, p. 415-429, 2004.

TOMASELLA, J.; HODNETT, M.G.; CUARTAS, L.A.; NOBRE, A.D.; WATERLOO, M.J.; OLIVEIRA, S.M. The water balance of Amazonian micro-catchment: the effect of interannual variability of rainfall on hydrological behaviour. **Hydrological Processes**, v.22, p. 2133-2147, 2008.

TOY, T.J. **Erosion: research techniques, erodibility and sediment delivery**. 1. ed. Norwich, England: GeoBooks, 2008. 86p. ISBN: 0860940009.

TUCCI, C.E.M. (Organizador). **Hidrologia -** ciência e aplicação. Porto Alegre, Brasil: Editora da Universidade/UFRGS, 1993.

TUCCI, C.E.M. Impactos da variabilidade climática e uso do solo sobre os recursos hídricos. **Fórum Brasileiro de Mudanças Climáticas – Câmara Temática de Recursos Hídricos**, Brasília, Brasil. 2002.

TUCCI, C.E.M. **Modelos hidrológicos**. 2.ed. Porto Alegre: UFRGS, 2005.

TUCCI, C.E.M. **Hidrologia:** ciência e aplicação. 3.ed. Porto Alegre: UFRGS, 2009.

UNITED NATIONS ENVIRONMENT PROGRAMME (UNEP). **Developing a national action plan to reduce and, where feasible, eliminate mercury use in artisanal and small-scale gold mining**. Guidance Document. Annex II, working draft. August, 2015.

UNITED STATES DEPARTMENT OF AGRICULTURE (USDA). **National Engineering Handbook.** Hydrology Section 4, Chapter 4-10. 1972.

UNITED STATES DEPARTMENT OF AGRICULTURE (USDA). **EPIC – Erosion/Productivity Impact Calculator:** 1. Model Documentation. Agricultural Research Service. 1990. Technical Bulletin n. 1768.

UNITED STATES GEOLOGICAL SURVEY (USGS). **Landsat5/TM archive**. https://earthexplorer.usgs.gov/. Accessed in Jan/2017.

UNITED STATES GEOLOGICAL SURVEY (USGS). **SRTM - Shuttle Radar Topography Mission**. https://earthexplorer.usgs.gov/. Accessed in Feb/2016.

UZEIKA, T.; MERTEN, G.H.; MINELLA, J.P.G.; MORO, M. Use of the SWAT model for hydro-sedimentologic simulation in a small rural watershed. **Revista Brasileira de Ciência do Solo**. v.36, n.2, 2012.

Van GENUCHTEN, M.T. A closed form equation for predicting the hydraulic conductivity of unsaturated soils. **Soil Science Society of America Journal**. v. 44, p. 892-898, 1980.

Van GRIENSVEN, A.; MEIXNER, T. Dealing with unidentifiable sources of uncertainty within environmental models. In: INTERNATIONAL ENVIRONMENTAL MODELLING AND SOFTWARE SOCIETY, 2004, Osnabrück, Germany. **Proceedings…** 2004.

Van GRIENSVEN, A.; MEIXNER, T. Methods to quantify and identify the sources of uncertainty for river basin water quality models. **Water Science and Technology**, v.53, n.1, p.51-59, 2006.

Van GRIENSVEN, A.; MEIXNER, T. A global efficient multi-objective auto-calibration and uncertainty estimation method for water quality catchment models. **Journal of Hydroinformatics**. v.9, n.4, p.277-291, 2007.

VEDOVATO, L.B.; FONSECA, M.G.; ARAI, E.; ANDERSON, L.O.; ARAGÃO, L.E.O.C. The extent of 2014 forest fragmentation in the Brazilian Amazon. **Regional Environmental Change**. v.16, n.8, p.2485-2490, 2016.

VEIGA, M.M.; ANGELOCI, G.; HITCH, M.; VELASQUEZ-LOPEZ, P.C. Processing centres in artisanal gold mining. **Journal of Cleaner Production**. v.64, n.1, p.535-544, 2014.

WAGNER, P.D.; FIENER, P.; WILKEN, F.; KUMAR, S.; SCHNEIDER, K. Comparison and evaluation of spatial interpolation schemes for daily rainfall in data scarce regions. **Journal of Hydrology**. v. 464-465, p. 388-400, 2012.

WANDERS, N.; BIERKENS, M.F.P.; DE JONG, S.M.; DE ROO, A.; KARSSENBERG, D. The benefits of using remotely sensed soil moisture in parameter identification of large-scale hydrological models. **Water Resources Research**. v.50, n.8, p. 6874-6891, 2014.

WATZEN, K.M.; MOL, J.H. Soil erosion from agriculture and mining: a threat to the tropical stream escosystems. **Agriculture**. v.3, p. 660-683, 2013.

WESTON, D.P.; YOU, J.; LYDY, M.J. Distribution and toxicity of sediment-associated pesticides in agriculture-dominated water bodies of California's Central Valley. **Environmental Science and Technology**. v.38, n.10, p.2752-2759, 2004.

WHITE, K.L.; CHAUBEY, I. Sensitivity analysis, calibration and validations for multisite and multivariable SWAT model. **Journal of American Water Resources Association**. v.41, n.5, p. 1077-1089, 2005.

WORLD HEALTH ORGANIZATION (WHO). **Environmental and occupational health hazards associated with artisanal and small-scale gold mining**. Geneva, 2016.Technical paper #1.

WILLIAMS, J.R. The EPIC model. p. 909-1000. In: Singh, V. P. (ed.) **Computer models of watershed hydrology**. Water Resources Publications, 1995. Chapter 25

WILLIAMS, J.R.; BERNDT, H.D. Sediment yield prediction based on watershed hydrology. **Transactions of ASAE**. v. 20, n.6, p. 1100-1104, 1977.

WILLIAMS, J.R.; JONES, C.A.; DYKE, P.T. A modelling approach to determining the relationship between erosion and soil productivity. **Transactions of ASAE**. v. 27, p. 12-144, 1984.

WILLIAMS, M.; SHIMABUKURO, Y.E.; RASTETTER, E.B. **LBA-ECO CD-09 soil and vegetation characteristics, Tapajós National Forest, Brazil**. Dataset. Available on-line [http://daac.ornl.gov] from Oak Ridge National Laboratory Distributed Active Archive Centre, Oak Ridge, Tennessee, USA, 2012.

WITTMANN, F.; JUNK, W.J. Amazon River Basin. In: FINLAYSON, C. M. et al (eds.). **The wetland book**. Springer Netherlands, 2016. p.1-20.

WORLD METEOROLOGICAL ORGANIZATION (WMO). **Guide to hydrological practices**. 5.ed. Geneva,1994. WMO-n°168.

YU, M.; CHEN, X.; LI, L.; BAO, A.; de la PAIX, M.J. Streamflow simulation by SWAT using different precipitation sources in large arid basins with scarce rain gauges. **Water Resources Management**. v. 25, p. 2669-2681, 2011.

ZHANG, A.; ZHANG, C.; FU, G.; WANG, B.; BAO, Z.; ZHENG, H. Assessments of impacts of climate change and human activities on runoff with SWAT for the Huifa River Basin, Northeast China. **Water Resources Management**. v. 26, p. 2199-2217, 2012.

ZULKAFLI, Z.; BUYTAERT, W.; ONOF, C.; MANZ, B.; TARNAVSKY, E.; LAVADO, W.; GUYOT, J.L. A Comparative Performance Analysis of TRMM 3B42 (TMPA) Versions 6 and 7 for Hydrological Applications over Andean-Amazon River Basins. **Journal of Hydrometeorology**. v. 15, p. 581-592, 2014.

APPENDIX A – LAND COVER MAPS AND SCENARIOS

Tables A.1, A.2, and A.3 show the confusion matrix of mapped scenarios, the overall accuracy and the Kappa index.

Table A.1. Confusion matrix of 1998 scenario.

Classification 1998 Scenario	Reference - Image: Forest	Non-forest	Water	Bare Soil	Total	
Forest	98	4	10	1	113	**Overall Acurracy:** 91.21%
Non-forest	1	84	0	5	90	
Water	1	11	90	1	103	**Kappa Index:** 0.88
Bare Soil	0	1	0	93	94	p-value < 0.05
Total	100	100	100	100	400	

Table A.2. Confusion matrix of 2003 scenario.

Classification 2003 Scenario	Reference - Image: Forest	Non-forest	Water	Bare Soil	Total	
Forest	98	20	12	0	130	**Overall Acurracy:** 88.50%
Non-forest	1	78	2	6	87	
Water	1	2	85	1	89	**Kappa Index:** 0.85
Bare Soil	0	0	1	93	93	p-value < 0.05
Total	100	100	100	100	400	

Table A.3. Confusion matrix of 2010 scenario.

Classification 2010 Scenario	Reference - Image: Forest	Non-forest	Water	Bare Soil	Total	
Forest	99	12	8	5	124	**Overall Acurracy:** 90.50%
Non-forest	0	81	0	5	86	
Water	1	5	92	0	98	**Kappa Index:** 0.87
Bare Soil	0	2	0	90	92	p-value < 0.05
Total	100	100	100	100	400	

Table A.4 show the rates of increase (positive values) and decrease (negative values) of each land cover calculated regarding the land cover changes observed in the period between 1998 and 2010.

Table A.4. Rates of increase and decrease of the land cover classes for the period of 1998-2010, 1 year and 2010-2040.

Land Cover	Increase/decrease rate for the period of 1998-2010 (%)	Increase/decrease rate for the period of 1 year (%)	Increase/decrease rate for the period of 2010-2040 (%)
Forest	-1.161	-0.089	-2.67
Non-forest	78.839	6.065	181.95
Water	0	0	0
Bare Soil	41.875	3.221	96.63

APPENDIX B - VEGETATION PARAMETERS

Table B.1. Parameter values of Non-forest and Forest land cover classes.

Crop	Parameter	Description	SWAT (Initial) value	Value used (manually calibrated)	Reference
FRSE	BIO_E	Biomass-energy ratio ((kg/ha)/(MJ/m²))	15	20	Strauch and Volk (2013)
PAST			35		
FRSE	BLAI	Maximum potential leaf area index (-)	5	9	Williams et al. (2012); Costa and Cohen (2013); Strauch and Volk (2013)
PAST			4	2.1	Strauch and Volk (2013)
FRSE	FRGRW1	Fraction of the plant growing season or fraction of total potential heat units corresponding to the 1st point on the optimal leaf are development curve (-)	0.15	0.07	
PAST			0.05	0.07	
FRSE	LAIMX1	Fraction of the maximum leaf area index corresponding to the 1st point on the optimal leaf area development curve (-)	0.7	0.15	
PAST			0.05	0.15	
FRSE	FRGRW2	Fraction of the plant growing season or fraction of total potential heat units corresponding to the 2nd point on the optimal leaf area development curve (-)	0.25	0.5	
PAST			0.49	0.4	
FRSE	LAIMX2	Fraction of the maximum leaf are index corresponding to the 2nd point on the optimal leaf area development curve (-)	0.99	0.95	
FRSE	DLAI	Fraction of growing season when leaf area begins to decline (-)	0.99	0.53	
PAST			0.99	0.58	
FRSE	CHTMX	Maximum canopy height (m)	10	30	Malhi et al. (2002)
FRSE	GSI	Maximum stomatal conductance at high solar radiation and low vapor pressure deficit ($m.s^{-1}$)	0.002	0.003	Strauch and Volk (2013)
PAST			0.005	0.0008	
FRSE	VPDFR	Vapor pressure deficit (kPa) corresponding to the second point on the stomatal conductance curve (-)	4	1.6	
PAST			4	1.1	
FRSE	ALAI_MIN	Minimum leaf area index for plant during dormant period (m²/m²)	0.75	3.2	Williams et al. (2012); Costa and Cohen (2013)
PAST			0	0.7	William et al. (1993); Strauch and Volk (2013)

APPENDIX C - SOIL PARAMETERS

Table C.1. Number and depth of soil layers.

	Soil Types							
	Acrisols	**Cambisols**	**Gleysols**	**Yellow Ferralsols**	**Red-Yellow Ferralsols**	**Fluvisols**	**Plinthosols**	**Arenosols**
Layer #	**Layer Depth (mm)**							
1	70	50	100	100	50	150	150	130
2	350	250	200	220	200	400	360	340
3	800	550	600	460	400	700	460	580
4	1200	850	900	730	800	1000	730	860
5	1600	1250	1500	950	1500	-	900	1200
6	-	1850	-	1330	-	-	1100	1600
7	-	2500	-	2000	-	-	1520	2150

Table C.2. Soil texture, Rock and Organic Carbon contents.

	Soil Types							
	Acrisols	**Cambisols**	**Gleysols**	**Yellow Ferralsols**	**Red-Yellow Ferralsols**	**Fluvisols**	**Plinthosols**	**Arenosols**
Layer #	**SAND (%)**							
1	62.50	28.75	38.60	77.30	47.50	53.37	49.16	93.81
2	12.97	23.43	40.35	74.88	38.50	53.11	43.72	88.83
3	9.92	21.79	38.31	71.36	31.00	52.56	38.40	83.15
4	8.98	22.38	38.88	69.36	29.75	50.37	34.69	81.50
5	10.24	20.50	38.03	68.64	30.00		34.75	81.50
6		17.25		68.23			30.35	81.00
7		17.25		68.00			38.55	81.00
Layer #	**SILT (%)**							
1	17.75	37.00	26.73	6.30	16.50	32.31	15.13	3.38
2	18.97	37.61	25.78	7.27	15.00	27.01	15.67	4.83
3	15.39	35.52	26.83	7.21	13.00	30.28	16.00	7.77
4	14.03	34.09	24.13	7.64	12.88	27.73	16.72	7.63
5	14.00	33.63	24.23	7.18	12.00		16.74	7.50
6		33.00		6.50			16.98	8.00
7		33.00		6.25			14.36	7.50
Layer #	**CLAY (%)**							
1	19.75	34.25	34.68	16.40	36.00	14.32	35.71	2.81
2	34.28	38.96	33.88	17.85	46.50	19.88	40.62	6.33
3	46.36	42.69	34.86	21.43	56.00	17.17	45.59	9.08
4	49.75	43.53	37.00	23.00	57.38	21.90	48.59	10.88
5	51.00	45.88	35.23	24.18	58.00		48.51	11.00

6		49.75		25.27			52.68	11.00
7		49.75		25.75			47.09	11.50
Layer #	**ROCK (%)**							
1	3.75	1.75	0.00	0.25	9.00	0.00	12.40	0.00
2	3.27	2.56	0.00	0.25	8.00	0.00	30.70	0.50
3	2.86	4.75	0.00	0.50	12.00	0.00	25.37	0.50
4	3.00	7.50	0.00	2.25	10.25	0.00	22.42	0.50
5	3.00	7.50	0.00	1.75	13.00		30.78	0.50
6		7.50		1.50			33.06	1.00
7		7.50		1.78			34.61	2.50
Layer #	**SOL_CBN (%)**							
1	2.96	1.99	2.30	1.06	1.59	1.30	2.33	1.08
2	1.04	1.11	1.63	0.80	0.97	0.58	1.15	0.80
3	0.49	0.63	0.89	0.49	0.57	0.45	0.90	0.74
4	0.39	0.52	0.40	0.33	0.40	0.45	0.70	0.55
5	0.35	0.49	0.22	0.27	0.29		0.48	0.43
6		0.47		0.26			0.43	0.42
7		0.47		0.25			0.36	0.39

SOL_CBN: Soil Organic Carbon Content.

Table C.3. Soil Hydrological Group, Maximum Root Depth, Humid Soil Albedo and USLE erodibility factor.

	Soil Types							
	Acrisols	**Cambisols**	**Gleysols**	**Yellow Ferralsols**	**Red-Yellow Ferralsols**	**Fluvisols**	**Plinthosols**	**Arenosols**
Hydgrp (-)	B	C	D	A	A	C	D	B
Sol_zmx (mm)	1600	1700	800	3500	3500	500	1100	3500
Sol_Alb (-)	0.15	0.20	0.19	0.15	0.20	0.18	0.18	0.20
USLE_K (0.013(metric ton m^2 hr)/(m^3-metric ton cm))	0.12	0.16	0.12	0.10	0.11	0.16	0.12	0.07

HYDGRP: Soil Hydrological Group.
SOL_ZMX: Maximum Root Depth in the soil.
SOL_ALB: Albedo of Humid Soil.
USLE_K: USLE erodibility factor.

Table C.4. Initial estimated values of Saturated Hydraulic Conductivity, Bulk Density and Available Water Capacity.

	Soil Types							
	Acrisols	**Cambisols**	**Gleysols**	**Yellow Ferralsols**	**Red-Yellow Ferralsols**	**Fluvisols**	**Plinthosols**	**Arenosols**
Layer #	**SOL_K (mm/h)**							
1	1702.57	806.09	973.53	1573.96	764.94	1485.42	1320.15	2256.60
2	679.15	560.03	862.74	1428.03	531.76	1070.82	957.77	1800.11
3	487.82	466.71	753.66	1205.15	459.57	993.70	721.63	1531.70
4	449.88	463.23	606.07	1092.34	434.91	936.11	678.55	1367.69
5	425.91	428.90	583.93	1047.70	423.47		595.40	1315.62
6		398.09		1003.39			462.55	1304.38
7		398.09		1002.64			601.39	1266.35
Layer #	**SOL_BD (Mg/m^3 or g/cm^3)**							
1	1.233	1.112	1.155	1.418	1.249	1.243	1.219	1.488
2	1.271	1.136	1.200	1.420	1.250	1.314	1.260	1.480
3	1.274	1.160	1.230	1.423	1.245	1.314	1.251	1.455
4	1.274	1.171	1.264	1.422	1.250	1.308	1.246	1.459
5	1.271	1.166	1.280	1.424	1.259		1.257	1.466
6		1.156		1.424			1.242	1.464
7		1.156		1.424			1.284	1.466
Layer #	**SOL_AWC ($mmH_2O/mmSoil$)**							
1	0.137	0.194	0.182	0.088	0.108	0.200	0.127	0.069
2	0.116	0.178	0.157	0.089	0.097	0.161	0.115	0.076
3	0.095	0.158	0.163	0.087	0.089	0.187	0.107	0.087
4	0.089	0.151	0.143	0.089	0.087	0.159	0.106	0.084
5	0.089	0.147	0.145	0.087	0.085		0.103	0.083
6		0.142		0.084			0.102	0.085
7		0.142		0.084			0.095	0.083

SOL_K: Soil Saturated Hydraulic Conductivity.
SOL_BD: Soil Bulk Density.
SOL_AWC: Soil Available Water Capacity.

APPENDIX D - SENSITIVITY ANALYSIS AND CALIBRATION

Table D.1. Parameters manually calibrated (except soil parameters).

Vegetation of soil type associated	Parameter	Description	Initial value	Value manually calibrated	Reference
Vegetation	**Vegetation parameters**				
FRSE	BIO_E	Biomass-energy ratio ((kg/ha)/(MJ/m²))	15	20	Strauch and Volk (2013)
PAST			35		
FRSE	BLAI	Maximum potential leaf area index (-)	5	9	Williams et al. (2012); Costa and Cohen (2013); Strauch and Volk (2013)
PAST			4	2.1	
FRSE	FRGRW1	Fraction of the plant growing season or fraction of total potential heat units corresponding to the 1st point on the optimal leaf are development curve (-)	0.15	0.07	Strauch and Volk (2013)
PAST			0.05	0.07	
FRSE	LAIMX1	Fraction of the maximum leaf area index corresponding to the 1st point on the optimal leaf area development curve (-)	0.7	0.15	
PAST			0.05	0.15	
FRSE	FRGRW2	Fraction of the plant growing season or fraction of total potential heat units corresponding to the 2nd point on the optimal leaf area development curve (-)	0.25	0.5	
PAST			0.49	0.4	

FRSE	LAIMX2	Fraction of the maximum leaf are index corresponding to the 2nd point on the optimal leaf area development curve (-)	0.99	0.95	
FRSE	DLAI	Fraction of growing season when leaf area begins to decline (-)	0.99	0.53	
PAST			0.99	0.58	
FRSE	CHTMX	Maximum canopy height (m)	10	30	Malhi et al. (2002)
FRSE	GSI	Maximum stomatal conductance at high solar radiation and low vapor pressure deficit ($m.s^{-1}$)	0.002	0.003	Strauch and Volk (2013)
PAST			0.005	0.0008	
FRSE	VPDFR	Vapor pressure deficit (kPa) corresponding to the second point on the stomatal conductance curve (-)	4	1.6	
PAST			4	1.1	
FRSE	ALAI_MIN	Minimum leaf area index for plant during dormant period (m^2/m^2)	0.75	3.2	Williams et al. (2012); Costa and Cohen (2013)
PAST			0	0.7	William et al. (1993); Strauch and Volk (2013)
Vegetation	**Parameters from files .hru (HRU)**				
FRSE	CANMX	Maximum canopy storage (mm H_2O)	0	1.049	Pineda (2008)
PAST				0.34	Trial and error
FRSE	EPCO	Plant uptake compensation factor (-)	1	0.95	Trial and error and Strauch and Volk (2013)
PAST				0.4	
FRSE	ESCO	Soil evaporation compensation factor (-)	0.95	0.016	Trial and error and Strauch and Volk (2013)
PAST				0.49	
Vegetation	**Parameters from files .gw (groundwater)**				
FRSE	GW_REVAP	Groundwater "revap" coefficient (-)	0.02	0.52	Trial and error and Strauch and Volk
PAST				0.17	

					(2013)
FRSE	REVAPMN	Threshold depth of water in the shallow aquifer for "revap" or percolation to the deep aquifer to occur (mm H_2O)	750	614	Trial and error
PAST				1000	Trial and error

Table D.2. Soil parameters manually calibrated.

	SOL_K (mm/h)							
	Acrisols	**Cambisols**	**Gleysols**	**Yellow Ferralsols**	**Red-Yellow Ferralsols**	**Fluvisols**	**Plinthosols**	**Arenosols**
Initial values	1702.57	806.09	973.53	1573.96	764.94	1485.42	1320.15	2256.6
	679.15	560.03	862.74	1428.03	531.76	1070.82	957.77	1800.11
	487.82	466.71	753.66	1205.15	459.57	993.7	721.63	1531.7
	449.88	463.23	606.07	1092.34	434.91	936.11	678.55	1367.69
	425.91	428.9	583.93	1047.7	423.47		595.4	1315.62
		398.09		1003.39			462.55	1304.38
		398.09		1002.64			601.39	1266.35
	Manually calibrated values							
Manually calibrated values	201.27	175.60	197.41	203.60	187.29	209.78	208.03	215.85
	180.24	116.79	188.38	184.10	125.97	159.12	144.66	164.68
	145.50	91.69	137.57	153.95	108.72	138.27	108.61	130.97
	48.10	100.52	118.74	135.52	102.91	134.10	101.71	116.80
	44.90	90.54	111.33	130.92	101.32		90.50	112.23
		81.90		126.08			68.74	110.24
		81.90		126.47			95.99	107.08

Table D.3. Parameters included in the sensitivity analysis.

File	**Parameter code**	**Description**	**Variation method**	**Minimum value**	**Maximum value**
gw	ALPHA_BF.gw	Baseflow alpha factor (1/days)	replace	0	1
rte	ALPHA_BNK.rte	Baseflow alpha factor for bank storage (days)	replace	0	1
mgt	BIOMIX.mgt	Biological mixing efficiency (-)	relative change	-0.5	0.2
hru	CANMX.hru____FRSE*	Maximum canopy storage (mm H_2O)	relative change	0	1
hru	CANMX.hru____PAST*		relative change	-0.2	1

sub	CH_K1.sub	Effective hydraulic conductivity in tributary channel alluvium (mm/hr)	replace	0	300
rte	CH_K2.rte	Effective hydraulic conductivity in main channel alluvium (mm/h)	replace	0	130
rte	CH_N2.rte	Manning's "n" value for the main channel (-)	replace	0.05	0.15
mgt	CN2.mgt____CX__FRSE	Initial SCS runoff curve number for moisture condition II (-)	replace	70	73
mgt	CN2.mgt____FF__FRSE		replace	77	79
mgt	CN2.mgt____FF__PAST		replace	77	79
mgt	CN2.mgt____GX__FRSE		replace	30	36
mgt	CN2.mgt____GX__PAST		replace	73	89
mgt	CN2.mgt____LA__FRSE		replace	30	36
mgt	CN2.mgt____LA__PAST		replace	55	60
mgt	CN2.mgt____LV__FRSE		replace	30	68
mgt	CN2.mgt____LV__PAST		replace	30	68
mgt	CN2.mgt____PA__FRSE		replace	55	60
mgt	CN2.mgt____PA__PAST		replace	70	73
mgt	CN2.mgt____RQ__FRSE		replace	48	79
mgt	CN2.mgt____RQ__PAST		replace	48	79
mgt	CN2.mgt____RY__FRSE		replace	73	89
hru	EPCO.hru____FRSE	Plant uptake compensation factor (-)	relative change	-0.15	0.05
hru	EPCO.hru____PAST		relative change	-0.5	0
hru	ESCO.hru____FRSE	Soil evaporation compensation factor (-)	relative change	0	3.3
hru	ESCO.hru____PAST		relative change	0	0.93
gw	GW_DELAY.gw	Groundwater delay time (days)	replace	1	450
gw	GW_REVAP.gw____FRSE	Groundwater "revap" coefficient (-)	relative change	-0.5	1.33
gw	GW_REVAP.gw____PAST		relative change	-0.5	1.33
gw	GWQMN	Threshold depth water in the shallow aquifer required for return flow to occur (mm H_2O)	replace	0	5000
hru	OV_N.hru	Manning's "n" value for overland flow (-)	replace	0.01	30
gw	REVAPMN.gw____FRSE	Threshold depth of water in the shallow aquifer for	relative change	-1	1.19

gw	REVAPMN.gw____PAST	"revap" or percolation to the deep aquifer to occur (mm H_2O)	relative change	-1	0
sol	SOL_AWC(1).sol_____FRSE	Available water capacity of the soil layer (mm H_2O/mm soil)	relative change	-0.03	0.05
sol	SOL_AWC(1).sol_____PAST		relative change	-0.03	0.05
sol	SOL_AWC(2).sol_____FRSE		relative change	-0.03	0.05
sol	SOL_AWC(2).sol_____PAST		relative change	-0.03	0.05
sol	SOL_AWC(3).sol_____FRSE		relative change	-0.03	0.05
sol	SOL_AWC(3).sol_____PAST		relative change	-0.03	0.05
sol	SOL_BD(1).sol_____FRSE	Moist bulk density (Mg/m^3 or g/cm^3)	relative change	-0.05	0.05
sol	SOL_BD(1).sol_____PAST		relative change	-0.05	0.05
sol	SOL_BD(2).sol_____FRSE		relative change	-0.05	0.05
sol	SOL_BD(2).sol_____PAST		relative change	-0.05	0.05
sol	SOL_BD(3).sol_____FRSE		relative change	-0.05	0.05
sol	SOL_BD(3).sol_____PAST		relative change	-0.05	0.05
sol	SOL_K(1).sol_____FRSE	Saturated hydraulic conductivity (mm/h)	relative change	-0.05	0.1
sol	SOL_K(1).sol_____PAST		relative change	-0.05	0.1
sol	SOL_K(2).sol_____FRSE		relative change	-0.05	0.1
sol	SOL_K(2).sol_____PAST		relative change	-0.05	0.1
sol	SOL_K(3).sol_____FRSE		relative change	-0.05	0.1
sol	SOL_K(3).sol_____PAST		relative change	-0.05	0.1
sol	SOL_ZMX.sol____CX**	Maximum rooting depth of soil profile (mm)	relative change	-0.5	1
sol	SOL_ZMX.sol____FF**		relative change	-0.5	1
sol	SOL_ZMX.sol____GX**		relative change	-0.5	1
sol	SOL_ZMX.sol____LA**		relative change	-0.2	0.042
sol	SOL_ZMX.sol____LV**		relative change	-0.2	0
sol	SOL_ZMX.sol____PA**		relative change	-0.2	0.5
sol	SOL_ZMX.sol____RQ**		relative change	-0.2	0
sol	SOL_ZMX.sol____RY**		relative change	-0.2	1
bsn	SURLAG.bsn	Surface runoff lag coefficient (-)	replace	1	12

*FRSE and PAST refer to the land covers 'Forest Evergreen' and 'Pasture', respectively, from SWATv.2012 database.
**CX, FF, GX, LA, LV, PA, RQ and RY refer to the soil types: Cambisols, Plinthosols, Gleysols, Yellow Ferralsols, Red-Yellow Ferralsols, Acrisols, Arenosols and Fluvisols, respectively.